Milan Vujinović

Vertices and Bound States in Strongly Interacting Theories

Dissertation
zur Erlangung des Doktorgrades der Naturwissenschaften
verfasst am Institut für Physik
an der Karl-Franzens-Universität Graz
Betreuer: Univ.-Prof. Dr. R. Alkofer
Graz, 2015

Contents

1 Introduction **5**

2 Basic Aspects of QCD **8**
2.1 Field content and symmetries 8
2.2 Quantisation and primitively divergent vertices 10
2.3 Phenomenological features 14
2.4 Other strongly interacting theories 18

3 Dyson-Schwinger and Bethe-Salpeter formalism **20**
3.1 General considerations 20
3.2 DSEs for proper vertices 22
3.3 The Bethe-Salpeter equation 24

4 Technicolor theories **30**
4.1 Standard Model Higgs sector and the hierarchy problem 30
4.2 General aspects of Technicolor 33
4.3 Walking Technicolor 35
4.4 Large N_f theories 38
4.5 Non-fundamental quarks 39
4.6 QCD-like model: a Dark Matter candidate theory 40

5 The three-gluon vertex **42**
5.1 Vertex DSE 43
5.2 Ghost/gluon input and models for vertices 44
5.3 Results and discussion 46

6 Bound states in an $SU(2)$ theory **54**
6.1 The matter sector 54
6.2 The Yang-Mills input 59
6.3 Numerical procedure 61
6.4 Ground state mesons 64

7 Conclusions and outlook **68**

A Utilities **71**
A.1 Euclidean conventions 71
A.2 Chebyshev expansion 72

B Basis construction and numerics for three-gluon vertex **74**
B.1 Bose-symmetric basis 74
B.2 Orthonormal basis 77
B.3 Solution method 79

C Technicalities of bound state studies **82**
C.1 Quark DSE in the complex plane 82
C.2 The quark-gluon vertex: basis and interpolation 85
C.3 Solving the BSE 89

D Constructing the Bethe-Salpeter kernel **91**
D.1 Axial Ward-Takahashi identity 91
D.2 DSE and BSE truncations from the effective action 92

Chapter 1

Introduction

Gauge symmetry is a concept of central importance in modern theoretical particle physics. The usefulness of the gauge principle for the description of fundamental laws of Nature was first made evident through many successes of quantum electrodynamics (QED), a quantum field theory of electromagnetic interaction based on the $U(1)$ gauge symmetry group. QED is still today a paragon of a successful field theory, as some of its predictions agree with experimental observations with unprecedented accuracy on the order of 10^{-8} [1, 2]. Owing to its beautiful results, QED served as a natural template when various theoretical descriptions of other fundamental forces were considered.

Today, the two 'nuclear' forces (whose range of influence is limited to atomic nuclei) are both described by non-Abelian generalisations of QED. The strong colour force, responsible for formation of nucleons and all other strongly interacting particles (hadrons), is described by an $SU(3)$ gauge theory named quantum chromodynamics (QCD). The weak interaction, which governs some types of radioactive decay, is described by an $SU(2)$ theory and is usually considered together with the electromagnetic force within the electroweak theory framework. Together, QCD and the electroweak theory form what is known as the Standard Model of particle physics.

On the outset, the fact that nuclear interactions are apparently successfully described by gauge field theories seems at odds with experimental data. Gauge invariance prohibits the mass terms for gauge field quanta, and yet the only massless particle known to us to this day is the photon. This inconsistency is however by now well understood. In the case of the strong interaction, the force-mediating bosons, called gluons, are confined within hadrons and their presence can be detected only indirectly. It is strongly believed that confinement (which is valid for strongly interacting matter fields, called quarks, as well) is due to the non-Abelian nature of QCD and the associated self-interactions of the gluon field. In weak interactions, there are no massless gauge field quanta because of the spontaneous breaking of a global symmetry corresponding to gauge invariance [3–6]. This so-called Higgs mechanism leads to very massive force-mediating bosons, which is the main reason for the 'weakness' of this fundamental force.

In this thesis we will be primarily concerned with QCD and similar strongly interacting theories. We wish to study both their fundamental and phenomenological aspects. On the fundamental side, we want to gather information about Greens functions, or vertices, as basic building blocks of these theories. On the phenomenological side, we want to be able to calculate hadronic observables like masses, decay constants and others, directly from the underlying dynamics. The study of bound states already excludes the use of perturbative methods. Also,

the vertex functions of QCD can be studied perturbatively only in the high-energy, or ultraviolet (UV) region, owing to asymptotic freedom [7–9]. Investigation of vertices for arbitrary four-momentum requires the use of tools which do not rely on the small coupling expansion. A continuous, manifestly covariant and non-perturbative framework which is almost ideally suited to this kind of investigation is that of Dyson-Schwinger and Bethe-Salpeter equations, for reviews see [10–13]. In this formalism, the vertex functions are studied by solving their equations of motion, while the connection between the fundamental degrees of freedom and physical observables is provided through the bound state equations. Basic aspects of QCD are reviewed in Chapter 2. These include the relevant symmetries, the quantisation procedure and the main phenomenological features. The combined formalism of Dyson-Schwinger and Bethe-Salpeter equations (DSEs/BSEs) is described in Chapter 3. It is immediately applied to QCD bound states within the rainbow-ladder (RL) framework. This serves both to establish our approach to hadrons in a simple way, as well as to show the shortcomings of the RL method and the need to use more sophisticated tools when investigating generic strongly interacting theories. For some examples of the application of the RL approach to QCD, see [14–18].

The success of QCD has led to ideas that a non-Abelian gauge field theory could offer a solution to some problematic aspects of the Higgs sector of the Standard Model. This culminated in the formulation of Technicolor (TC) as a theory of dynamical breaking of electroweak symmetry [19, 20]. Motivation for Technicolor theories, as well as some general ideas connected to these endeavors are given in Chapter 4. There we also give a short review of scenarios which are presently thought to be most appealing from the phenomenological perspective. Apart from the obvious motivation, connected to the fact that these models might solve some of the shortcomings of the Standard Model, we have two additional reasons to study them. One is that by investigating Technicolor we improve our intuition on how strongly interacting theories work. This is especially interesting in the context of TC phenomenology, since it seems that phenomenologically viable models need to have the so-called nearly conformal, or 'walking' dynamics [21], a feature which is very different from what is encountered in QCD. It would be highly rewarding for our understanding of strongly-interacting matter to study how walking behaviour affects both the fundamental Greens functions and hadronic observables. While we do not tackle this task directly here, concentrating instead on purely QCD-like models, we do develop some techniques which should be useful in future investigations of nearly conformal templates. The second reason to study different non-Abelian gauge theories is that they provide an additional testbed for some of the newer methods that were employed during our calculations, mostly in the area of bound state investigations.

In Chapter 5 we describe a Dyson-Schwinger evaluation of the three-gluon vertex. This is the simplest Greens function which encodes the self-interaction of the gluon field and is thus intrinsically interesting for our understanding of strong interactions. Additionally, it is an important ingredient in the evaluation of some other Greens functions, for instance the gluon propagator [22–24] and the quark-gluon vertex [25]. Unfortunately, our results for the gluon three-point function strongly suggest that there are important contributions missing in the calculation. It is suspected that these are primarily related to the unquenching effects, the neglected two-loop terms and the inadequate description of the gluonic four-point correlator. At the end of Chapter 5 we comment on how can at least some of the shortcomings be mitigated with minimal changes to the overall computational method. Our results for this vertex function can also be found in [26].

Through the quark-gluon interaction, the three-gluon vertex enters the calculations of hadronic properties. In the context of bound states, the fact that its tree-level dressing has a zero crossing can have some interesting consequences, depending on the location (in momentum space) of this sign flip. These matters are considered in detail in Chapter 6.

The centerpiece of our beyond rainbow-ladder (BRL) treatment of hadrons is the quark-gluon vertex. It is here calculated in a semi-self-consistent manner (as opposed to a fully self-consistent approach) to make the Bethe-Salpeter bound-state equation solvable. This is one of the very first instances where the quark-gluon interaction was evaluated in such a fashion and used in the calculation of hadronic observables, see also [27, 28]. These novel techniques are applied and tested in the study of the ground state spectrum of light hadrons in an $SU(2)$ gauge theory, which is described in Chapter 6. We studied the $SU(2)$ theory because it potentially offers a unified description of dynamical electroweak symmetry breaking and Dark Matter [29–31]. Although this model has some drawbacks as a Technicolor scenario, it still might be a useful starting point, and future investigations will show if it can be modified to better meet the demands of Technicolor phenomenology. More details on these matters are provided in Chapters 4 and 6. We conclude in Chapter 7.

While some more technical aspects and derivations are discussed in the main text as well, most of these are delegated to the Appendices. In Appendix A we provide some basic utilities related to the Euclidean spacetime conventions and the Chebyshev expansion, a computational tool which we frequently employ here. Appendix B contains the description of our solution method for the three-gluon vertex, including the construction of a Bose-symmetric basis and the numerical setup. Details related to the numerics of bound-state calculations can be found in Appendix C, and some more formal aspects of BSE/DSE truncations in Appendix D. We finally note that in terms of organisation and notation this thesis was greatly influenced by [32].

Chapter 2

Basic Aspects of QCD

2.1 Field content and symmetries

In Euclidean spacetime, the classical action of QCD can be written as (see e. g. [33]):

$$S_{\rm QCD}[A,\bar\psi,\psi] = \int d^4x \left[\bar\psi(-\not{D} + \mathrm{M})\psi + \frac{1}{4}F_{\mu\nu}^2\right]. \tag{2.1}$$

Here, ψ is the quark field, while D_μ and $F^a_{\mu\nu}$ are respectively the covariant derivative and the gluon field strength tensor, given by

$$\begin{aligned} D_\mu &= \partial_\mu + igA_\mu \ , \\ F_{\mu\nu} &= \partial_\mu A_\nu - \partial_\nu A_\mu + ig[A_\mu, A_\nu]. \end{aligned} \tag{2.2}$$

g is the gauge coupling. By its very construction, $S_{\rm QCD}$ is invariant under the gauge transformations (we suppress the matrix indices)

$$\psi' = U\psi, \qquad A'_\mu = UA_\mu U^\dagger - \frac{i}{g}U(\partial_\mu U^\dagger), \qquad F'_{\mu\nu} = UF_{\mu\nu}U^\dagger. \tag{2.3}$$

$U(x)$ is a local gauge rotation of the form $e^{i\varepsilon(x)} = e^{i\sum_a \mathbf{t}_a\varepsilon_a(x)}$, with the index $a = 1\ldots 8$ and $\mathbf{t}^a$ the generators of the $SU(3)$ colour group. $\varepsilon_a(x)$ are transformation parameters. Gluon fields are represented by A_μ, and can be written in component notation as $A_\mu = A^a_\mu \mathbf{t}^a$. The quarks transform according to the fundamental representation of $SU(3)_c$, with $\mathbf{t}_a$ given by the Gell-Mann matrices $\lambda_a/2$. Due to the non-Abelian nature of colour rotations, the commutator of gluon fields in Eq. (2.2) does not vanish, leading to terms proportional to A^3 and A^4 in $F^2_{\mu\nu}$. These self-interactions of the gluon field are largely believed to be responsible for some unique features of the strong interaction, like the confinement phenomenon.

While the gauge invariance is exact, the QCD action has other symmetries which are approximate and are related to the flavour structure encoded within the quark mass matrix M. The quarks come in six different flavours distinguished by their bare masses. These masses range from the very light 'up' state with $m_u \approx 2$ MeV, to the very heavy 'top' quark state with $m_t \approx 170$ GeV. These masses come from the electroweak sector [34, 35], and can be considered as external input for QCD calculations. Obviously, in reality the flavour symmetry is very badly broken. It will prove useful to temporarily ignore this and consider a general case of

a theory with N_f flavours with unspecified quark masses. We are then interested in how the theory behaves under global flavour rotations of the quark fields $\psi'(x) = U\psi(x)$, with[1]

$$\begin{aligned} SU(N_f)_V: &\quad U = e^{i\sum_f \mathbf{t}_f \alpha_f} \ , \\ SU(N_f)_{\mathcal{A}}: &\quad U = e^{i\gamma_5 \sum_f \mathbf{t}_f \alpha_f}. \end{aligned} \tag{2.4}$$

Here, the $\mathbf{t}_f$ are the generators of $SU(N_f)$, and the flavour index f takes on values from 1 to $N_f^2 - 1$. Indices 'V' and '$\mathcal{A}$' respectively denote the vector and axialvector currents associated with these rotations. For the flavour-singlet case of $U(1)_V$ and $U(1)_{\mathcal{A}}$ transformations, one needs to make replacements $\mathbf{t}_f \to 1$ and $\alpha_f \to \alpha$ in Eqs. (2.4). It is straightforward to work out the corresponding currrents:

$$U(1)_V: \quad V^\mu = \bar{\psi}\gamma^\mu\psi \ , \tag{2.5}$$

$$SU(N_f)_V: \quad V_f^\mu = \bar{\psi}\gamma^\mu \mathbf{t}_f \psi \ , \tag{2.6}$$

$$SU(N_f)_{\mathcal{A}}: \quad \mathcal{A}_f^\mu = \bar{\psi}\gamma^\mu\gamma_5 \mathbf{t}_f \psi \ , \tag{2.7}$$

$$U(1)_{\mathcal{A}}: \quad \mathcal{A}^\mu = \bar{\psi}\gamma^\mu\gamma_5\psi \ , \tag{2.8}$$

and their divergences:

$$\partial_\mu V^\mu = 0 \ , \tag{2.9}$$

$$\partial_\mu V_f^\mu = i\bar{\psi}[\mathrm{M}, \mathbf{t}_f]\psi \ , \tag{2.10}$$

$$\partial_\mu \mathcal{A}_f^\mu = i\bar{\psi}\{\mathrm{M}, \mathbf{t}_f\}\psi \ , \tag{2.11}$$

$$\partial_\mu \mathcal{A}^\mu = 2i\bar{\psi}\mathrm{M}\gamma_5\psi. \tag{2.12}$$

The vanishing divergence of Eq. (2.9) entails baryon number conservation in processes governed by the strong interaction. It is the only 'flavour' conservation law which does not depend on the properties of the quark mass matrix. As can be seen from Eq. (2.10), divergence of V_a^μ is zero only in the case of mass-degenerate quarks, which is not even approximately realised in Nature. If one considers only the light states, the up, down and strange quark, with masses (the values cited below are for the $\overline{\mathrm{MS}}$ scheme at the scale $\mu^2 \approx 4$ GeV^2 [36]):

$$m_u \approx 2 \text{ MeV}, \quad m_d \approx 5 \text{ MeV}, \quad m_s \approx 100 \text{ MeV}, \tag{2.13}$$

then the symmetry $SU(N_f)_V$ offers a good approximate description. This is because the differences between m_u, m_d and m_s are relatively small compared to the intrinsic scale of the strong interaction $\Lambda_{\mathrm{QCD}} \approx 1$ GeV [36]. Additionally, for the lightest states the currents $\mathcal{A}_a^\mu$ and $\mathcal{A}^\mu$ should also be conserved to a high degree, since the light quarks can be considered 'massless' compared to Λ_{QCD}, cf. Eqs. (2.11) and (2.12). However, none of the axial symmetries can be seen in the hadronic spectrum, see Table 2.1 in section 2.3. In strong interactions, the approximate conservation law for $\mathcal{A}_f^\mu$, valid on the classical level, is removed by the non-perturbative dynamical effects. Similarly, the quantity $\partial_\mu \mathcal{A}^\mu$ receives anomalous contributions upon quantisation [37, 38]. While both of these phenomena are highly interesting and have deep implications for QCD phenomenology, in this thesis we will be primarily concerned with the dynamics which affects the divergence of equation (2.11).

[1] While we use the 'group' notation $SU(N_f)_{\mathcal{A}}$ for axial non-singlet transformations, it should be noted that they actually form a *semigroup*.

In the limit of vanishing quark masses, the $SU(N_f)_V \times SU(N_f)_{\mathcal{A}}$ symmetry of $S_{\rm QCD}$ is equivalent to an invariance under chiral rotations $SU(N_f)_L \times SU(N_f)_R$. Here, the labels '$L$' and '$R$' denote left- and right- handed components of fermion fields ψ. This equivalency can be easily made apparent by defining the chiral projection operators:

$$\mathrm{P}_{\pm} = \frac{1}{2}(\mathbf{1} \pm \gamma_5), \quad \mathrm{P}_{\omega}\psi = \psi_{\omega}, \quad \bar{\psi}\mathrm{P}_{\omega} = \bar{\psi}_{-\omega} \ . \tag{2.14}$$

ω can have values '+' and '−', which respectively stand for right-handed and left-handed projectors/components. With the help of the identities $\mathrm{P}_{\omega}\gamma^{\mu} = \gamma^{\mu}\mathrm{P}_{-\omega}$ and $\mathrm{P}_{\omega}\mathrm{P}_{-\omega} = 0$, it is straightforward to show that in the massless limit the quark part of Eq. (2.1) decouples into left-handed and right-handed components:

$$S_{\rm quark} = \int d^4x \ \bar{\psi} \not{D} \psi = \int d^4x \sum_{\omega} \bar{\psi}_{\omega} \not{D} \psi_{\omega} \ . \tag{2.15}$$

The resulting theory is invariant under seperate $SU(N_f)_L \times SU(N_f)_R$ rotations, and is said to possess chiral symmetry. With the same arguments one can show that the Dirac structure $\gamma^{\mu}\gamma_5$ is also chirally invariant, whereas $\mathbf{1}$ (mass term), γ_5 and $\sigma^{\mu\nu}$ are not. In the case of QCD there is already explicit chiral symmetry breaking due to non-vanishing quark masses. As previously mentioned, the $SU(N_f)_V$ part is still approximately correct in the light quark sector, whereas the $SU(N_f)_{\mathcal{A}}$ component is spontaneously broken by the strong interaction itself. The associated pattern of symmetry breaking is

$$SU(3)_L \times SU(3)_R \to SU(3)_V \ . \tag{2.16}$$

The mechanism behind this phenomenon, as well as its consequences on the hadronic spectrum are further discussed in section 2.3. We also note that the 2-flavour counterpart of equation (2.16) has some important implications for Technicolor theories, see section 4.2.

2.2 Quantisation and primitively divergent vertices

Basic objects in any quantum field theory are its Greens functions (and amongst them the vertex functions), which encode the propagation and interaction of various fields. A convenient starting point in deriving the vertices and relations among them is to define the generating functional of the theory Z. All relevant details about the formalism can be found in Chapter 3. Here we immediately give the 'naive' version of the generating functional for QCD (henceforth, we label $S_{\rm QCD}$ simply as S):

$$Z[J, \eta, \bar{\eta}] = \int \mathcal{D}[A, \bar{\psi}, \psi] e^{i\left(S[A,\bar{\psi},\psi] - \int_x (J_\mu A^{\mu}, + \bar{\psi}\eta + \bar{\eta}\psi)\right)} \ . \tag{2.17}$$

J^{μ}, η and $\bar{\eta}$ are the source terms. Like the quark fields themselves, the sources $\eta, \bar{\eta}$ are Grassmann-valued. We call the generating functional of Eq. (2.17) naive because it is not well defined as it stands. We can see what is wrong with it by looking at the inverse gluon propagator in momentum space:

$$F^a_{\mu\nu} F^{\mu\nu}_a \sim A^a_{\mu}(k)(k^2\delta^{\mu\nu} - k^{\mu}k^{\nu})A^a_{\nu}(k) + \dots \ . \tag{2.18}$$

The object in the bracket is a transverse projector. Since it has zero modes (all longitudinal field configurations), it cannot be inverted and the gluon propagator does not exist. Another way to look at this is to consider the functional integral itself. If we write an arbitrary gluon field configuration in terms of transverse and longitudinal components, $A_\mu = A_\mu^T + A_\mu^L$, then only the A_μ^T part contributes to the propagator in Eq. (2.18). However, the integral measure $\int \mathcal{D}A$ still contains the 'spurios' longitudinal degrees of freedom, and the functional integral overcounts the physically equivalent gauge field configurations. A method which is frequently used to overcome this difficulty is due to Faddeev and Popov [39]. The basic idea is to introduce a gauge fixing condition of the form $f[A] = 0$ into the functional integral. In this way one singles out the gauge field configurations which fufill this condition, and avoids redundant information in the generating functional. There is a certain level of freedom available in making a particular choice for the function $f[A]$. In a slight abuse of terminology, this is often called 'choosing a gauge'. We shall briefly outline the Faddeev-Popov procedure here. Let A^U denote a gauge transformation of the gluon fields, with U as defined below Eq. (2.3). The Faddeev-Popov operator is then defined as

$$M[A] = \frac{\delta f[A^U]}{\delta \varepsilon}\Big|_{f[A^U]=0} \, . \tag{2.19}$$

Note that the above operator does not depend on U: this dependence is lost when taking the derivative. One then employs the 'functional unity'

$$\int \mathcal{D}U \, \det \, M[A] \, \delta\big(f[A^U]\big) = 1, \tag{2.20}$$

to transform the gauge part of QCD generating functional into

$$Z = \int \mathcal{D}U \int \mathcal{D}A \, \det \, M[A] \, \delta\big(f[A^U]\big) e^{iS[A]} \, . \tag{2.21}$$

By performing a gauge transformation $A^U \to A$ it is easy to see that the expression inside the outer integral is U-independent, and $\int \mathcal{D}U$ produces a constant which drops out upon normalisation. The U-integral can be ignored and in principle, we have our desired result: we are now integrating only over physically distinct field configurations which are picked out by the delta function. This procedure assumes that each gauge orbit intersects the hypersurface $f[A] = 0$ only once. If this were not the case, we would still have some redundancy left over in the system in the form of Gribov copies, see Fig. 2.1.

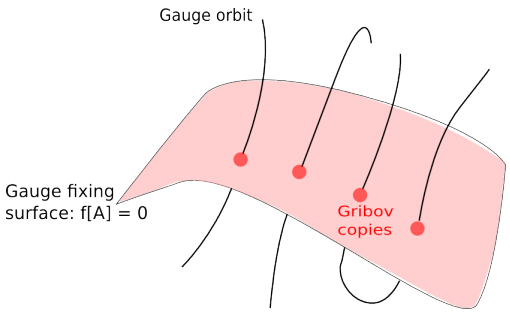

Figure 2.1: Schematic representation of the Faddeev-Popov gauge-fixing procedure.

Unfortunately, in QCD the Faddeev-Popov method is not sufficient to completely address this issue, and a full solution for the problem of Gribov copies is yet to be found [40]. While it holds importance for some formal considerations of QCD (e. g. the non-perturbative failure of the BRST symmetry, which we shortly discuss below), we shall mostly ignore this aspect in the rest of the thesis. What remains to be done is to manipulate the expression of Eq. (2.21) so as to bring the delta function and the Faddeev-Popov determinant inside the action. We shall not provide the details, which can be found in [39]. We cite the final result for linear covariant gauges $f[A] = \partial_\mu A^\mu$:

$$Z[J,\eta,\bar{\eta},\sigma,\bar{\sigma}] = \int \mathcal{D}[A,\bar{\psi},\psi,c,\bar{c}] e^{i\left(S[A,\bar{\psi},\psi]+S_{\rm GF}+S_{\rm C}\right)}, \tag{2.22}$$

with $S_{\rm GF}$ and S_C respectively being the gauge fixing and source terms, given by

$$S_{\rm GF} = -\int_x \frac{f[A]^2}{2\xi} + \int_x\int_y i\bar{c}_a M[A]_{ab} c_b = \int_x \left(-\frac{(\partial_\mu A^\mu_a)^2}{2\xi} + \frac{i}{g}\bar{c}_a \partial_\mu D^\mu_{ab} c_b \right) , \tag{2.23}$$

$$S_{\rm C} = -\int_x (J_\mu A^\mu, +\bar{\psi}\eta + \bar{\eta}\psi + \bar{\sigma}c + \bar{c}\sigma). \tag{2.24}$$

The auxiliary fields c and $\bar{c}$ come from the Faddeev-Popov determinant and are called Faddeev-Popov ghosts, or simply ghosts. They are anticommuting scalars and thus do not obey the spin-statistics theorem. This is not a problem since they are merely a part of the formalism and do not represent real physical excitations. The corresponding sources in the functional integral are σ and $\bar{\sigma}$. The ξ variable in Eq. (2.23) is a gauge parameter. It can take on any finite value, and a specific choice usually depends on the problem which is being tackled. Throughout we will be working with $\xi = 0$, which defines the Landau gauge. We briefly note that in this gauge the ghost and gluon propagator, $D_G(k)$ and $D_{\mu\nu}(k)$ respectively, take the simple form

$$D_G(k) = -\frac{G(k^2)}{k^2}, \quad D_{\mu\nu}(k) = T_{\mu\nu}(k)\frac{Z(k^2)}{k^2} , \tag{2.25}$$

where $T_{\mu\nu}(k) = \delta_{\mu\nu} - k_\mu k_\nu / k^2$ is a transverse projector with respect to momentum k. The fact that the gluon propagator in Landau gauge is a purely transverse object will entail some important simplifications in our upcoming calculations. Other reasons for this choice of gauge will become clear as we go along.

An arguably more economical way to arrive at the quantised theory of equation (2.22) is to impose the BRST symmetry [41, 42]. Let us look at the infinitesimal gauge transformation with the ghost field as the rotation parameter $c(x) = c_a(x) \cdot \mathbf{t}_a$. Under this so-called BRST variation, the fields in the classical QCD action transform as

$$\delta\psi = ic\psi, \quad \delta\bar{\psi} = -i\bar{\psi}\bar{c}, \quad \delta A_\mu = \frac{1}{g} D_\mu c, \quad \delta F_{\mu\nu} = i[c, F_{\mu\nu}] \ . \tag{2.26}$$

Requirement that this variation be nilpotent ($\delta^2 = 0$) fixes the transformation of the ghost field itself from any of the above relations: $\delta c = \frac{i}{2}[c,c]$. Conserved charge associated with the $U(1)$ symmetry of the ghost fields is called the ghost number, and it is raised by one unit with each application of δ. When acting on the antighost $\bar{c}$, the BRST transformation

should produce a scalar field with ghost number equal to zero, the so-called Nakanishi-Lautrup field, with $\delta\bar{c} = -iB$. Nilpotency of δ then fixes $\delta B = 0$. Since the classical QCD action is gauge-invariant and the BRST variation is a gauge transformation, it should be clear that $S[A, \psi, \bar{\psi}]$ is also BRST-invariant. The most general BRST-symmetric object is then obtained by adding to the classical action a term of the form $S_{\rm GF} = \delta\mathcal{O}$. In this approach, choosing a gauge amounts to picking out a particular $\mathcal{O}$. The generating functional of Eqs. (2.22), (2.23) and (2.24) follows from the following choice:

$$S_{\rm GF} = \delta \int_x i\bar{c}_a \left(f_a[A] + \frac{\xi}{2} B_a \right) = \int_x B_a \left(f_a[A] + \frac{\xi}{2} B_a \right) + \int_x \int_y i\bar{c}_a M[A]_{ab} c_b \ . \tag{2.27}$$

Employing the equation of motion for the B field, $f_a + \xi B_a = 0$ [39] then gives the middle expression in equation (2.23). Thus, imposing BRST symmetry provides both the ghost fields and the gauge-fixing terms. This formalism can also be used for derivation of helpful identities among the Greens functions (and consequently, the renormalisation factors) of the theory, some of which will be cited below and used extensively in our calculations. In non-Abelian models it is usually more convenient to exploit the BRST invariance than the 'ordinary' gauge symmetry when obtaining these relations.

Upon quantisation, one ends up with seven primitively divergent vertex functions of QCD. Three of them are the inverse propagators, and these are the quark, gluon, and ghost two-point function. The other four are interaction vertices, namely the quark-gluon, ghost-gluon, three-gluon and four-gluon vertex. QCD contains infinitely many different Greens functions, but the primitively divergent ones are of special importance. One of the reasons is that they 'carry' the renormalisation of the theory: after the basic vertices have been rendered finite by renormalisation, all higher n-point functions should be finite as well. In addition, the approximations which include all superficially divergent vertices are expected to provide qualitatively reliable information about the theory. The general structure of functional equations for Greens functions suggests that all the non-analytic behaviour (e. g. poles) should come from the vertices which have a tree-level counterpart [11]. This means that the inclusion of higher-point functions, while possibly having important quantitative impact, will almost surely not give rise to any kind of unexpected, fundamentaly different results.

A remark is in order regarding renormalisation. One would naively expect that it takes nine renormalisation contacts to remove infinites from QCD: one for the gauge coupling, two for the quark propagator, and one for each of the remaining tree-level terms. Fortunately, owing to the gauge symmetry and associated Slavnov-Taylor identities [43, 44], the actual number of renormalisation conditions is significantly reduced. We will only need the following ones:

$$A^a_\mu \to \sqrt{Z_3} A^a_\mu, \quad \bar{c}_a c_b \to \tilde{Z}_3 \bar{c}_a c_b, \quad \bar{\psi}\psi \to Z_2 \bar{\psi}\psi, \quad g \to Z_g g \ . \tag{2.28}$$

All other constants can be derived from these via Slavnov-Taylor relations (see e. g. [45] and references therein):

$$Z_1 = Z_g Z_3^{3/2}, \quad \tilde{Z}_1 = Z_g \tilde{Z}_3 Z_3^{1/2}, \quad Z_{1F} = Z_g Z_3^{1/2} Z_2, \quad Z_4 = Z_g^2 Z_3^2 \ . \tag{2.29}$$

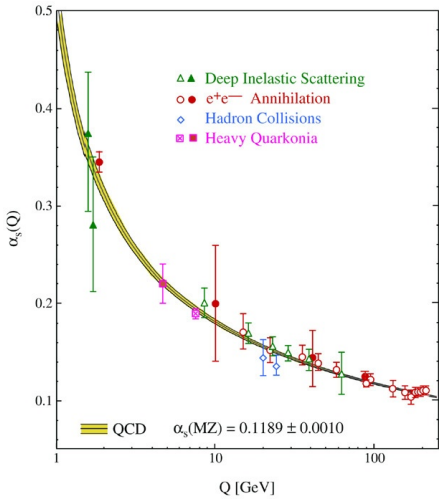

Figure 2.2: Scale dependence of the strong interaction running coupling [46].

$Z_1, \tilde{Z}_1, Z_{1F}$ and Z_4 are respectively renormalisations of the three-gluon, ghost-gluon, quark-gluon and four-gluon interaction. As we shall see in section 5.2 and onwards, in Landau gauge there are additional simplifications to these identities, which make it especially convenient for non-perturbative calculations.

2.3 Phenomenological features

Chiral limit QCD is a conformally invariant theory, at least on the classical level. The quark masses are the only thing which sets the scale in the classical action of QCD, and without them the theory is completely symmetric with respect to rescaling of distances and fields.[2] This symmetry is lost upon quantisation, as the integral measure $\mathcal{D}[A\psi\bar{\psi}c\bar{c}]$ in Eq. (2.22) is affected in a non-trivial way by conformal transformations. Among other things, this implies that the coupling(s) of the theory become scale-dependent quantities. In the case of QCD, the evolution of this 'running coupling' $\alpha_S(\mu)$ (with $\mu = p^2$ denoting the energy scale) is such that the theory becomes asymptotically free at high energies [7–9]. The coupling gets weaker as one goes further into the UV region, and quarks behave as almost-free particles. Measurements on the scale dependence of α_S are shown in Figure 2.2. From a theoretical perspective, importance of asymptotic freedom lies in the fact it enables the use of perturbative methods for the study of QCD at high energies, and this in turn also guarantees that the non-Abelian gauge theories are fundamentantally well defined.

The converse of this is that the running coupling becomes stronger as the mid- and low-energy region is approached, and at a certain point it gets large enough to invalidate the use of perturbative tools. In fact, as can be seen in Figure 2.2, this transition to the non-perturbative regime happens relatively fast, as it takes α_S 'only' a few orders of magnitude in $\sqrt{\mu}$ to become $O(1)$. As we will see in section 4.3, the fact that the gauge coupling changes relatively quickly with the scale has some very important implications for QCD-based theories of electroweak

[2]Conformal symmetry is a broader concept than scaling symmetry. As there are no known examples of field theories which are scale invariant but not conformally invariant, we will use the two names interchangeably.

symmetry breaking. Two phenomena which are inherently tied to low energies and the associated strong coupling are confinement and dynamical chiral symmetry breaking. These are truly unique features of the colour interaction which set it apart from other fundamental forces of Nature, and are crucial for understanding the spectrum of bound states in QCD. We shall now discuss each of these aspects in turn.

Confinement entails the absence of isolated coloured states, quarks and gluons, from the asymptotic state space of QCD. It is an experimental fact that quarks and gluons are always bound inside hadrons, and we can detect their presence only indirectly. A satisfactory theoretical explanation of this phenomenon is still lacking, and it is an open question whether it is at all possible to describe it within the framework of a local theory. Different methods have been developed over time that tackle different aspects of this problem. For instance, in Coulomb gauge confinement implies a linearly rising potential between a quark and an antiquark [47–50], whereas in Landau gauge it is intimately tied to the infrared properties of the Yang-Mills propagators, where the gluon is IR suppressed while the ghost is not [51–54]. Yet another way of looking at this issue is to attempt to identify the subspace of physical states from the asymptotic state space of the theory. These attempts include the Kugo-Ojima confinement scenario [55] and the Osterwalder-Schrader axiom of reflection positivity for an Euclidean field theory [56, 57]. We shall see in this section that it is possible, within a simple Dyson-Schwinger treatment, to obtain a quark propagator which has complex conjugate poles, ensuring that the quark is a very short-lived excitation [58]. These results will however be both gauge- and truncation- dependent and should be seen merely as an illustration of some principal ideas.

Dynamical chiral symmetry breaking is arguably easier to understand and describe theoretically. As was mentioned in connection with Eqs. (2.10) and (2.11), both $SU(N_f)_V$ and $SU(N_f)_{\mathcal{A}}$ symmetries are expected to be realised to a good approximation in the light quark sector. However, while a semblance of $SU(N_f)_V$ is indeed visible in the spectrum of light hadrons, the $SU(N_f)_{\mathcal{A}}$ part seems to be completely absent. In order to clarify this, let us look at the charge associated with $SU(N_f)_{\mathcal{A}}$ symmetry, the generator of flavour non-singlet chiral rotations:

$$Q_f^{\mathcal{A}}(t) = \int d^3x \; \bar{\psi}\gamma^0\gamma_5\mathbf{t}_f\psi \; . \tag{2.30}$$

It is not very hard to see that in the chiral limit $m_u = m_d = m_s = 0$ this operator commutes with the Hamiltonian of QCD. From this we would expect to see chiral parity partners in the hadronic spectrum. If $|\lambda\rangle$ is an eigenstate of $H_{\rm QCD}$ with positive parity, then its negative parity partner $Q_f^{\mathcal{A}}|\lambda\rangle$ should also be an eigenstate with the same mass. Chiral symmetry is explicitly broken due to non-zero quark masses, but since these are small compared to hadronic scales, we still except to see some of its remnants in the spectrum. The pseudoscalar mesons should be approximately degenerate with scalars, vectors with pseudovectors and so on. By looking at the ground state spectrum in Table 2.1 it is quite obvious that this is not realised in Nature (note that η and η' masses are affected by $U(1)_{\mathcal{A}}$ anomaly, see Eq. (2.12) and the paragraph below).

Absence of chiral parity partners and unusually light masses of pseudoscalar mesons are clues that the axial $SU(N_f)$ symmetry is spontaneously broken in strong interactions. Spontaneous symmetry breaking is a phenomenon where the vacuum, due to interactions in the system, does not respect some symmetries of the field theory Lagrangian/Hamiltonian. Ac-

I	S	PS (0^{-+})	S (0^{++})	V (1^{--})	A (1^{+-})	A (1^{++})
1	0	π (0.14)	a_0 (0.98)	ρ (0.78)	b_1 (1.23)	a_1 (1.23)
0	0	η (0.55)	f_0 (0.50)	ω (0.78)	h_1 (1.17)	f_1 (1.28)
0	0	η' (0.96)	f_0' (0.99)	ϕ (1.02)	h_1'(1.39)	f_1' (1.42)
$\frac{1}{2}$	± 1	K (0.50)	K_0^*(0.68)	K^*(0.90)	K_1(1.27)	K_1(1.40)

Table 2.1: Spectrum of $SU(3)_f$ mesons according to their J^{PC}, isospin I and strangeness S [36]. All units are in GeV. Grey entries are not well enough identified or there are multiple candidates. Note that C-parity is only well defined for neutral mesons.

cording to the Goldstone theorem, in the cases of spontaneous symmetry breaking there always arise massless spinless excitations called Nambu-Goldstone bosons [59, 60]. The number of massless bosons grows with the number of Lagrangian symmetries which are broken by the vacuum. In QCD, the strong interaction leads to dynamical mass generation, wherein a large constituent quark mass is created from the tiny (for the light quarks) bare mass. Associated pseudo-Nambu-Goldstone bosons would be the pseudoscalar mesons, thus explaining their extraordinarily small masses (again, they are not exactly massless due to explicit symmetry breaking effects).

While the names 'dynamical mass generation' and 'dynamical chiral symmetry breaking' are sometimes used interchangeably, it should be pointed out that the latter is actually a broader concept: chiral symmetry breaking implies both the generation of large quark mass from the strong interaction, as well as the generation of chirally non-symmetric terms in Greens functions of QCD (e. g. in the quark propagator and the quark-gluon vertex). We shall now present a simple Dyson-Schwinger calculation for the quark propagator which features both 'confinement' of quarks and dynamical mass generation. As stated earlier, our conclusions will be gauge- and model- dependent and cannot be used as a basis for any rigorous arguments. The inverse quark propagator can be decomposed as

$$S^{-1}(p) = i\not{p}A(p^2) + B(p^2) \ , \tag{2.31}$$

where $A(p^2)$ and $B(p^2)$ are respectively called the vector and scalar dressing functions of the inverse propagator. The tree-level form is given by $S_0^{-1}(p) = i\not{p} + Z_m m$, with Z_m being the mass renormalisation constant. The exact Dyson-Schwinger equation for this Greens function is (for its derivation, see section 3.2):

$$S^{-1}(p) = \ Z_2 S_0^{-1}(p) \ + \ g^2 Z_{1f} C_F \int_k \gamma^\mu S(k+p)\Gamma^\nu(k+p,p) D_{\mu\nu}(k) \ . \tag{2.32}$$

$\Gamma^\nu(p,k)$ is the full quark gluon vertex, while the gluon propagator $D_{\mu\nu}(k)$ takes the form given in Eq. (2.25). We use the shorthand notation $\int_k = \int d^4k/(2\pi)^4$ in the above equation and onwards. $C_F = (N_c^2 - 1)/2N_c$ is the colour Casimir operator in the fundamental representation. In QCD, $C_F = 4/3$. The Dyson-Schwinger equations (DSEs) constitute an infinite tower of coupled integral equations and in general they cannot be solved exactly. Approximations need to be made to render the system analytically and numerically tractable.

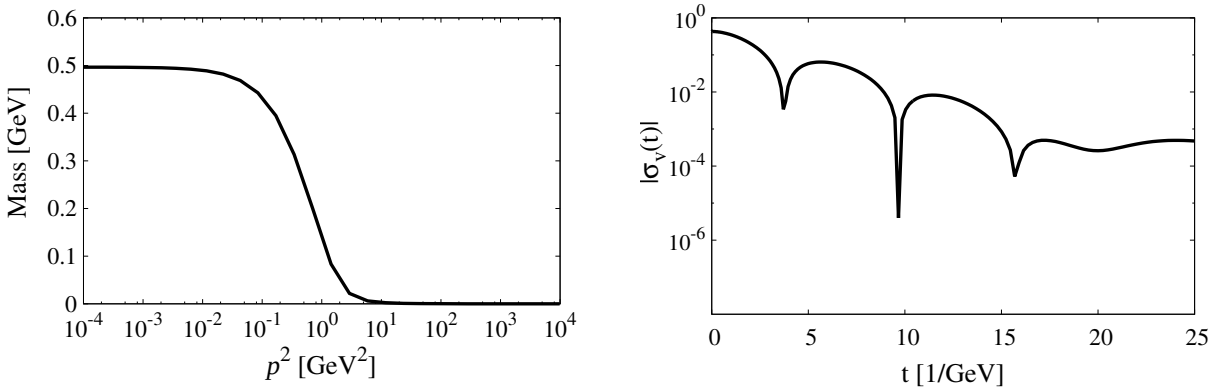

Figure 2.3: Dynamical quark mass (*left*) and the test of the quark propagator positivity violation (*right*).

For our illustrative purposes, a simple 'rainbow' approximation of the quark DSE will suffice, wherein we replace the quark-gluon vertex by its enhanced tree-level form:

$$\Gamma^\mu(p,k) \to \lambda(k^2)\gamma^\mu \ . \tag{2.33}$$

$\lambda(k^2)$ is a model dressing function, and it is usually defined to absorb the gluon propagator dressing as well. This approximation is often employed in connection with bound state studies, where the effective interaction is fitted to some hadronic observables. We will use the setup and fit parameters as given in [61] for the Maris-Tandy interaction. The resulting dynamical quark mass, defined as $M(p^2) = B(p^2)/A(p^2)$ is given in the right panel of Figure 2.3. The large accumulation of mass in the IR is mostly a result of appropriately chosen model dressing $\lambda(k^2)$. Note that within the rainbow approximation it is only the explicit mass term m and the $B(p^2)$ part that break chiral symmetry in Eq. (2.32). Had we set $B(p^2) = 0$ from the beginning, there would have been no solutions of the quark DSE which feature dynamical mass generation. This is an example of our previous remark that dynamical chiral symmetry breaking implies both the large accumulation of quark mass in the IR, as well as a generation of chirally non-symmetric structures in Greens functions of QCD. In the left panel of Fig. 2.3 we show the test of positivity violation for the quark, by plotting the absolute value of the Fourier transform

$$\sigma_V(t) = \int d^3x \int \frac{d^4p}{(2\pi)^4} e^{ip\cdot x}\sigma_V(p^2) \ . \tag{2.34}$$

$\sigma_V(p^2)$ is a vector coefficient function of $S(p)$, expressed in terms of $A(p^2)$ and $B(p^2)$ as $\sigma_V = A/(p^2A^2 + B^2)$. The fact that $\sigma_V(t)$ is positivity violating implies that the quark is a short-lived excitation, and is thus 'confined'. To a great extent, this result is a consequence of the fact that we only employ the tree-level tensor structure of the quark-gluon vertex, see [62] and references therein. However, as we will show in Chapter 6, the main conclusions and ideas presented here are valid also in considerably more elaborate approximation schemes, where the quark-gluon vertex is solved for in a semi-self-consistent manner and all of its tensor structures relevant in Landau gauge are included in the quark DSE. It thus seems that, despite

its simplicity, some of the qualitative statements of the rainbow truncation are more robust than one might initially suspect.

2.4 Other strongly interacting theories

The form of the generating functional of Eq. (2.22) is applicable not only to QCD but also to generic strongly interacting theories, where one can freely vary the number of colours, flavours and the representation of the gauge group to which the matter fields belong. Formally, these manipulations are very easy to do, but they have potentially great influence on the overall properties of the model. An example is provided by the asymptotic freedom of QCD, which is a result of a complex interplay between opposing screening effects of quarks and antiscreening effects of gluons. Parameters like N_f and N_c are directly related to this dynamics, and by changing their values one can arrive at theories whose behaviour is much different from that of QCD. The strong effect which adding a large number of chiral quark flavours can have on the overall properties of the theory can be most easily seen by looking at the one-loop perturbative expression for the beta function (henceforth we label the strong coupling simply as α):

$$\beta(\alpha) = \frac{\alpha^2}{\pi}\left(-\frac{11N_c}{6} + \frac{N_f}{3}\right) . \tag{2.35}$$

The beta function is defined as $\beta = d\alpha(t)/dt$, with $t = \ln(\mu)$. From its definition it is clear that β determines the scale evolution of the running coupling. In QCD the sign of β in the above expression is negative, and this is what brings about the asymptotic freedom. However, if the number of light quarks were to increase to around 16 the asymptotic freedom would be lost and the theory would enter the so-called Coulomb phase, behaving similar to quantum electrodynamics (QED). While the quantitative predicitions of Eq. (2.35) should be taken with some reserve due to the perturbative origin of the result, it is almost beyond doubt that the overall qualitative statement is correct, and that strongly-interacting models with a large number of fermions indeed behave like QED. What makes these considerations more intereseting is the possibility that there exists an intermediate phase, where the number of light quarks is greater than in QCD but still not big enough to entail the loss of asymptotic freedom. For certain values of N_f such models could still behave like QCD in the highy energy region, but in the infrared they would not feature dynamical chiral symmetry breaking and bound state formation [63–65].

Studies of strongly interacting theories which are close to the infrared conformal phase are important both from a phenomenological and a fundamental perspective. On the phenomenological side, they are helpful with resolving some problems faced by the models of dynamical electroweak symmetry breaking, see section 4.3. From a fundamental point of view, the vertex functions of nearly conformal (or 'walking') theories are expected to be considerably different from what is seen in QCD, and in the upcoming sections we will point to a few results which support this idea. Exploring how the walking dynamics influences the principal building blocks should aid in our understanding of strongly interacting theories in general. This is an important remark which holds independently of any other applications of these models. Apart from being interesting in themselves, these investigations might also pave the path for studies of more challenging phase transitions, like the properties of strongly interacting matter at relatively high densities.

The vertex functions which are expected to be particularly affected by the (near) conformal phase transition are those which have certain components generated by the dynamical chiral symmetry breaking, like the quark propagator and the quark-gluon vertex. In this thesis we will however not tackle these interesting questions, instead dealing exclusively with QCD and QCD-like models. This is mainly because of the many technical problems which arise when one attempts to include the back-reaction of quarks onto other Greens functions in a Dyson-Schwinger framework, or any other functional approach. Since we do not consider the effects of fermion loops, most of our techniques cannot be directly applied to arbitrary asympotically free theories. We do however believe that we have laid down some ground work in this regard, and that it will not be too hard to modify some of our methods so as to include the matter sector in a dynamical way. In section 3.3 we will argue that even our approach to bound states, which relies heavily on chiral symmetry and its breaking, can be applied to walking or even exactly conformal scenarios, as long as the proper input from the Yang-Mills sector is provided.

Chapter 3

Dyson-Schwinger and Bethe-Salpeter formalism

3.1 General considerations

In quantum field theories, an n-point Greens function encodes the interaction of n 'particles'. In the functional formalism, these objects are given by the following expression [33]:

$$G(x_1 \dots x_n) = \frac{\int \mathcal{D}\varphi e^{iS[\varphi]} \varphi(x_1) \dots \varphi(x_n)}{\int \mathcal{D}\varphi e^{iS[\varphi]}}, \quad \mathcal{D}\varphi = \prod_{i=1} d\varphi(x_i) \ , \tag{3.1}$$

$S[\varphi]$ is the action and $\varphi(x)$ generically denotes various fields of the theory. The Dirac and Lorentz structure is left implicit. In the case of bosons, the fields φ are ordinary commuting numbers, whereas fermions are represented by Grassmann variables. In Minkowski spacetime, boundary conditions need to be imposed carefully in order for integrals of Eq. (3.1) to make sense. In our calculations we make these matters simpler by Wick-rotating to the Euclidean spacetime, see section A.1 for the corresponding conventions. However, in this and the next section we will still adhere to the Minkwoski metric. An efficient way of obtaining vertices and their equations of motion starts by defining the generating functional

$$Z = \int \mathcal{D}\varphi e^{i\left(S[\varphi] - \int_x \varphi(x) J(x)\right)} \ . \tag{3.2}$$

The source terms $J(x)$ are there to facilitate the derivation of Greens functions, which result from functional differentiation of Z:

$$G(x_1 \dots x_n) = \frac{i^n \delta^n}{\delta J(x_1) \dots \delta J(x_n)} \frac{Z[J]}{Z[0]}\Big|_{J=0} \ . \tag{3.3}$$

We have indicated in the above equation that the sources are to be set to zero at the end. Eqs. (3.1) and (3.3) can be straightforwardly generalised to the case of polynomial functions of fields at different spacetime points:

$$\langle f(\varphi) \rangle = \frac{\int \mathcal{D}\varphi e^{iS[\varphi]} f(\varphi)}{\int \mathcal{D}\varphi e^{iS[\varphi]}} = f\left(\frac{\delta}{\delta J}\right) \frac{Z[J]}{Z[0]}\Big|_{J=0} \ . \tag{3.4}$$

For some of the upcoming calculations it will prove useful to work with non-vanishing sources in the intermediate steps. We therefore also define a version of Eq. (3.4) in the presence of source terms:

$$\langle f(\varphi)\rangle_J = \frac{\int \mathcal{D}\varphi e^{i\left(S[\varphi]-\int_x \varphi(x)J(x)\right)} f(\varphi)}{\int \mathcal{D}\varphi e^{i\left(S[\varphi]-\int_x \varphi(x)J(x)\right)}} = \frac{1}{Z[J]} f\left(\frac{\delta}{\delta J}\right) Z[J] \ . \tag{3.5}$$

For any polynomial function f the following identity can be proven relatively easily with mathematical induction: $f(\partial_x)e^{W(x)} = e^{W(x)}f(\partial_x + \partial_x W)$. The expression is understood to act on some test function on the right. By defining $Z[J] = e^{iW[J]}$ and exploiting this relation we can reformulate Eq. (3.5) as

$$\langle f(\varphi)\rangle_J = f\left(-\frac{\delta W[J]}{\delta J} + \frac{i\delta}{\delta J}\right) \ . \tag{3.6}$$

$Z[J]$ is the generating functional of all Greens functions, but it is not necessary to use every piece of information contained within this object. In practice it is often convenient to restrict ones attention to a subset of all possible vertices. One such restriction is offered by the generating functional $W[J] = -i \ln Z[J]$ introduced above. In a diagrammatic language, $W[J]$ generates the connected Greens functions, where all the external spacetime points x_i of the function are connected to each other by propagators and interaction vertices (for a particularly elegant proof of this, see [66]). It is these vertex functions that enter the S-matrix elements and are thus interesting for physical applications. It is possible to go even further in constraining the available information by defining the following Legendre transform of $W[J]$:

$$\Gamma[\tilde{\varphi}] = W[J] + \int_x \tilde{\varphi}(x)J(x) \ . \tag{3.7}$$

$\tilde{\varphi}(x)$ is the quantum averaged field in the presence of sources:

$$\tilde{\varphi}(x) := -\frac{\delta W}{\delta J(x)} = \frac{i}{Z[J]}\frac{\delta Z[J]}{\delta J(x)} = \langle \varphi \rangle_J \ . \tag{3.8}$$

$\Gamma[\tilde{\varphi}]$ is the generating functional of one-particle-irreducible (1PI) vertices, meaning that it generates the connected Greens functions which cannot be broken into disjointed pieces by removing a single propagator line [66]. 1PI vertex functions are often also called proper vertices. Henceforth we will exclusively be working with proper Greens functions and their equations of motion. We will employ the following shorthand notation for functional derivatives of Γ and W:

$$\Gamma''_{xy}[\tilde{\varphi}] = \frac{\delta^2\Gamma[\tilde{\varphi}]}{\delta\tilde{\varphi}(x)\delta\tilde{\varphi}(y)}, \quad W''_{xy}[J] = \frac{\delta^2 W[J]}{\delta J(x)J(y)} \ . \tag{3.9}$$

From definitions in Eqs. (3.7) and (3.8) one can see that variables $\tilde{\varphi}(x)$ and $J(x)$ are conjugated to each other:

$$W'_x[J] = -\tilde{\varphi}(x), \quad \Gamma'_x[\tilde{\varphi}] = J(x) \ . \tag{3.10}$$

It immediately follows that the two-point function $\Gamma''_{xy}[0]$ is the inverse of the propagator $W''_{xy}[0]$:

$$\int_y W''_{xy}[J]\Gamma''[\tilde{\varphi}]_{yz} = -\int_y \frac{\delta\tilde{\varphi}(x)}{\delta J(y)}\frac{\delta J(y)}{\delta\tilde{\varphi}(z)} = -\frac{\delta\tilde{\varphi}(x)}{\delta\tilde{\varphi}(z)} = -\delta^4(x-z)\ . \tag{3.11}$$

Likewise, the derivative $\Gamma'''_{xyz}[0]$ represents a three-point function, $\Gamma''''_{xyzw}[0]$ a four-point one and so on. The two-point function in the presence of sources is of somewhat special importance and we denote it by $\Gamma''_{xy}[\tilde{\varphi}]^{-1} = \Delta_{xy}[\tilde{\varphi}]$. By using the relation

$$\frac{\delta}{\delta J(x)} = \int_y \frac{\delta\tilde{\varphi}(y)}{\delta J(x)}\frac{\delta}{\delta\tilde{\varphi}(y)} = \int_y \Delta_{xy}[\tilde{\varphi}]\frac{\delta}{\delta\tilde{\varphi}(y)}\ , \tag{3.12}$$

we can rewrite Eq. (3.6) in terms of the 1PI generating functional and its derivatives:

$$\langle f(\varphi)\rangle_J = f\left(\tilde{\varphi}(x) + \int_y \Delta_{xy}[\tilde{\varphi}]\frac{\delta}{\delta\tilde{\varphi}(y)}\right)\ . \tag{3.13}$$

We have arrived at one of the master equations for obtaining relations among proper vertex functions. If there is more than one field present in the theory then the superindex y in the above equation is understood to stand both for an integration variable and a summation index for various types of fields (i. e. all possible 'mixed propagators' $\Delta_{xy}[\tilde{\varphi}]$ should be summed over). In the next section we shall use this relation to set up the formalism of Dyson-Schwinger equations (DSEs) and apply them to QCD.

3.2 DSEs for proper vertices

Dyson-Schwinger equations for Greens functions follow from the invariance of the path-integral under the field translations $\varphi(x) \to \varphi'(x) = \varphi(x) + \epsilon(x)$: since this amounts to a mere relabeling of variables and all field configurations are integrated over, the generating functional should stay the same. By assuming that the integral measure $\mathcal{D}\varphi$ also does not change, we arrive at a condition $Z'[J] = Z[J]$. For infinitesimal field variations this translates into:

$$\begin{aligned} Z'[J] = &\int \mathcal{D}\varphi' e^{i\left(S[\varphi'] - \int_x \varphi'(x)J(x)\right)} = \\ &\int \mathcal{D}\varphi e^{i\left(S[\varphi] - \int_x \varphi(x)J(x)\right) + i\int_x \epsilon(x)\left(\frac{\delta S[\varphi]}{\delta\varphi(x)} - J(x)\right)} = \\ &Z[J]\left\langle e^{i\int_x \epsilon(x)\left(\frac{\delta S[\varphi]}{\delta\varphi(x)} - J(x)\right)}\right\rangle := Z[J]\ . \end{aligned} \tag{3.14}$$

From the last equality we gain the master Dyson-Schwinger equation:

$$\left\langle \frac{\delta S[\varphi]}{\delta\varphi}\right\rangle_J = J\ . \tag{3.15}$$

We immediately recast the above expression in the language of 1PI vertices by employing Eqs. (3.10) and (3.13):

$$\Gamma'_x[\tilde{\varphi}] = \frac{\delta S[\varphi]}{\delta \varphi} \left(\tilde{\varphi}(x) + \int_y \Delta_{xy}[\tilde{\varphi}] \frac{\delta}{\delta \tilde{\varphi}(y)} \right) \ . \tag{3.16}$$

One can see from this relation why is the generating functional of proper vertex functions $\Gamma[\tilde{\varphi}]$ also referred to as the quantum effective action. The y integral in Eq. (3.16) accounts for quantum loop corrections to the classical equations of motion: in its absence, the $\tilde{\varphi}$ dependence of $\Gamma'_x[\tilde{\varphi}]$ would be exactly the same as the φ dependence of $S'_x[\varphi]$. By differentiating the above master equation $n-1$ times with respect to the various fields $\tilde{\varphi}$ and setting all sources to zero at the end, one obtains the Dyson-Schwinger equation for the n-point function $\Gamma^{(n)}_{x_1 \ldots x_n}[0]$. Thus one arrives at an infinite tower of coupled non-linear integral equations for vertices of the theory. In practical computations, one usually needs to employ truncations to 'collapse' this tower and end up with a finite closed set of equations. To illustrate these points we will now derive one of the simplest DSEs in QCD, that of the quark propagator. The relevant part of the action is

$$S = \bar{\psi} \left(-\not{\partial} + m \right) \psi + ig \ \bar{\psi} \not{A} \psi \quad \longrightarrow \quad \frac{\delta S}{\delta \bar{\psi}} = \left(-\not{\partial} + m \right) \psi + ig \ \not{A} \psi \ . \tag{3.17}$$

According to Eq. (3.16) the corresponding derivative of quantum effective action is (we drop the 'tilde' notation for fields in the presence of sources)

$$\frac{\delta \Gamma}{\delta \bar{\psi}(x)} = (-\not{\partial} + m)\psi(x) + ig \ \not{A}(x)\psi(x) + ig \ \gamma^\mu \Delta_{\psi A^\mu}(x,x) \ . \tag{3.18}$$

To gain the DSE for the inverse quark propagator, we differentiate the above equation with respect to $\psi(y)$, using the product rule

$$\frac{\delta}{\delta \varphi(z)} \Delta_{xy}[\varphi] = \Delta_{xa}[\varphi] \Gamma'''_{azb}[\varphi] \Delta_{by}[\varphi], \tag{3.19}$$

and setting all sources to zero at the end (this entails the loss of $ig\not{A}$ term):

$$\Delta^{-1}_{\psi\bar{\psi}}(x,y) = (-\not{\partial} + m)\delta^4(x-y) + ig \int_z \int_w \gamma^\mu \Delta_{\psi\bar{\psi}}(x,z) \Gamma'''_{\bar{\psi}\psi A^\nu}(z,y,w) \Delta_{A^\nu A^\mu}(w,z) \ . \tag{3.20}$$

$\Gamma'''_{\bar{\psi}\psi A^\nu}$ and $\Delta_{A^\nu A^\mu}$ are respectively the full quark-gluon vertex and gluon propagator. By performing the Fourier transformation of the above equation and taking into account the renormalisation and other numerical factors, one finally arrives at Eq. (2.32). The diagrammatical representation of quark DSE is given in Figure 3.1. Further differentiation of $\Gamma''_{\bar{\psi}\psi}$ with respect to the gluon field yields the DSE for the quark-gluon vertex and so on. Since the derivation of equations of motion for three- and higher- point functions is considerably more involved, we will leave them out of this thesis. A convenient automated way of obtaining the functinal relations for vertices is offered by the *CrazyDSE* and *DoFun* packages, see [67, 68].

It should be pointed out that DSEs offer merely one out of many ways to study Greens functions in the functional framework. Popular alternative methods include functional renormalisation group (FRG) [69], nPI formalisms [70], and others. Differences between these various approaches mostly come from the way in which the resummation of diagrams is performed,

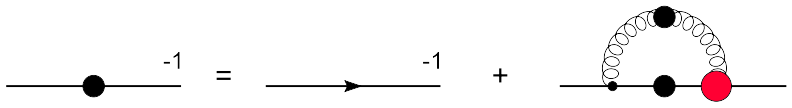

Figure 3.1: The quark propagator Dyson-Schwinger equation.

and each method has its advantages and drawbacks. In the context of this thesis, the DSE framework is convenient because it can be straightforwardly connected to the bound state calculations in a way which preserves relevant symmetries. Such a connection would be much harder to make with any of the other functional techniques (see however [71–73] for some of the advancements in the FRG bound state studies). We will further elaborate on this issue in the next section.

Note that the arguments very similar to the ones which lead us to equation (3.15) can be employed to obtain other useful relations among vertex functions. For instance, the generating functional should be invariant under gauge rotations, as they too represent nothing more than relabeling of fields. By using the gauge symmetry of the classical action and manipulations akin to those of Eq. (3.14), it is quite straightforward to derive the following relation

$$\langle \delta S_{\mathrm{GF}} + \delta S_{\mathrm{C}} \rangle_J = 0 \ . \tag{3.21}$$

This is the general form of a Ward-Takahashi identity (WTI). These identities connect various n-point Greens functions to each other and can be used for modelling purposes, or to reduce the total number of renormalisation conditions needed to render the theory finite. For non-Abelian gauge groups it is more efficient to use the BRST symmetry instead. In that case S_{GF} in the above expression vanishes as well, but the field variations inside δS_{C} are non-linear functions of fields themselves, see equation (2.26). This results in the Slavnov-Taylor identities. Along similar lines one can derive the symmetry relations associated with axial (chiral) rotations. One of these, the axial-vector Ward-Takahashi identity, plays a special role in the DSE/BSE treatment of bound states, as we demonstrate in the next section. The identity is derived in section D.1.

3.3 The Bethe-Salpeter equation

Derivation of n-body bound state equations(s) relies on a general field theory principle that these bound states should appear as poles in the corresponding $2n$-point Greens functions. In this thesis we are particularly interested in bound states of 2 valence particles, and we immediatelly specialise to this case in the following discussion. The method which we outline here can be easily generalised to composite states made out of an arbitrary number of constituents. We begin by considering the Dyson equation for a four-point function G:

$$G = S_1 S_2 + S_1 S_2 K_{12} G, \tag{3.22}$$

with S_1 and S_2 being the propagators of the two particles, and K_{12} is the interaction kernel. In principle, K encodes infinitely many ways in which the two constituents can interact. Now let us denote the total momentum as P, and the mass of some particular bound state $\langle \eta |$ as M_η. With these labels, the energy-momentum condition for the bound state formation is, in

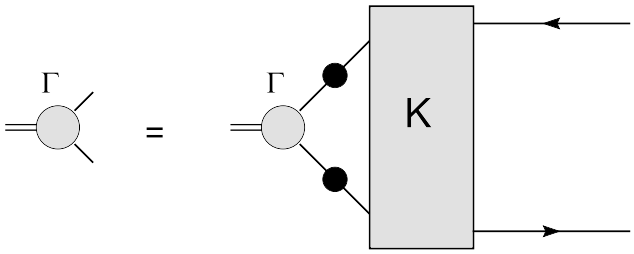

Figure 3.2: The homogeneous meson Bethe-Salpeter equation.

Euclidean spacetime, $P^2 = -M_\eta^2$. Exactly at this pole we introduce the following *ansätze* for the four-point function:

$$G \approx \mathcal{N}_\eta \frac{\Gamma_\eta \overline{\Gamma}_\eta}{P^2 + M_\eta^2} \ . \tag{3.23}$$

Γ_η is the bound state amplitude and $\overline{\Gamma}_\eta$ its charge conjugated version. $\mathcal{N}_\eta$ is the state-dependent normalisation factor. By combining Eqs. (3.22) and (3.23) and comparing the pole residues at both sides of the resulting expression, one arrives at a homogeneous Bethe-Salpeter equation (BSE) for the amplitude Γ_η:

$$\Gamma_\eta = S_1 S_2 K_{12} \Gamma_\eta \ . \tag{3.24}$$

If we now consider mesons as two-body bound states of QCD, and explicitly write all the momentum variables, the BSE takes the form (we drop the label η):

$$\Gamma\left(P,p\right) = \int_k S\left(k_-\right) \Gamma\left(P,k\right) S\left(k_+\right) K\left(P,p,k\right) \ . \tag{3.25}$$

In the above expression $S(k_\pm)$ are the quark propagators, k and p the relative momenta among them, and $k_\pm = k \pm P/2$. Diagrammatic representation of the meson BSE is given in Figure 3.2. Since we wish to give some examples of its application already in this section, we will comment on how are the solutions of Eq. (3.25) obtained. An apparent obstacle in solving the homogeneous BSE is the fact that it is defined only for those total meson momenta for which the pole condition $P^2 = -M^2$ holds. As we do not know in advance the meson masses, we cannot formulate the BSE at the correct P values. A way to circumvent this problem is to introduce the auxiliary continuous eigenvalue $\lambda(P^2)$. In a succinct notation, we are then solving the equation:

$$\Gamma_i = \lambda\left(P^2\right) M_{ij} \Gamma_j \ . \tag{3.26}$$

Indices i, j denote the components of the meson amplitude and M_{ij} symbolically stands for the entire rotation operation of Eq. (3.25). By solving this equation at various values of P^2 we can locate the solutions for which $\lambda\left(P^2\right) = 1$: these then correspond to the actual BSE. Since we are dealing with a homogeneous equation, the amplitude Γ needs to be normalised somehow: in terms of the eigenvalue λ, a proper normalisation condition is [74, 75]:

$$\left(\frac{d\lambda}{dP^2}\right) = 3 \ \mathrm{tr} \int_k \overline{\Gamma}(k,-P) S(k_+) \Gamma(k,P) S(k_-) \ . \tag{3.27}$$

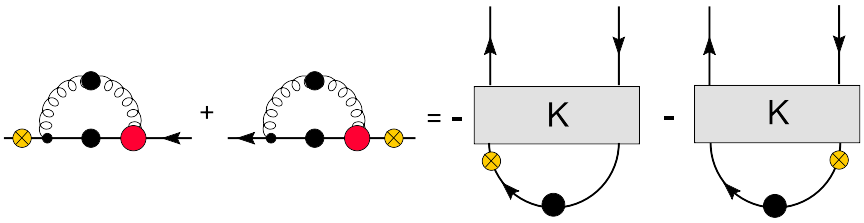

Figure 3.3: The axial-vector Ward-Takahashi identity for flavour non-singlet mesons. Yellow blob denotes the insertion of a γ_5 matrix.

An alternative way to study hadronic observables is to consider the inhomogeneous, or vertex, Bethe-Salpeter equation:

$$\Gamma\left(P,p\right) = \Gamma_0\left(P,p\right) + \int_k S\left(k_-\right)\Gamma\left(P,k\right)S\left(k_+\right)K\left(P,p,k\right) \ . \tag{3.28}$$

The inhomogeneous term Γ_0 carries the appropriate J^{PC} quantum numbers of the meson under investigation. Bound state solutions of the above expression are found by looking for poles in any of the vertex dressing functions $\Gamma_i\left(P^2\right)$, or alternatively searching for zero crossings of the inverses $1/\Gamma_i\left(P^2\right)$. Either of the equations (3.25) and (3.28) can be used for bound state studies, and the choice between the two is a matter of preference. We will employ both methods in our calculations, but in Chapter 6 we ultimately settle for the vertex approach since it is much better suited for extrapolations, see section 6.3. We also note that in Euclidean spacetime the pole condition $P^2 = -M^2$ entails working with the complex-valued total momentum. Some of the techniques of dealing with the BSE (and the closely related quark DSE) in the complex plane are given in section C.1.

We wish to make some remarks concerning the interaction kernel K itself. As noted earlier, this object subsumes an infinity of interactions among constituent particles, and any practical consideration of the Bethe-Salpeter equation requires the kernel to be truncated. Since we are mostly interested in bound states of light quarks, an important guiding principle when making these approximations is offered by chiral symmetry and its dynamical breaking. We wish for our theory to be 'aware' that the light pseudoscalar mesons are both quark-antiquark bound states, as well as (pseudo) Goldstone bosons associated with dynamical chiral symmetry breaking. This can be accomplished if the truncations do not break the axial-vector Ward-Takahashi identity (axWTI), given in a diagrammatic form in Figure 3.3 for flavour non-singlet mesons. In a flavour singlet case, there is an additional contribution due to the axial anomaly.

As Figure 3.3 suggests, the axWTI imposes a tight connection between the Bethe-Salpeter kernel and the quark propagator self-energy. Thus any truncation of the quark DSE severely constrains the possible form of the meson BSE. Depending on the employed approximations, this construction scheme is not always easy to implement, but at least in principle it enables one to include systematic improvements without breaking the relevant symmetries. This is one of the reasons why the combined DSE/BSE approach is so convenient for bound state studies. To the best of our knowledge, a similar principle has not yet been employed in any of the other functional frameworks. We shall now illustrate some of these points by considering the simplest possible truncation scheme that preserves the axWTI, the so-called rainbow-ladder approach.

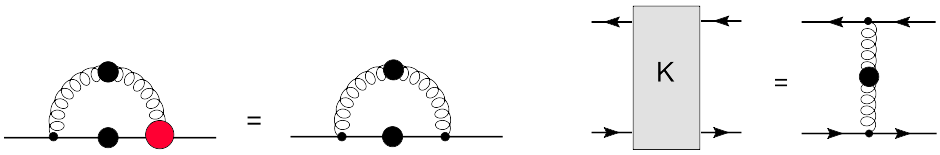

Figure 3.4: The rainbow approximation of quark DSE (*left*) and the corresponding axWTI-preserving ladder truncation of meson BSE (*right*).

Let us start by writing the quark propagator DSE of Eq. (3.20) in a symbolic notation

$$S^{-1}(x,y) = S_0^{-1}(x,y) + \Sigma(x,y) \ , \tag{3.29}$$

with $\Sigma(x,y)$ being the quark self-energy. For a generic approximation of the above equation, the axWTI-preserving Bethe-Salpeter kernel can be obtained by applying the following functional derivative :

$$K(x,y,x',y') = -\frac{\delta\Sigma(x,y)}{\delta S(x',y')} \ . \tag{3.30}$$

For a 'proof' of this statement see section D.2. In a diagrammatic language the operation of Eq. (3.30) corresponds to the cutting of internal quark lines in the quark self-energy. From this it should not be too hard to see that to the rainbow truncation of quark DSE, shown in Eq. (2.33) and in the left panel of Figure 3.4, there corresponds a ladder truncation of the meson BSE, shown in the right panel of Fig. 3.4.

As noted in section 2.3, in the rainbow-ladder approach the dressings of the gluon propagator and the quark-gluon vertex are usually combined into an effective model interaction which is fitted to some hadronic observables. When working light quarks/hadrons, one usually uses pion mass and decay constant to set the parameters of the model. In the DSE/BSE framework, the pion decay constant can be calculated as [76]:

$$f_\pi = \frac{Z_2 N_c}{\sqrt{2}P^2}\mathrm{tr}\int_k S(k_+)\Gamma_\pi(k,P)S(k_-)\gamma_5 \not{P} \ . \tag{3.31}$$

In the above relation we employ the conventions for which $f_\pi = 93$ MeV in QCD. With a careful choice of model dressing functions and corresponding parameters, the rainbow-ladder (RL) approach has been applied extensively and relatively successfully to QCD hadron phenomenology [14–18, 61, 76–84]. We provide an example on how RL works in Table 3.1. The results shown there were obtained with the fit parameters for the Maris-Tandy effective coupling used in [61]. Since the m_π and f_π were employed for model fitting, it is not surprising that they come out correctly. A more surprising result is that the m_ρ and f_ρ also turn up in a very nice agreement with experiments. It is not yet fully understood why the RL truncation seems to offer a good description of the light vector meson. A possible explanation is that there is a strong connection between dynamical chiral symmetry breaking and the hyperfine splitting for orbital ground states (in the language of non-relativistic quark models, pseudoscalar mesons correspond to $S = 0$ states and the vectors to $S = 1$).

	f_π	m_π	f_ρ	m_ρ	m_σ	m_{b1}
RL result	93	140	151	743	635	907
Experiment	93	138	156	776	400-550	1230

Table 3.1: RL results for light mesons compared to experimental values. All units are in MeV. We used the fit parameters for the Maris-Tandy interaction as shown in [61].

From Table 3.1 one can also see that in certain meson channels some of the inadequacies of the rainbow-ladder treatment start to show up. In the scalar and axial-vector channels the interaction is respectively too repulsive and too attractive. It should be pointed out that the bad results for the σ meson might not entirely due to the RL tratement, as the interpretation of ground state scalars as $q\bar{q}$ states might be wrong, see e. g. [85–87] for alternative explanations. Even with this in mind, the fact remains that the RL does not provide a satisfactory description for all mesonic bound states: see [81] for additional comments on the performance of the RL method for various J^{PC} quantum numbers. It would be very hard, if not impossible, to account for the shortcomings of the rainbow-ladder by simply adjusting the model dressing functions. The prime reason is that the framework has very little flexibility because of its limited interaction structure ($\gamma^\mu \times \gamma^\nu$), which offers no variation in the projected strength across different bound state channels. This can only be remedied if additional tensor structures of the quark-gluon vertex are included in the calculation.

An additional drawback of the RL approach is that it is not easy to translate it to other strongly interacting theories, especially to those which have potentially very different dynamics in comparison to QCD. The concept of constructing effective interactions to reproduce hadronic observables of QCD entails the loss of a connection to the underlying gauge sector. If the ghost and gluon propagators undergo significant changes due to a different colour/flavour content of the theory (see e. g. [88, 89]), it would be very hard to mimic these effects reasonably well in the RL method. These arguments should make it clear that the investigations of generic non-Abelian gauge theories, as well as more 'serious' studies of QCD itself, demand more elaborate beyond rainbow-ladder (BRL) techniques. One such method is presented and applied to the study of an $SU(2)$ gauge theory with 2 fundamental Dirac fermions in Chapter 6.

We wish to remark on the possibility to use the described bound state formalism in walking scenarios, or even exactly conformal ones (in the conformal phase all hadron masses and decay constants are equal to zero, but one can still meaningfully study the ratios like M_σ/f_π). In the absence of dynamical chiral symmetry breaking the pion does not have the special status of the Goldstone boson, and it seems pointless to use a truncation scheme which centers on the axWTI. The fact is however that the procedure which we outlined would remain exactly the same. The cutting method used to obtain the interaction kernel K from a propagator self-energy guarantees a consistent truncation for Dyson-Schwinger and Bethe-Salpeter equations, as long as they are both derived from the same effective action, see [90] and references therein. Any global symmetries of the effective action will not be broken by these DSE/BSE approximations, and for this reason the approach is often used even for systems which have nothing to do with chiral properties, for instance in the studies of glueballs [91].

The one thing which could introduce a potentially big difference to the formalism presented here would be the fact that for nearly and exactly conformal theories one has to explicitly consider the effects of quarks on the Yang-Mills propagators. Apart from complicating the

ghost/gluon equations themselves, this would also mean that the fermionic loops would show up in the quark self-energy, thus producing additional contributions in the bound state equation according to the cutting technique. Such additional terms in the BSE would vanish in the isovector meson channels. Even if isoscalars need to be explicitly considered (e. g. in Technicolor the isoscalar scalar meson is quite important), the complication of the BSE itself is actually a minor issue compared to the unquenching of the ghost/gluon sector. The first and foremost problem for these kinds of investigations is to reliably solve the coupled system of DSEs for the quark, the Yang-Mills propagators, and the quark-gluon vertex.

Chapter 4

Technicolor theories

4.1 Standard Model Higgs sector and the hierarchy problem

Weak interaction, which governs the radioactive decays of atomic nuclei, is very short-ranged: distance scales where it has any appreciable influence are on the order of 10^{-17} m. This and other features of the weak force could be understood naturally if the particles which mediate it were very massive. The problem is that the force-mediating bosons cannot be 'given a mass' in a naive way. Theories which allow explicit mass terms for particles that mediate the interaction have issues with violations of unitarity and non-renormalisability, the same ones which plague the models with contact four-fermion interactions [92]. A way to resolve this issue is offered by the Higgs mechanism, which was developed my numerous authors in the 1960s [3–6, 93–95]. The mechanism hinges on the idea that gauge bosons (the force carriers) can be bestowed with a mass in a way which is consistent with gauge invariance: the gauge degrees of freedom can then be used to eliminate the non-renormalisable terms. This can can be easily illustrated as follows. At arbitrary order of perturbation theory, the gauge boson propagator is given by the following expression (we made the choice of gauge $\xi = 1$, which does not affect the argument):

$$D_{\mu\nu}(k) = \frac{\delta_{\mu\nu}}{k^2(1 + \Pi_\gamma(k^2))} \ . \tag{4.1}$$

$\Pi_\gamma(k^2)$ is related to the one-particle-irreducible gauge boson self-energy $\Pi_{\mu\nu}(k^2)$ by

$$\Pi_{\mu\nu}(k^2) = (k^2\delta_{\mu\nu} - k_\mu k_\nu)\Pi_\gamma(k^2) \ . \tag{4.2}$$

Equation (4.2) depicts the transversality property of $\Pi_{\mu\nu}(k^2)$ which arrises from current conservation. Now let us assume that $\Pi_\gamma(k^2)$, and hence also $\Pi_{\mu\nu}(k^2)$, has a contribution of the form A^2/k^2, with $A^2 > 0$. Then the propagator of Eq. (4.1) would become

$$D_{\mu\nu}(k) = \frac{\delta_{\mu\nu}}{k^2 + A^2} \ . \tag{4.3}$$

The above expression corresponds to the propagator of a massive particle. The contribution proportional to A^2/k^2 in the self-energy arises from an exchange of a single massless particle and is illustrated in Figure 4.1. Since $\Pi_\gamma(k^2)$ and $\Pi_{\mu\nu}(k^2)$ are 1PI, this particle cannot be the gauge boson itself. The problem can be easily remedied if the theory contains other massless

excitations which couple to gauge bosons. As already mentioned in section 2.3, massless Goldstone bosons always accompany the phenomenon of spontaneous symmetry breaking. If a global symmetry corresponding to gauge invariance is spontaneously broken,[1] Goldstone and gauge bosons will interact, leading to self-energy contributions depicted in Figure 4.1. Formal summation of an infinity of such diagrams gives the expression for the propagator of a massive gauge particle [98]:

$$D_{\mu\nu}(k) = \left[\delta_{\mu\nu} + \frac{(1-\xi)k_\mu k_\nu}{k^2 - \xi M^2}\right](k^2 - M^2)^{-1} \ . \tag{4.4}$$

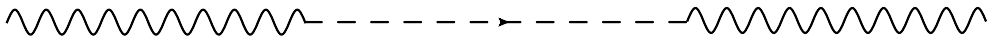

Figure 4.1: Contribution to a gauge boson self-energy from an exchange of a single massless particle.

Choice $\xi = 1$ in the above expression gives the propagator of Eq. (4.3). Despite the gauge boson now being massive, the constraints which follow from gauge invariance, like the one shown in Eq. (4.2), still hold. This fact is of crucial importance for the renormalisability of the theory. For an explicit proof that theories with the gauge boson of Eq. (4.4) are indeed manifestly renormalisable (for any finite choice of ξ), look up [98]. The Higgs mechanism thus provides a way to obtain theories with massive intermediate vector bosons which behave well at high energies.

It is important to note that, while the Goldstone fields are an essential part of this formalism, they do not appear in the physical spectrum of particles, in accordance with experiments. The Goldstone fields represent unphysical degrees of freedom and one can gauge them away by using the choice $\xi \to \infty$. In this so-called unitary gauge one directly works with physical states, the longitudinal polarisations for gauge bosons. While it is not useful for loop calculations (leading to issues with non-renormalisability), unitarity gauge is usually employed for tree-level arguments, as it makes matters relatively simple. We shall use this choice to sketch how is the Higgs mechanism implemented in the Standard Model (SM), keeping everything at zero-loop order. SM Higgs potential is given by

$$\mathcal{L}_{Higgs} = (D_\mu H)^\dagger (D^\mu H) + \mu^2 H^\dagger H - \frac{\lambda}{4}(H^\dagger H)^2 \ . \tag{4.5}$$

Here H is a Higgs field, which is an $SU(2)$ doublet:

$$H = \begin{pmatrix} \pi_2 + i\pi_1 \\ \sigma - i\pi_3 \end{pmatrix}. \tag{4.6}$$

$\mu^2 > 0$ is a Higgs 'mass' (note the wrong sign) and D_μ is a $SU(2)_L \times U(1)_Y$ covariant derivative, with Y being the weak hypercharge.

[1] Despite the common terminology, there is no 'gauge symmetry breaking' in the Higgs mechanism. The Higgs method requires the (local) gauge symmetry to be *explicitly* broken, with additional subtle points related to the actual ground state of the theory. It is more correct to say that the mechanism relies on the non-zero vacuum expectation vale for the Higgs field, see [96, 97].

Electroweak symmetry (EW) breaking is caused by the vacuum expectation value for the Higgs field:

$$\langle H \rangle = \begin{pmatrix} 0 \\ v/\sqrt{2} \end{pmatrix} . \tag{4.7}$$

The electroweak scale is set by putting $v = 246$ GeV. This value follows from comparing predictions of EW theory with experiment: so far, no theory has been able to derive it from first principles. The electroweak group $SU(2)_L \times U(1)_Y$ has 4 generators, while the choice of Eq. (4.7) breaks 3 symmetries, with the pattern

$$SU(2)_L \times U(1)_Y \to U(1)_Q \ . \tag{4.8}$$

$U(1)_Q$ is a gauge symmetry of electromagnetic interaction, where $Q = I_3 + Y/2$ is the electric charge and I_3 the third component of weak isospin. This pattern produces 3 Goldstone particles which become the longitudinal degrees of freedom for the $W^{\pm}$ and Z^0 bosons, the mediators of the weak interaction. Since the symmetry $U(1)_Q$ of electrodynamics is left unbroken, the photon does not acquire a mass. Additionaly, there is one massive scalar excitation left in the spectrum, the remnant of 4 degrees of freedom of Eq. (4.6). It is this scalar particle that is called the 'Higgs boson' and which was apparently discovered at CERN in 2012 [99, 100]. For now, the measurements of its properties seem to be in excelent agreement with Standard Model predictions.

It is hard to argue against the fact that the Higgs mechanism provides a convenient and economical way to break the electroweak symmetry. However, as it stands, it has some undesirable features. Firstly, the Higgs potential does not have a dynamical origin: it does not follow from a gauge principle, nor does it arise as an effective description of some deeper dynamical mechanism. The potential of Eq. (4.5) (including the crucial sign for the Higgs mass term) is simply put in by hand into the Standard Model to produce the desired pattern of EW symmetry breaking. A more fundamental model which does the same job as the Higgs field would be highly welcome. The second problem has to do with the 'naturalness' of the Higgs sector. In a generic field theory which includes scalar particles, the mass of the scalar receives radiative corrections which are quadratically divergent:

$$m_{ren}^2 = m_0^2 \Big(1 + f_1(\lambda, g_i) \log \frac{\Lambda}{m_0^2} \Big) + f_2(\lambda, g_i) \Lambda^2 \ . \tag{4.9}$$

Here λ is the coupling of ϕ^4 term, while g_i denote other dimensionless renormalised couplings of the theory. Λ is the cutoff scale, and the precise form of the functions f_1 and f_2 is irrelevant. One can see that even if the bare mass m_0 is zero, the renormalised (physical) mass will receive contributions governed by the quadratically divergent piece. Since the new physics scale Λ is generaly thought to be quite high (for instance, the Planck scale of 10^{19} GeV), one needs to employ a very fine tuning of parameters λ and g_i to explain the physical Higgs mass of 126 GeV. The large discrepancy between the observed Higgs mass and the cutoff scale Λ is termed the hierarchy problem. This is actually not a problem of the Standard Model itself, since the mass of the Higgs boson cannot be calculated within the SM framework. The hierarchy problem has to do with the expectation that a more fundamental theory, which will be able to predict the mass of the Higgs, should not feature excessive fine tuning.

A number of beyond Standard Model (BSM) theories has been constructed in an attempt to address these issues. In supersymmetric scenarios there are intricate cancellations of quadratic divergences in the Higgs self-energy [101]. This would provide for a natural solution of the hierarchy problem, but so far there have been no experimental proofs of supersymmetry. There are also attempts to describe the Higgs as a pseudo-Goldstone boson: while the basic idea is simple, its practical implementation is usually forbiddingly complicated if supersymmetry is not involved, see [102] and references therein. We shall concentrate on the class of theories which resolve this problem by describing the Higgs boson as a composite particle of strongly interacting fermions [19, 20]. These scenarios are collectively known as Technicolor, and we review some of their basic aspects in the next section. It should be noted that the hierarchy problem is not the only motivation for studying BSM theories: there are many other issues and phenomena which cannot be addressed within Standard Model, such as neutrino masses, strong CP problem, nature of Dark Matter/Dark Energy, and others. Some of these highly interesting topics can also be tackled with composite Higgs theories.

4.2 General aspects of Technicolor

We begin the argument by rewriting the Higgs field of Eq. (4.6) as a right column of the following 2×2 matrix Σ:

$$\Sigma = \sigma + \vec{\tau} \cdot \vec{\pi} \ . \tag{4.10}$$

In terms of Σ, the Lagrangian of Eq. (4.5) becomes

$$\mathcal{L}_{Higgs} = \mathrm{Tr}[D_\mu \Sigma^\dagger D^\mu \Sigma] + \mu^2 \mathrm{Tr}[\Sigma^\dagger \Sigma] - \frac{\lambda}{4} \mathrm{Tr}[\Sigma^\dagger \Sigma]^2 \ . \tag{4.11}$$

Now let us temporarily ignore the electroweak interactions implicit in the covariant derivative, by setting $D^\mu = \partial^\mu$ in Eq. (4.11). The resulting Lagrangian is that of a linear σ model, the low-energy effective theory of two-flavour QCD. This Lagrangian is invariant under an $SU(2)_L \times SU(2)_R$ transformation, which acts on Σ in a bilinear fashion:

$$\Sigma \to g_L \Sigma g_R^\dagger \quad \text{with} \quad g_{L/R} \in SU(2)_{L/R} \ . \tag{4.12}$$

The Higgs vacuum expectation value of Eq. (4.7) breaks the above symmetry to its diagonal subgroup

$$SU(2)_L \times SU(2)_R \to SU(2)_{L+R} \ . \tag{4.13}$$

This is the pattern of chiral symmetry breaking of two-flavour QCD. In reality, the right-handed particles do not feel the weak force. If the EW sector is included, only the $U(1)_Y$ subgroup of $SU(2)_R$ will be gauged under it, and the actual symmetry breaking pattern is that of Eq. (4.8). This should make it clear that, barring the electroweak interactions, the SM Higgs potential can be seen as an effective description of some strongly interacting gauge theory. In these QCD-like models, the actual origin of spontaneous symmetry breaking is the formation of a fermion bilinear, the chiral condensate:

$$\langle \bar{q}_L q_R \rangle \ . \tag{4.14}$$

In unitary gauge the Goldstone bosons associated with chiral symmetry breaking, the three technipions $\pi^{\pm}, \pi^0$ become the longitudinal degrees of freedom for the vector bosons $W^{\pm}, Z^0$. In this framework there is no hierarchy problem because the Higgs is a composite particle, analogous to the σ meson of QCD: its mass is determined by the electroweak scale v, just as the masses of ordinary hadrons are determined by Λ_{QCD}. By using the analogy with the linear σ model, the EW scale v can be put in Technicolor terms by equating it with the technipion decay constant, $v = f_\pi^{tc}$. Thus, in its original form, Technicolor was nothing more than a scaled-up version of QCD. It should be noted that the somewhat naive identification $f_\pi^{tc} = v$ only works if the theory is regarded in isolation. A soon as couplings to Standard Model or other sectors are included, the actual value of f_π^{tc} might change in any numbers of ways. This is the prime reason why some TC scenarios, which at face value seem to be completely inapplicable for phenomenology, are still considered as viable descriptions of Nature. To the best of our knowledge, so far there has been no systematic investigation performed on the influence of Standard Model interactions on Technicolor observables.

One should however not forget that bestowing the W and Z bosons with a mass is not the only role of the Higgs sector. It should also provide masses for Standard Model fermions, through gauge-invariant terms of the form

$$\mathcal{L}_{fermion} = \bar{\psi} \not{D} \psi + G_\psi \bar{\psi} H \psi \ . \tag{4.15}$$

G_ψ is a (*a priori* unknown) Yukawa coupling. In Technicolor approach these Yukawa interactions are effectively modeled as four-fermion operators. Their explicit consideration leads to Extended Technicolor (ETC) theories [20, 103]. As ETC includes non-renormalisable terms, it should be regarded as a low-energy description of some yet unknown dynamics. Accepting this viewpoint, one can write down the most general form of four-fermion interactions as (ψ denote SM fermions, while Q are techniquarks):

$$\alpha \frac{\bar{Q}Q\bar{\psi}\psi}{\Lambda_{ETC}^2} + \beta \frac{\bar{Q}Q\bar{Q}Q}{\Lambda_{ETC}^2} + \gamma \frac{\bar{\psi}\psi\bar{\psi}\psi}{\Lambda_{ETC}^2} \ . \tag{4.16}$$

α and β operators, respectively, give rise to masses of Standard Model fermions and Goldstone bosons, whereas γ terms produce flavour-changing neutral currents (FCNCs). Λ_{ETC} is a scale at which the gauge symmetry of Extended Technicolor spontaneously breaks, leaving behind the symmetry of ordinary Tehnicolor as an unbroken subgroup. The general 'theory' of Eq. (4.16) includes many free parameters and therefore does not have much predictive power. However, there are certain experimental results which allow one to put stringent restrictions on possible Technicolor dynamics. The γ terms include operators of the form

$$\frac{1}{\Lambda_{ETC}^2} (\bar{s}\gamma^5 d)(\bar{s}\gamma^5 d) \ . \tag{4.17}$$

These operators would induce a mass difference between a 'short' and 'long' kaon. Current experimental upper bound on this mass difference is on the order of 10^{-12} MeV [36]. Combining this and other results with a seemingly reasonable assumption that γ coefficients should be $O(1)$, leads to an estimate of the lowest Λ_{ETC} scale of about 10^3 TeV [103]. This in turn puts a restriction on how much mass can be 'naturally' given to SM particles through α operators. A naive estimate is that, unless the parameters of the model are unexpectedly large or small, one cannot account for SM particles heavier than 100 MeV. This result holds under the assumption

that Technicolor possessees QCD-like dynamics, and it could be significantly altered if different strongly interacting theories are considered. This observation led to the idea of near-conformal Technicolor.

We would like to make one last remark regarding the general ETC operators of (4.16), in particular the β interactions which provide (pseudo) Goldstone bosons with a mass. They are of principal importance for many TC scenarios. The reason is that in a generic strongly interacting theory the pattern of chiral symmetry breaking can be considerably richer than that of a two-flavoured QCD. These more complex patterns will not only produce the desired technipions but also many other Goldstone excitations, none of which has been seen in experiments. The absence of these massless states can be explained owing to the β operators. In certain TC scenarios the would-be Golstones are not merely a nuisance but an important part of the physical spectrum of particles, see section 4.6 as an example.

4.3 Walking Technicolor

Following the condensation of techniquarks, Standard Model fermions will gain masses of the magnitude

$$m_f \sim \frac{g^2}{M_{ETC}^2} \langle \bar{Q}Q \rangle_{ETC} \ . \tag{4.18}$$

M_{ETC} is the ETC gauge boson mass, and g and $\langle \bar{Q}Q \rangle_{ETC}$ are respectively the gauge coupling and technifermion condensate, both evaluated at the scale(s) Λ_{ETC}. Condensate at the scale Λ_{ETC} can be connected to the one at Λ_{TC} by using the renormalisation group (RG):

$$\langle \bar{Q}Q \rangle_{ETC} = \exp\Big(\int_{\Lambda_{TC}}^{\Lambda_{ETC}} d(\ln \mu) \gamma_m(\alpha(\mu)) \Big) \langle \bar{Q}Q \rangle_{TC} \ . \tag{4.19}$$

γ_m is the anomalous dimension for the techniquark mass operator. If we assume that Technicolor possesses QCD-like dynamics, the running coupling should behave as $\alpha(\mu) \sim 1/\ln(\mu)$ at scales above Λ_{TC}. This implies that the anomalous mass dimension γ_m depends linearly on the coupling $\alpha(\mu)$. The integral of Eq. (4.19) would then yield the result

$$\langle \bar{Q}Q \rangle_{ETC} = \ln \Big(\frac{\Lambda_{ETC}}{\Lambda_{TC}} \Big)^{\gamma_m} \langle \bar{Q}Q \rangle_{TC} \ . \tag{4.20}$$

The logarithmic enhancement of technifermion condensate does not help much in alleviating the tension between experiments and naive ETC calculations. However, if we instead consider a situation where the coupling α changes very slowly over a wide range of energies from Λ_{TC} to Λ_{ETC} (i. e. the coupling 'walks' instead of 'runs'), the resulting enhancement of TC condensate is significantly larger, with

$$\langle \bar{Q}Q \rangle_{ETC} = \Big(\frac{\Lambda_{ETC}}{\Lambda_{TC}} \Big)^{\gamma_m(\alpha^*)} \langle \bar{Q}Q \rangle_{TC} \ . \tag{4.21}$$

α^* is the value of the coupling at the approximate fixed point. Using this results in the estimate of Eq. (4.18), one can see that within the walking scenario it is much easier to explain masses of heavy quarks without giving any additional strength to operators which induce flavour-changing neutral currents. The fact that $\alpha(\mu)$ is almost constant over several

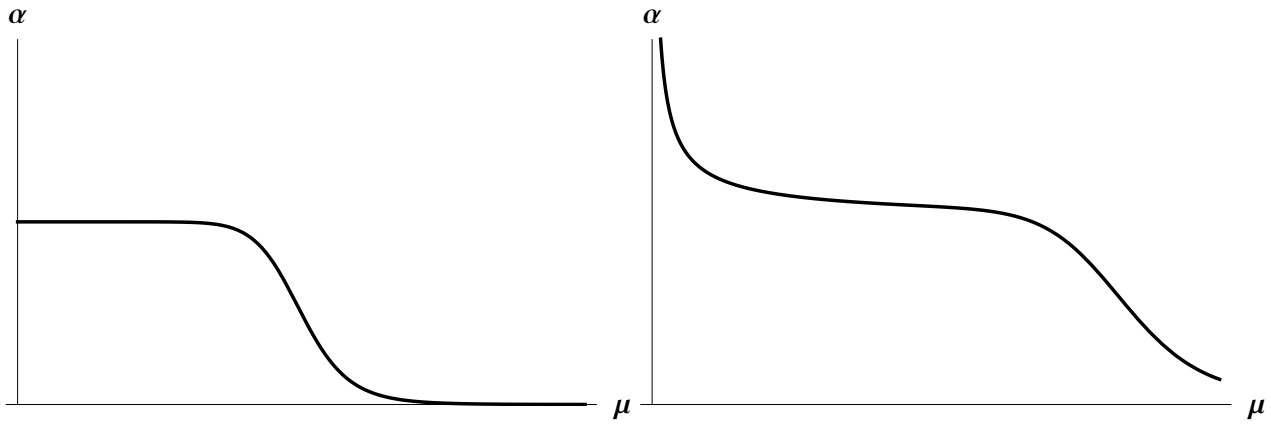

Figure 4.2: Gauge coupling in a theory with an exact (*left*) and approximate (*right*) IR fixed point. Despite (near)-conformality in the IR, the theories are still asymptotically free.

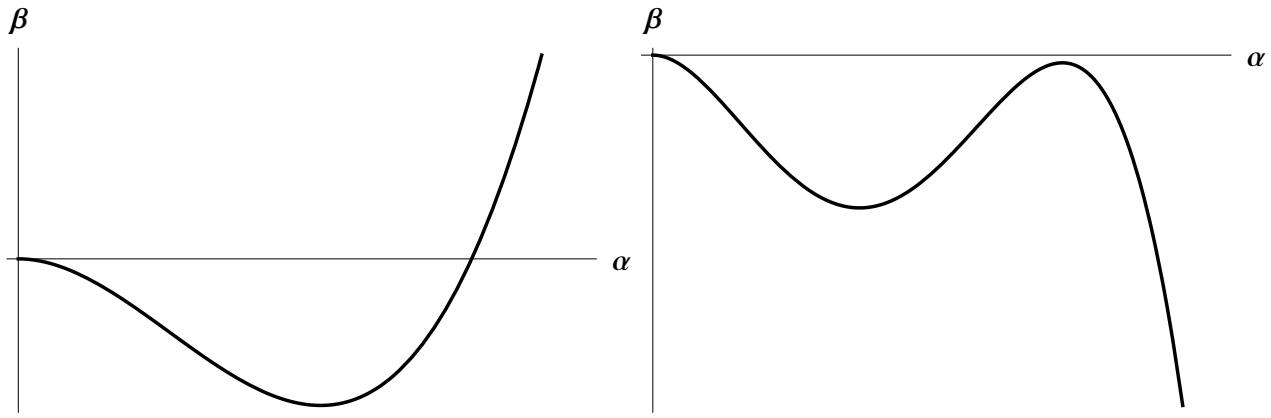

Figure 4.3: β functions in a theory with an exact (*left*) and approximate (*right*) IR fixed point. Despite (near)-conformality in the IR, the theories are still asymptotically free.

orders of magnitude in μ implies that the theory possesses an approximate fixed point in the parameter space, with

$$\beta(\alpha^*) \approx 0 \ . \tag{4.22}$$

This basic assumption of Walking Technicolor makes no reference on the nature of the fixed point, meaning that it can correspond to either an ultraviolet ($\beta(\alpha^*) > 0$) or infrared ($\beta(\alpha^*) < 0$) limit. The first investigation of a walking scenario dealt with an UV case [21], but there are only a few examples of four-dimensional theories with this kind of dynamics, and all require the presence of fundamental scalars [104]. On the other hand, as already mentioned in section 2.4, asymptotically free theories with an IR fixed point are thought to arrise naturally if the number of chiral fermion flavours is increased up to some critical value N_f^{cr} [63–65].

Theories which have an exact IR fixed point are sometimes referred to as conformal, since there is no intrinsic scale generated in the IR: $\alpha^* = \text{const.}$ implies that there is no fermion condensate and therefore the masses and decay constants of all hadrons are equal to zero. However, these theories might still be asympotically free, and thus not conformal in the most

strict sense of the word. Conformal and near-conformal (walking) dynamics are compared in Figures 4.2 and 4.3. Note the big qualitative differences as compared to a QCD coupling in Figure 2.2. These illustrations should be taken with a bit of caution, however. There are multiple ways to define the strong gauge coupling, depending on what Greens functions are used to impose the renormalisation conditions. While the various definitions should agree to a high degree in the UV (as the deviations only set in at higher-loop orders), in the non-perturbative regime the different couplings can behave completely differently, as is explicitly demonstrated at the end of section 5.3. It is not yet clear if all of the various α can develop an infrared plateau-like structure in the conformal phase, and if not, which of them should be regarded as indicative of the onset of a phase transition. For this reason the discussions of the 'walking gauge couplings' should be seen as representations of some principal ideas, pending more rigorous studies in the future.

The condensate enhancement of Eq. (4.21) will not be significant if γ_m is much smaller that unity. In [105] it is argued that $\gamma_m \approx 1$ signals dynamical chiral symmetry breaking, with $\gamma_m(\alpha_{\chi SB}) = 1$. If the theory posseses walking dynamics, α should not change much as the scale is varied from Λ_{TC} to Λ_{ETC}, and subsequently γ_m should have a value close to unity in the relevant energy range. This essentially leads to a condensate enhancement which is linear in $\Lambda_{ETC}/\Lambda_{TC}$. Despite this significant 'boost', there are concerns that the mass of the top quark cannot be accounted for without resorting to unnatural values for model parameters. This difficulty led to the development of topcolor-assisted Technicolor [106] and other similar ideas. We shall not discuss this problem and its possible solutions further here.

Constructing a strongly interacting gauge theory with an approximate IR fixed point is a very non-trivial task. Appearance of walking dynamics is a result of complicated interplay between the number of fermion flavours, number of colours, and the gauge group representation to which the fermion fields belong. In the following sections we will review some of the theories which are expected to feature walking dynamics. Despite the fact that the construction of these scenarios requires a certain level of fine-tuning, there are good reasons to study these unusual theories, and some of them were already shortly discussed in section 2.4. An especially attractive feature which walking models are expected to have, is the overall supression of hadron masses. Bound states in nearly-conformal models are expected to be very light with respect to some intrinsic scale like v_{EW}. An effective field theory approach gives the following result for masses of scalar mesons as one approaches the critical number of flavours N_f^{cr} from below [107]:

$$M_\sigma^2 \sim N_f^{cr} - N_f \ . \tag{4.23}$$

Due to its effective field theory origin, the validity of the above formula should not be taken for granted. However, it is not hard to convince oneself that its overall statement is correct, and that the Higgs boson mass should go down very fast (at least, faster than f_π^{tc}) as one approaches the conformal phase. Some lattice results which corroborate this idea are discussed in section 4.5. Without this feature, it would be very hard to obtain a composite Higgs boson with a mass of just 126 GeV, even if one takes into consideration the radiative corrections to the scalar self-energy from top-quark loops [108]. Similar conclusions were reached in the Dyson-Schwinger/Bethe-Salpeter calculations of [109, 110].

4.4 Large N_f theories

There are quite a few studies which attempted to estimate the critical number of fermion flavours for which no chiral symmetry breaking takes place. One of the most often cited results was obtained in [111] and has the form:

$$N_f^{cr} = N_c\Big(\frac{100N_c^2 - 66}{25N_c^2 - 16}\Big) \ . \tag{4.24}$$

This expression holds for fermions in the fundamental representation of $SU(N)_c$. In the large N_c limit it reduces to $N_f^{cr} \approx 4N_c$. Since these calculations were based on perturbative arguments, their validity is doubtful in a strong coupling regime. Despite the somewhat crude origins, the approximate value $N_f^{cr} \approx 4N_c$ served as a valuable guidance for early non-perturbative investigations. A considerable effort has been invested in the study of $SU(3)$ theory with 12 light fermions [112–117]. Clues were found that the actual N_f^{cr} is somewhat below the above estimate, and most new investigations use different colour/flavour combinations [89, 118, 119]). So far there is no general consensus on the location of the conformal window in the (N_f, N_c) plane. Studies on the existence of (approximate) IR fixed points require the probing of deep IR regime, and all calculations should in principle be performed in the exact chiral limit. Both the deep IR and the chiral quarks are very hard to study on the lattice (lattice being the most often used method of investigation), leading to many uncertainties in the final results.

One thing which is almost certain is that theories with a large number of fundamental flavours will not be used much for Technicolor phenomenology. One of the reasons for this was mentioned earlier: their pattern of chiral symmetry breaking is expected to result in a great number of Goldstone bosons. All the excess Goldstones can in principle be given a mass through β operators of Eq. (4.16), but most theorists prefer working with a framework which does not include a large number of extra particles. For this reason models with a smaller N_f are given an advantage. The second reason has to with the electroweak precision parameters. EW oblique parameters are quantities which parameterise potential new physics in the electroweak sector [120–122]. For now, their values are in excelent agreement with the Standard Model. One of the biggest constraints for Technicolor comes from the S parameter, which is supposed to be very small according to current experimental results [123]. A perturbative calculation predicts that S should grow linearly as the number of quarks and neutrinos is increased [35]. Thus any BSM model which features a great number of extra fermions will generally have problems when faced with EW precision data. While large N_f templates are in principle not yet excluded by experiments, the general attitude is in favour of scenarios which have as little matter content as possible[2]. In theories with small N_f, the walking dynamics can be achieved by considering fermions in higher-dimensional representations of the gauge group: matter belonging to the higher-dimensional representation generally screens more that the fundamentally charged matter.

[2]The 'matter content' might refer to other particles besides techniquarks. There are models which require the presence of additional neutrinos in order to ensure the cancellation of topological anomalies [107, 124]

4.5 Non-fundamental quarks

In [125] a study was performed on the existence of the conformal window for theories where quarks belong to non-fundamental representations of $SU(N)_c$. For the sextet (six-dimensional) representation of $SU(2)_c$, it was found $N_f^{cr} \approx 2$. This was the first investigation which showed that it is not neccessary to consider large N_f scenarios to obtain conformal dynamics. Many similar techniques were used over time to arrive at theories which are naively expected to be nearly conformal. A comprehensive list of Walking Technicolor candidates can be found in [35]. Here we shall concentrate on two representations for matter fields which are currently considered attractive from a phenomenological perspective: two-index symmetric (sextet) representation of $SU(3)$, and the adjoint representation of $SU(2)$.

Lattice investigations of sextet QCD with two flavours were performed in [126–128]. As with fundamental fermions, so far there is no agreement on whether the theory possesses an approximate or an exact IR fixed point. The meson mass spectrum as calculated in [128] has some peculiar features. The first peculiarity is that the theory shows an inversion in the hierarchy of masses when compared to QCD-like models: in the isovector channel the scalar particle is the lightest state, instead of being the heaviest. Second peculiarity is that there is an overall supression of technimeson masses with respect to the intrinsic EW scale, with $M_\sigma/f_\pi^{tc} \in [1,3]$. While this is not a neccessarily unexpected result, it is nice to see that walking scenarios might indeed lead to naturally light mesons, including the Higgs state. Another appealing feature of this model is that the pattern of chiral symmetry breaking is equal to the one of two-flavoured QCD. This should not come as a surprise, as the theory essentially represents $SU(2)_f$ QCD with enhanced quarks. The only Goldstone bosons are the three technipions, and there are no excess particles floating around. In this regard the template provides a minimal extension of the Standard Model.

Another interesting scenario is an $SU(2)$ gauge theory with 2 adjoint quarks. It is a Walking Technicolor candidate with a minimal matter content, and thus often called Minimal Walking Technicolor (MWT). Despite the small number of fermionic particles, there is a surprisingly rich pattern of chiral symmetry breaking, with no less than nine Goldstone particles, see [35] for details. Lattice results strongly suggest that this scenario is not of walking type, but is rather well inside the conformal window [130–132]: it is not possible to make definitive statements about this as the finite size effects were not fully understood in these investigations. [130] gives an estimate for the light vector meson, with $M_\rho/f_\pi^{tc} \in [5,6]$. That makes the ρ very light if the theory is not in the conformal phase, suggesting that other hadrons might have small masses as well. This is also one of the rare Technicolor models for which lattice studies of fundamental Greens functions were performed, most notably the propagators of Yang-Mills and matter sectors [88, 133]. While there are uncertainties caused by discretisation artifacts, their results strongly imply that fermion and gluon two-point functions undergo a significant change as compared to theories with QCD-like dynamics. This corroborates the idea that the conformal window has a great impact on Greens functions of the theory: a similar conclusion for fundamentally charged matter was reached in the Dyson-Schwinger study of [89].

4.6 QCD-like model: a Dark Matter candidate theory

Initial interest in $SU(2)$ gauge theories (either with fundamental or higher-dimensional quarks) with even N_f arose form the fact that their lattice simulations at non-zero chemical potential μ do not suffer from the sign problem. This makes the said models convenient for lattice investigations of the phase diagram of strongly interacting matter [134–144]. Relatively recently a template which includes 2 fundamental quarks was proposed as a possible unified description of Technicolor and Dark Matter (DM) [29–31]. In this context the properties of light mesons at zero temperature and chemical potential are also important, and it is this hadronic spectrum that will be the central focus of our study in Chapter 6.

An $SU(2)$ gauge theory possesses an enhanced flavour symmetry (the Pauli-Gürsey symmetry), leading to mesons and baryons (diquarks) which are chiral parity partners of each other. In these models the 3 usual Goldstone bosons, the pseudoscalar mesons ('pions') are accompanied by 2 additional scalar diquarks. When considering the theory as a Dark Matter template, it is these scalar diquarks which are usually suggested as the DM candidate and its antiparticle. Through Extended Technicolor interactions they are provided with a mass on the order of a few GeV, in accordance with experimental searches [147, 148].

Models which describe the Dark Matter as a composite particle of a new strongly coupled sector have several attractive features. Firstly, the fact that the constituent fermions are charged under the electroweak interaction provides several plausible mechanisms that explain the relic abundance of scalar Dark Matter, see e. g. [149–151]. Secondly, the bound states in these theories are EW neutral, and thus their interactions with Standard Model particles would be highly suppressed. This would explain naturally why it is so hard for us to detect these mysterious objects. And finally, the global flavour symmetries (e. g. the baryon number symmetry $U(1)$) would render the DM stable without the need to invoke any additional conservation principles. In this regard it should however be noted that it is not yet clear if an $SU(2)$ gauge theory can provide 'enough' of this baryon number conservation. This is due to the Pauli-Gürsey symmetry (i. e. mesons and baryons which are essentially indistinguishable from each other) and the fact that an $SU(2)$ template allows dimension-5 couplings to certain sectors of the Standard Model, which is arguably not a sufficiently large suppresion to explain an apparent long lifetime of Dark Matter. We will however not comment on this problematic issue any further in this thesis, and refer to [152] and references within for a more thorough discussion of these matters.

From the purely dynamical point of view, it should be clear that this model is not walking, and that it is is in fact very much QCD-like. Along with the problem of flavour-changing neutral currents, this also entails that the theory is expected to feature an isoscalar scalar meson (the Higgs boson) which is very massive, with M_σ no less than 1 TeV. The expectation is corroborated by group theory scaling arguments [108] and Dyson-Schwinger calculations, see [27] and Chapter 6. Some of these issues can be at least partially remedied by employing more general electroweak embeddings [153] or taking into account the couplings to Standard Model particles [108]. It is however generally believed that this model cannot be regarded as a truly viable Technicolor candidate until its dynamics is significantly modified. Possible modifications include the addition of an adjoint quark which would not be charged under the EW sector, thus bringing the overall dynamics closer to the conformal phase. This and similar scenarios will probably be investigated in future lattice and DSE calculations.

For us, the fact that this scenario does not really work as a TC template is not so prob-

lematic. We see it as an interesting opportunity to test our relatively novel beyond rainbow ladder (BRL) approach, precisely because the model is close, but not exactly equal to QCD. We describe our BRL framework in some detail in Chapter 6 and show that it gives a significant improvement, when compared to lattice results, over the rainbow-ladder treatment. We do not however go further than evaluating masses and the pion decay constant, which is used to set the scale of the calculation. While there are many other things which can be evaluated (e. g. the electromagnetic form factors, decay widths), these computations would be technically very involving, especially in a BRL setting. We thus leave these topics for future endeavors.

Chapter 5

The three-gluon vertex

The three-gluon vertex is the simplest primitively divergent Greens function which encodes the self-interaction of gluon fields. While it is a fairly interesting object to study in its own right, the main motivation for investigating it comes from the significant role it is expected to play in fundamental and phenomenological studies of QCD and QCD-like theories. In the context of this thesis, the three-gluon coupling is important as an input in our treatment of bound states and the Dyson-Schwinger equation for the quark-gluon vertex. This chapter and the corresponding Appendix are largely based on [26].

While it has been quite some time since the first perturbative studies of the three-gluon coupling were performed [154–157], it is only fairly recently that this function became a subject of elaborate investigations which do not rely on the small coupling expansion. Some initial interest in its non-perturbative properties arose from the fact that it represent an important piece in the functional calculations of the gluon propagator. Owing to limited computational resources, in most of these evaluations the three-gluon vertex was included simply via carefully constructed models. Main guidelines for modelling were based on constraints from Slavnov-Taylor identities and Bose symmetry [154, 158, 159]. In other cases, the three-gluon coupling was deliberately tuned to produce the correct anomalous dimension for the gluon propagator or eliminate spurious quadratic divergences which arise as a consequence of truncations [22, 160]. A somewhat elaborate construction is presented in [23] and has multiple desirable features: it is Bose-symmetric, gives the correct gluon anomalous dimension, and leads to a gluon two-point function which fares well when compared with lattice results. The model also captures the qualitative behaviour of three-pont function in the infrared region, which is by now known from continuum [161] and lattice studies [162–164].

It is certainly true that cleverly constructed vertex models can, to some extent, be a good replacement for the actual evaluation of the function. There are however some potentially important properties of vertices which can only be assessed if they are explicitly calculated. What is particularly interesting about the gluon three-point function is that its tree-level dressing seems to feature a sign flip in the deep IR region, as first seen in lattice simulations in two and three dimensions [162, 163]. In four dimensions lattice results are plagued by large uncertainties in the IR, but they are at least suggestive of a similar behaviour. The location (in momentum space) of this zero-crossing is expected to have some bearing on hadronic observables when the three-point function is employed in bound state studies, as was first done in [165]. To gain further insight into these matters, we will perform a DSE study of this function in Landau gauge.

The very first such investigation was conducted in [24]. There only the tree-level tensor structure was considered, and the back-coupling of the vertex onto ghost/gluon system was explicitly taken into account. Since we are primarily interested in this function as a tool for phenomenological studies, we will ignore its dynamical influence on the Yang-Mills sector and will instead use fixed model input for ghost and gluon propagators. This simplification is well justified by the results of [24], which show that the back-coupling does not affect the Yang-Mills propagators appreciably. We complement the results of forementioned investigation by including all the tensor structures of the three-gluon vertex relevant in Landau gauge.

5.1 Vertex DSE

We will not write down the full DSE for the three-gluon vertex: for the entire equation see e.g. [166] and references within. We immediatelly work with the approximated form, where only the one-loop diagrams containing primitively divergent vertices are kept, see Figure 5.1. Note that, while the full DSE for this function is Bose-symmetric (i. e. it is symmetric under the interchange of external gluon legs), the truncated equation is not. Since Bose symmetry plays a crucial role in our treatment, we enforce it on the approximate equation by including cyclic permutations of all diagrams. We will be working with the reduced form for all vertices, wherein the colour structures and gauge couplings are isolated, for instance $\Gamma^{abc}_{\mu\nu\rho} = igf^{abc}\,\Gamma_{\mu\nu\rho}$. In terms of the reduced functions, the truncated Dyson-Schwinger equation reads

$$\Gamma_{\mu\nu\rho} = \Gamma^{(0)}_{\mu\nu\rho} + \Lambda^{\text{ghost}}_{\mu\nu\rho} + \Lambda^{\text{gluon}}_{\mu\nu\rho} + \Lambda^{\text{sword 1}}_{\mu\nu\rho} + \Lambda^{\text{sword 2}}_{\mu\nu\rho}\ . \tag{5.1}$$

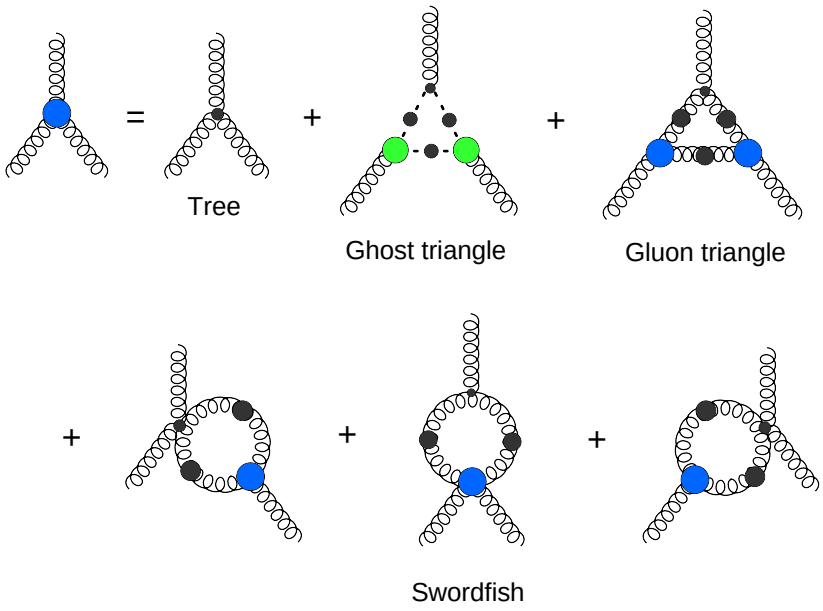

Figure 5.1: Truncated DSE for the three-gluon vertex. Equation is Bose-symmetrised by including cyclic permutations with respect to external gluon legs.

Labels **ghost** and **gluon** in equation (5.1) refer to ghost and gluon triangle diagrams, whereas **sword 1** and **sword 2** are swordfish loops with the dressed four-gluon and three-gluon vertex respectfully. It is understood that each term in the above equation depends on external momenta (p_1, p_2, p_3). Explicit expressions for the self-energies are (all momenta p_i are outgoing)

$$\Lambda^{\text{ghost}}_{\mu\nu\rho}(p_1,p_2,p_3) = -g^2 N_c \int_k D_G(k_1^2) D_G(k_2^2) D_G(k_3^2) \Gamma_\mu(-k_1,k_3,p_1) \Gamma^{(0)}_\rho(-k_3,k_2,p_3) \Gamma_\nu(-k_2,k_1,p_2),$$

$$\Lambda^{\text{gluon}}_{\mu\nu\rho}(p_1,p_2,p_3) = \frac{g^2 N_c}{2} \int_k D_{\alpha\tau}(k_1^2) D_{\gamma\sigma}(k_2^2) D_{\beta\eta}(k_3^2) \Gamma_{\alpha\beta\mu}(-k_1,k_3,p_1) \Gamma^{(0)}_{\eta\gamma\rho}(-k_3,k_2,p_3) \Gamma_{\sigma\tau\nu}(-k_2,k_1,p_2),$$

$$\Lambda^{\text{sword 1}}_{\mu\nu\rho}(p_1,p_2,p_3) = -\frac{3g^2 N_c}{4} \int_k D_{\alpha\eta}(k_3^2) D_{\beta\sigma}(k_2^2) \Gamma^{(0)}_{\alpha\beta\rho}(-k_3,k_2,p_3) \Gamma_{\eta\sigma\mu\nu}(k_3,-k_2,p_1,p_2),$$

$$\Lambda^{\text{sword 2}}_{\mu\nu\rho}(p_1,p_2,p_3) = -\frac{3g^2 N_c}{4} \int_k D_{\alpha\eta}(k_3^2) D_{\beta\sigma}(k_2^2) \Gamma_{\alpha\beta\rho}(-k_3,k_2,p_3) \Gamma^{(0)}_{\eta\sigma\mu\nu}(k_3,-k_2,p_1,p_2).$$

k is the loop momentum, and we employed the notation

$$k_3 = k + \frac{p_3}{2}, \quad k_2 = k - \frac{p_3}{2}, \quad k_1 = k_2 - p_2 \ . \tag{5.2}$$

Numerical coefficients in front of the integrals subsume the colour trace and symmetry factors coming from DSE derivation. Multiplicities arising from Bose-symmetrisation are also taken into account (this just gives the factor of 2 for 'swordfish 2' diagram, see Figure 5.1 as well as Figure 1 of [26]). Bare ghost-gluon, three-gluon and four-gluon vertex are given by

$$\begin{aligned}
&\Gamma^{(0)}_\mu(p_1,p_2,p_3) = \tilde{Z}_1 \cdot p_2^\mu \ , \\
&\Gamma^{(0)}_{\mu\nu\rho}(p_1,p_2,p_3) = Z_1 \cdot [\delta^{\nu\rho}(p_2-p_3)^\mu + \delta^{\mu\rho}(p_3-p_1)^\nu + \delta^{\mu\nu}(p_1-p_2)^\rho] \, , \\
&\Gamma^{(0)}_{\mu\nu\rho\sigma}(p_1,p_2,p_3,p_4) = Z_4 \cdot [\delta^{\mu\rho}\delta^{\nu\sigma} - \delta^{\mu\sigma}\delta^{\nu\rho}] \, .
\end{aligned} \tag{5.3}$$

The tensor structure for the four-point function is what remains of the tree-level term once the colour trace has been carried out in the swordfish diagrams. The ghost and gluon propagators, $D_G(k)$ and $D_{\mu\nu}(k)$, respectively, are given by Eq. (2.25) in Landau gauge. In our calculation their dressing functions are taken as model input.

5.2 Ghost/gluon input and models for vertices

For the Yang-Mills (YM) propagators we will use the results of a DSE study of [22]. In addition to a scaling scenario considered in that investigation, we will also work with some decoupling-type solutions within the same truncation. The scaling case corresponds to an infrared divergent ghost dressing function, whereas in the decoupling one the ghost dressing is IR finite. The dressing functions for the ghost and gluon propagators are shown in Figure 5.2. $\tilde{Z}_3 = 1.529$ and $Z_3 = 3.384$ are the ghost and gluon renormalisation constants, respectively. The ghost-gluon running coupling was used to impose the renormalisation conditions, with $\alpha_{gh}(\mu^2) = 0.7427$ at the point $\mu = 2.28$ GeV. The UV cutoff was $\Lambda^2_{\text{cut}} = 10^4$ GeV^2. By employing the Slavnov-Taylor identities of equation (2.29) it is possible to eliminate the gauge coupling renormalisation Z_g in favour of the one for the ghost-gluon vertex $\tilde{Z}_1$ and obtain:

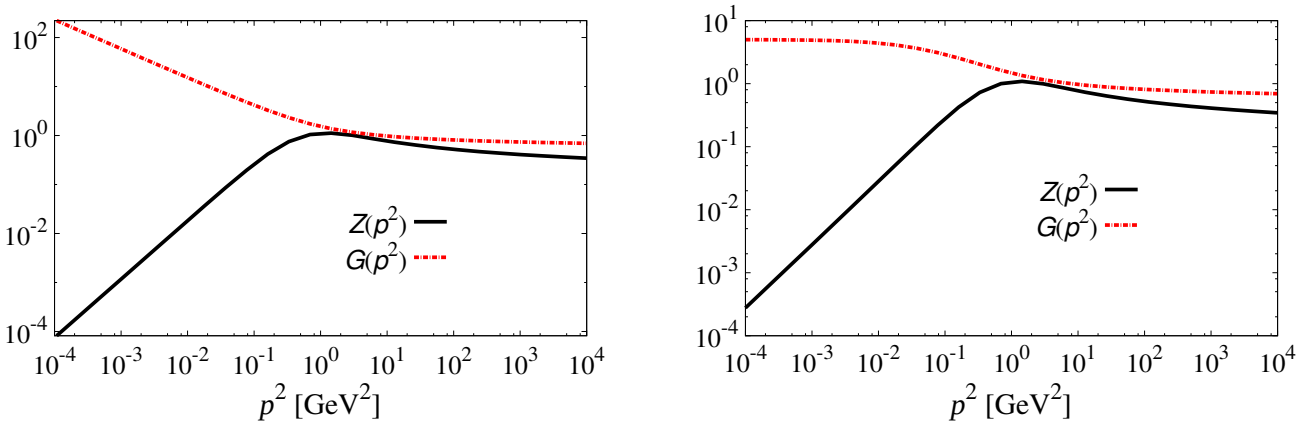

Figure 5.2: Ghost (G) and gluon (Z) dressing functions for scaling (*left*) and decoupling (*right*) scenarios. The IR boundary condition for the DC scenario was chosen such that $G(p^2 \to 0) = 5$.

$$Z_1 = \frac{\tilde{Z}_1 Z_3}{\tilde{Z}_3}, \quad Z_4 = \frac{\tilde{Z}_1^2 Z_3}{\tilde{Z}_3^2} \ . \tag{5.4}$$

Thus we only need the $\tilde{Z}_1$ to have the renormalisation of the three-gluon and four-gluon vertex uniquely determined. Since the ghost-gluon function does not get renormalised in Landau gauge [43], we simply set $\tilde{Z}_1$ equal to unity. This defines the miniMOM scheme [167]. It immediately follows that $Z_1 = 2.213$ and $Z_4 = 1.447$. The final two ingredients needed for the evaluation of equation (5.1) are the non-perturbative ghost-gluon and four-gluon vertex. We set the full ghost-gluon function equal to its bare counterpart, $\Gamma_\mu = \Gamma_\mu^{(0)}$. This is well justified by lattice and functional investigations in Landau gauge, which show that the dressed vertex does not deviate appreciably from its tree-level form [23, 162, 164, 168]. For the gluon four-point coupling we construct a model by employing its tree-level tensor structure and a suitably defined dressing function:

$$\Gamma_{\mu\nu\rho\sigma}(p_1, p_2, p_3, p_4) = f(x) \cdot \Gamma^{(0)}_{\mu\nu\rho\sigma}(p_1, p_2, p_3, p_4), \tag{5.5}$$

with the Bose-symmetric combination $x = (p_1^2 + p_2^2 + p_3^2 + p_4^2)/\Lambda^2$, and $\Lambda = 0.6$ GeV is the characteristic gluon scale. The model $f(x)$ is constructed out of ghost and gluon dressing functions as:

$$f(x) = Z_4 \cdot G^a(x) Z^b(x), \quad a, b = \text{const.} \tag{5.6}$$

a and b are chosen so that $f(x)$ qualitatively matches the known behaviour of the tree-level dressing in the UV [155, 169] and IR [170, 171] regions. They are given by the following set of parameters for the scaling and decoupling scenarios:

$$\begin{aligned} &\text{scaling:} \quad a = 2, \quad b = -1, \\ &\text{decoupling:} \quad a = \frac{1 + 4\delta}{\delta}, \quad b = 0. \end{aligned} \tag{5.7}$$

$\delta = -9/44$ is the ghost anomalous dimension. The resulting model dressing function is shown in Figure 5.3. Note that our choice for a, b gives a dressing which is constant in the IR for the decoupling case. According to [172], this function should actually be logarithmically diverging, at least in four dimensions. This difference would only set in in relatively deep IR, where most effects are anyway washed away by gluons. The numerics would change very little if we used the 'proper' four-gluon vertex model for the decoupling scenario, and we thus choose to stay with Eq. (5.7).

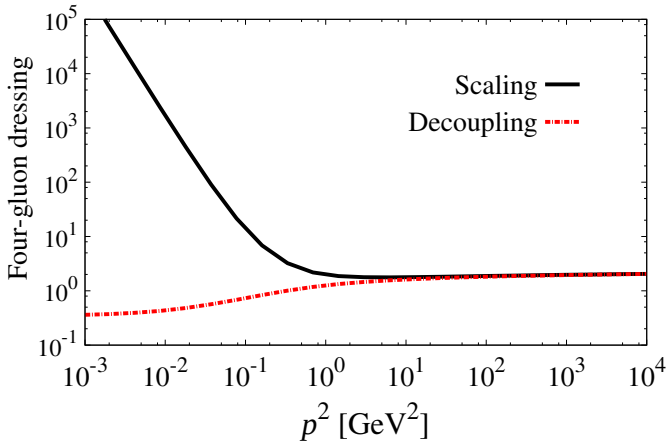

Figure 5.3: The model dressing function for four-gluon vertex, for the scaling and decoupling scenarios.

5.3 Results and discussion

We already noted that Bose-symmetry is very important for our treatment of the gluon three-point function. In order to make it explicitly manifest, one has to use appropriate kinematic variables and tensor basis elements, which can be obtained by using permutation group analysis. We provide all the necessary details about this construction principle in section B.1. For the sake of convenience, here we shall only give the definitions of the momentum variables which will be used for plotting of results:

$$S_0 = \frac{1}{6}(p_1^2 + p_2^2 + p_3^2),$$
$$a = \sqrt{3}\frac{p_2^2 - p_1^2}{p_1^2 + p_2^2 + p_3^2}, \quad s = \frac{p_1^2 + p_2^2 - 2p_3^2}{p_1^2 + p_2^2 + p_3^2}. \tag{5.8}$$

S_0 is obviously a symmetric singlet under the permutations of momenta, whereas angular variables a and s form a doublet representation of the S_3 permutation group. Although this is far from obvious, a and s also form the interior of a circle of unit radius, and Bose symmetry manifests itself as a rotational invariance under $2\pi/3$ and $4\pi/3$ rotations in the (a, s) plane. These matters are discussed in detail in [26]. The rotational symmetry can be nicely seen in our

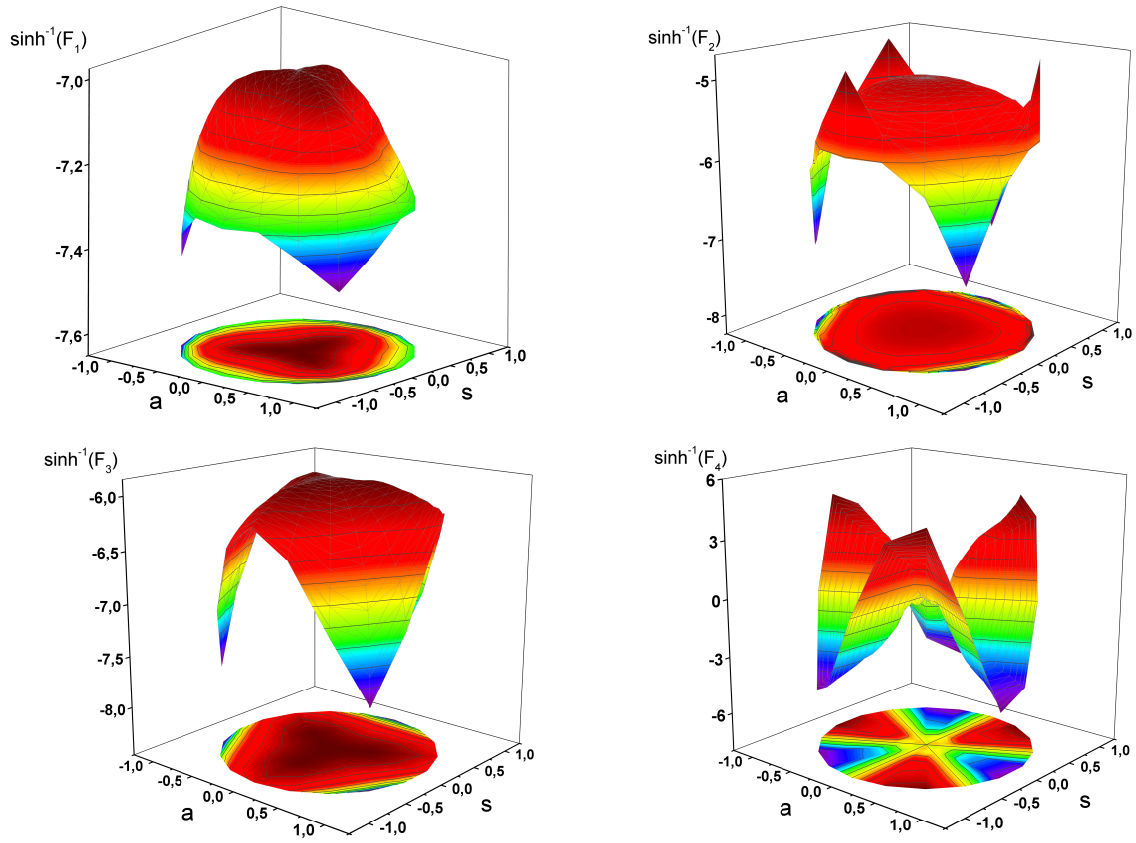

Figure 5.4: The vertex dressing functions in (a, s) plane for the scaling scenario, with fixed $S_0 = 7.64 \cdot 10^{-4}$ GeV^2. Basis is that of Eq. (B.17) and the definitions of variables (S_0, a, s) are provided by Eq. (5.8). For the interpretation of results, note that $F_1 \approx \sinh(-7) = -\mathrm{e}^7$.

results shown in Figure 5.4, where we plot the angular dependence of vertex dressings functions for a fixed value of $S_0 = 7.64 \cdot 10^{-4}$ GeV^2 (note that F_4 is actually antisymmetric, this choice is explained in B.3). Only the scaling scenario is considered, and the corresponding basis is given in equation (B.17). In Landau gauge it only takes 4 basis elements to fully describe the three-gluon vertex: this is due to the transversality property of the gluon propagator, which ensures that longitudinal components decouple from the system. In more general gauges it would take 14 tensors for the description of the three-gluon coupling, a significantly greater challenge. We also point to the fact that vertex dressing functions in Figure (5.4) were transformed with inverse hyperbolic sine. Significance of this transformation for the numerical procedure is elaborated on in section B.3.

The dressing function F_1 which corresponds to the tree-level term is apparently the dominant one, with F_3 being the only other component with comparable values. In our calculation we kept all four components when back-coupling the vertex, but for most practical purposes it would probable be a reasonable approximation to completely neglect F_2 and F_4 terms. Our result justifies, to some extent, the truncation made in [24], where only the tree-level part was self-consistently back coupled. Our rough estimate is that the inclusion of sub-leading components would have produced about a 10 percent difference in the final result. A peculiar feature

of the results displayed in Figure 5.4 has to do with the angular dependence of sub-leading amplitudes. While F_1 is a relatively flat function, other ones show a large enhancement in certain kinematical regions.

From the definitions of equation (5.8) it can be seen that the three soft kinematic limits ($p_i^2 \to 0$ for $i = 1, 2, 3$) correspond to directions $s = -2 \pm \sqrt{3}a$ and $s = 1$ in the (a, s) plane. This is exactly where the enhancements of $F_{2,3,4}$ dressings show up. The angular dependence of various components is shown more explicitly in Figure 5.5. It is yet unclear why the soft collinear divergences do not manifest themselves in the tree-level term. Non-uniform singularities are a relatively new research topic, see [174, 175] for some of the previous investigations. While the semi-perturbative results of [175] corroborate the idea that different dressing functions of the three-gluon coupling can have different IR exponents, a direct comparison with our approach is not possible since the basis construction employed there violates Bose symmetry. This remains an interesting topic for future investigations. We also note that a manifestly Bose-symmetric approach was a key in uncovering the soft infinities: had we broken this invariance in any of the steps the non-uniform divergences would have remained hidden.

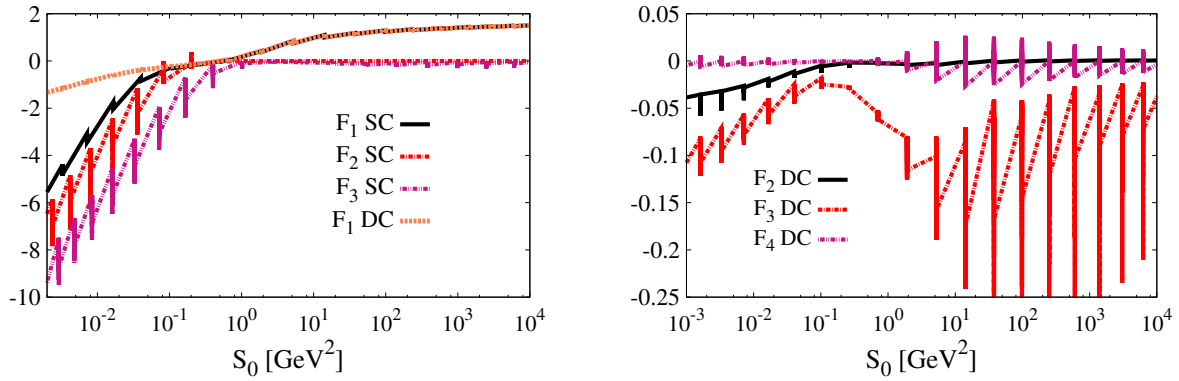

Figure 5.5: Angular dependence of various components of the the three-gluon vertex, for scaling (SC) and decoupling (DC) solution. All functions were transformed with $\sinh^{-1}(x)$. Sub-leading terms in the left panel were slightly moved to the right to ease comparison.

Separate contributions to vertex tree-level dressing are shown in Figure 5.6 for the symmetric limit $a = s = 0$. We first note that for the scaling case, all self-energy contributions behave in accordance with the IR scaling analysis of Yang-Mills vertices. If one considers the gauge sector alone, it can be shown that the following *ansätze* for vertex functions formally solves the infinite hierarchy of DSEs in the infrared [52, 161, 176]:

$$\Gamma^{(n,m)}_{p^2} \sim (p^2)^{2(m-n)\kappa}, \quad \text{as} \quad p^2 \to 0. \tag{5.9}$$

$\Gamma^{(n,m)}_{p^2}$ is a Greens function with $2n$ ghost and m gluon legs, and κ is an infrared scaling exponent. In our calculation κ is a part of the model input for the scaling Yang-Mills propagators, with $\kappa \approx 0.595$ [22]. By applying the above power counting scheme to the three-gluon equation (5.1) one can see, for instance, that the ghost loop diverges in the IR like $(p^2)^{-3\kappa}$.

With the appropriate function fitting we have checked that all the self-energies have IR exponents in quantitative agreement with Eq. (5.9). We will return to this point later, when we discuss the strong running coupling associated with the three-gluon vertex.

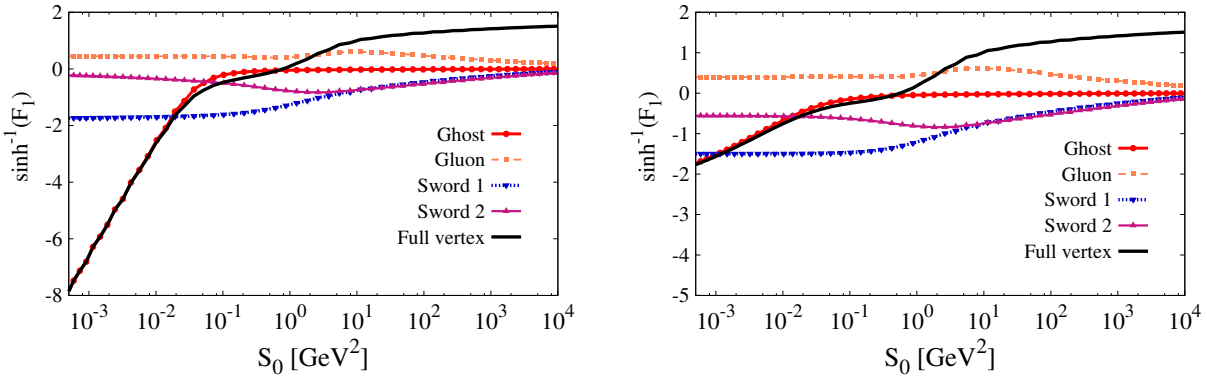

Figure 5.6: Contributions to tree-level dressing in the symmetric limit $a = s = 0$, for scaling (*left*) and decoupling (*right*) scenarios.

For the decoupling case the vertex is logarithmically diverging in the IR, in agreement with the results of [172, 177]. Apart from the big differences in the limit of vanishing momentum, the vertex dressing functions look very similar for the scaling and decoupling solutions. In fact, the zero-crossing of the tree-level component occurs at almost the same place for these two solutions, as is explicitly shown in the left panel of Figure 5.7. In this regard our results corroborate the idea that physical observables might be (almost) insensitive to the differences between scaling and decoupling vertex functions (while the three-gluon coupling is not an observable, the location of the sign flip potentially has some influence when the vertex is used in bound state studies). Even if this eventually turns out to be true, it should be noted that the issue of the two kinds of solution can still have bearing on formal aspects of QCD, see [178] and references therein.

From the left panel of Figure 5.7 one can see that the tree-level dressing function changes sign at the 'hadronic' scales of about 1 GeV. This is an unexpectedly high result, and it is in stark contrast with other investigations where the zero crossing happens much deeper in the IR [24, 172]. The large disagreement is due to different setups of these calculations. In the study of [172] only the ghost triangle part of vertex self-energy was considered. By employing the same approximation we obtained the results in good agreement with theirs. As for the computations performed in [24], there the so-called renormalisation group improvement (RGI) was employed to enhance the otherwise bare three-gluon and four-gluon vertex in the DSE [179]. This is done by replacing the vertex renormalisation constants with momentum-dependent functions of the form

$$Z_1 \to Z^{a1} \cdot G^{a2}, \quad Z_4 \to Z^{b1} \cdot G^{b2}. \tag{5.10}$$

We will only cite the values for constants a_i, b_i for the decoupling case, where $a_1 = 0$, $a_2 = -17/9$, $b = 0$ and $b_2 = -8/9$. The purpose of these RG improvements is to compensate

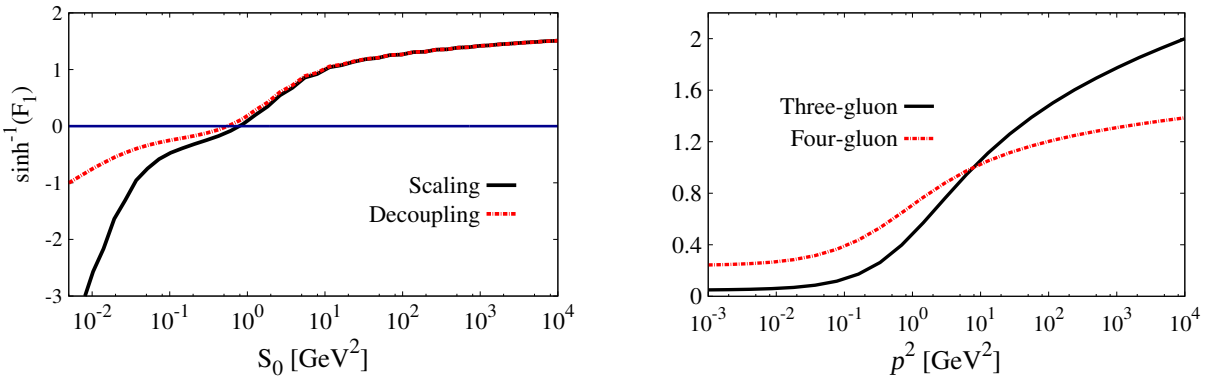

Figure 5.7: *Left*: Full dressings of the tree-level tensor structure for scaling and decoupling solutions. *Right*: RG improvements for the three- and four- gluon vertex for a decoupling scenario.

in the UV for the missing two-loop diagrams in the equation of motion. While it is certainly useful, the method also leads to a change in balance between different diagrams in the mid- and low- energy region. This is illustrated in the right panel of Figure 5.7, where we plot the RG improvements for the three- and four- vertex in a decoupling scenario. In the UV, these dressings approach the values of the corresponding renormalisation constants Z_1 and Z_4. For lower energies however they introduce a rather arbitrary momentum dependence which weakens the gluon triangle and swordfish diagrams. This is the main source of discrepancy between our results and those obtained in [24]. In this regard our calculation is more 'honest', but one has to admit that the full vertices shown in Figures 5.6 and 5.7 do look a bit worisome. As we show in Chapter 6, if such three-gluon couplings are used in our treatment of the quark propagator and quark-gluon vertex, they lead to solutions for the quark DSE where there is no chiral symmetry breaking.

Besides the sign flip at unnaturally high energies, there is another troubling aspect of our treatment of the three-gluon Greens function. This is the fact that the stability of iterations strongly depends on the employed model for the four-gluon vertex. Had we set this function equal to its bare counterpart, or employed a model which is 'too weak', there would have been no stable solutions due to the influence of the gluon triangle contribution, which would grow with every new iteration. We have checked that this is not a consequence of an inappropriate iteration method by using multiple approaches, including the Newton iteration technique. All the methods returned the same result, suggesting that this is a genuine instability of the truncated equation of motion.

These considerations lead to the conclusion that there are important pieces missing in our model. One of the possibilities is that our ghost/gluon input is inadequate: since we use the results of a DSE calculation where the two-loop terms were neglected, our gluon propagator is somewhat weaker in the mid-momentum region than what is seen on the lattice. To assess the importance of this we performed calculations with an artificially enhanced two-point function. Apart for some differences in the ghost-gluon running coupling (see below), our main conclusions remain the same as before. The next most obvious candidates for the missing

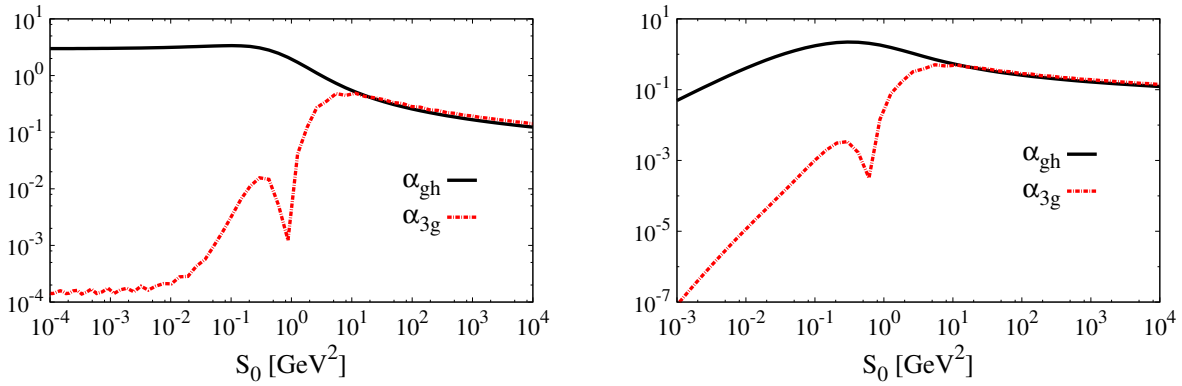

Figure 5.8: Three-gluon and ghost-gluon runnning couplings of equation (5.11) for scaling (*left*) and decoupling (*right*) scenarios.

contributions would be the full four-gluon vertex, the two-loop terms, and the unquenching effects. Out of these, the inclusion of (at least some) of the two-loop diagrams is arguably the easiest step to take. The four-gluon vertex has a forbiddingly rich tensor/colour basis and kinematic structure, meaning that even studies which use hard approximations are computationally expensive see e. g. [171]. In a similar way, the inclusion of fermionic loops beyond simple truncations for the quark-gluon interaction pose a serious challenge. Note however that the quark-gluon vertex is currently being investigated in FRG [25] and DSE frameworks, thus enabling eventual studies on the influence of unquenching on the gluonic three-point function. In the end, it will probably be a mixture of these various contributions which will hopefully give better results for the three-gluon correlator. At the end of this section we will comment how some of the two-loop diagrams can be at least partially included in a relatively simple way.

As one of the final checks on our calculation, we obtain the running coupling of the three-gluon vertex α_{3g}, and compare it with the one for the ghost-gluon coupling α_{gh} in Figure 5.8. These quantitites are defined as

$$\begin{aligned} \alpha_{gh}(p^2) &= \alpha(\mu^2) Z(p^2) G^2(p^2), \\ \alpha_{3g}(p^2) &= \alpha(\mu^2) Z^3(p^2) F_1^2(p^2). \end{aligned} \tag{5.11}$$

α_{3g} and α_{gh} agree relatively well in the UV: the slight discrepancy between them comes from the missing two-loop contributions in the vertex DSE (the mismatch cannot be so clearly seen here because of the log scale on the y axis). If two-loop terms are not explicitly taken into account, one can employ the RG improvements to reach better agreement for high energies, see [24]. This is a crucial step if back-coupling of the vertex onto the Yang-Mills propagators is considered, as otherwise the gluon anomalous dimension comes out wrong. In the mid-momentum and infrared region, the couplings for ghost-gluon and three-gluon vertex look very different. This is not surprising, as there is no unambiguous non-perturbative definition of the strong running coupling.

Even α_{3g} itself is not uniquely defined, as from the vertex dressing F_1 and Yang-Mills propagators one can construct infinitely many functions which look the same in the UV region:

$$\alpha_{3g}^{(n)} = \alpha(\mu^2) Z (G\Gamma_{gh})^2 \left[\frac{ZF_1}{G\Gamma_{gh}}\right]^n . \tag{5.12}$$

Γ_{gh} is the tree-level dressing of ghost-gluon vertex. The coupling α_{3g} of equation (5.11) is a special case of the above expression with $n = 2$. This is the only definition which is independent of the ghost-gluon vertex dressing. We note that in the scaling scenario both α_{gh} and α_{3g} develop and infrared fixed point, with $\alpha_{gh}(0) \approx 3$ and $\alpha_{3g}(0) \approx 1.5 \cdot 10^{-4}$. The existence of an low-energy plateau for these couplings is in accordance with the IR scaling analysis of [161]. This provides an additional check of our numerics, as the appearance of an IR fixed point in α_{3g} for the scaling scenario guarantees that the vertex dressing F_1 behaves correctly at small momenta.

Now let us describe how some of the two-loop contributions can be partially included with minimal modification to the framework presented here. To illustrate the main points we will concentrate on a single diagram, namely the ghost version of the swordfish loops. This procedure can be applied to almost all other two-loop terms, and is straightforwardly translated to the unquenching case (where one just replaces the ghost lines with quarks). The ghost swordfish diagram contains a non-primitively divergent vertex function, the ghost-gluon scattering kernel. By using the DSE for this kernel and neglecting the non-superficially divergent terms, one ends up with the equation depicted in Figure 5.9 (note that one of the gluon swordfish diagrams was left out for brevity).

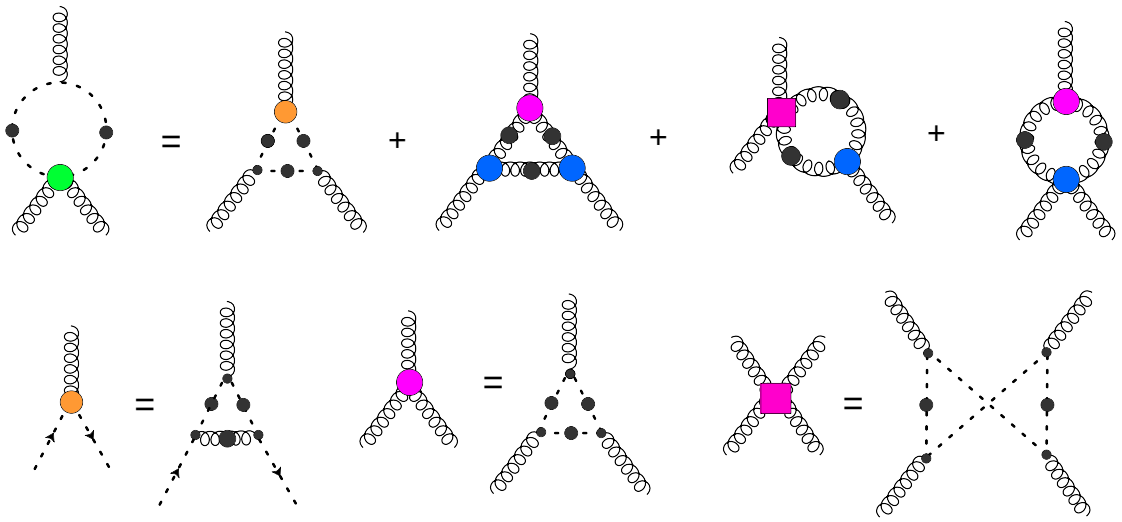

Figure 5.9: An approximated form of the ghost swordfish diagram, wherein the non-primitively divergent pieces are neglected. Note that one of the gluon swordfish diagrams was left out in the upper line for brevity.

From the resulting expression one can see that all the additional contributions take the form of corrections to the one-loop diagrams, where the bare vertices are replaced with their 'dressed' versions. What is good about these 'dressings' is that none of them depend on the three-gluon vertex itself, meaning that they can be calculated and stored prior to any iterations. Their

inclusion in the iteration process itself would then be achieved via interpolation. Even in the cases where the modifications of bare vertices do depend on $\Gamma_{\mu\nu\rho}$, one can still use this 'two-step' method with interpolation to effectively keep everything at one-loop order. This trick can be applied to almost all other two-loop diagrams. Additionally, since we are anyway modelling the gluon four-point interaction, it would probably make sense to neglect any diagrams which look like corrections to the gluonic swordfish loop with the bare three-gluon vertex. While this procedure certainly neglects a lot of information, it allows for an approximate inclusion of higher order terms with minimal change to the method employed in the one loop case. One could then see if the overall behaviour of the gluon three-point function starts to improve in comparison to what we have seen in our computations.

Chapter 6

Bound states in an $SU(2)$ theory

In section 3.3 we performed a simple rainbow-ladder (RL) computation of certain meson masses in QCD. The main purpose of this was to demonstrate a few basic ideas of our approach to bound states. However, the calculation also made apparent some of the shortcomings of the RL framework, wherein the masses for scalar and axial-vector meson come out in poor agreement with experimental values. Here we would like to apply the combined DSE/BSE formalism to the study of light mesons in an $SU(2)$ gauge theory with 2 fundamental chiral Dirac fermions. It should probably not come as a surprise that here the RL method proves to be inadequate as well, see Table 6.2 in section 6.4. We will attempt to remedy this by employing a more elaborate 'beyond rainbow-ladder' (BRL) technique based on the diagrammatic expansion of the quark-gluon vertex DSE [165, 180–189]. We wish to point out that there are alternative ways to construct bound-state equations in accordance with constraints from chiral symmetry [190–196], but this particular approach suits us due to its close connection to the underlying Yang-Mills sector. Since the quark-gluon vertex represents the centerpiece of this calculation, we will begin by providing some details about it and the corresponding Bethe-Salpeter truncation. This Chapter and the corresponding Appendix are largerly based on [27].

6.1 The matter sector

The quark-gluon vertex is arguably the single most important Greens function of QCD. It is expected to provide the mayority of strength needed to trigger the non-perturbative phenomena like dynamical chiral symmetry breaking and confinement, see [53] and references therein. Due to its supposed importance, it has been investigated on numerous occassions on the lattice and in functional approaches [25, 185, 187, 188, 197–201]. In the DSE framework, the most often used truncation to describe this interaction is the following:

$$\Gamma_\mu = \Gamma_\mu^{(0)} + \Lambda_\mu^{NA} + \Lambda_\mu^{AB} \ . \tag{6.1}$$

All terms depend on external momenta (p_1, p_2, p_3). We work with reduced vertices, e. g. $\Gamma_\mu^a = ig \cdot \mathbf{t}^a \Gamma_\mu$. The tree-level vertex is simply $\Gamma_\mu^{(0)} = Z_{1f}\gamma_\mu$, whereas Λ_μ^{NA} and Λ_μ^{AB} are, respectively, the non-Abelian and Abelian contributions to the self-energy.

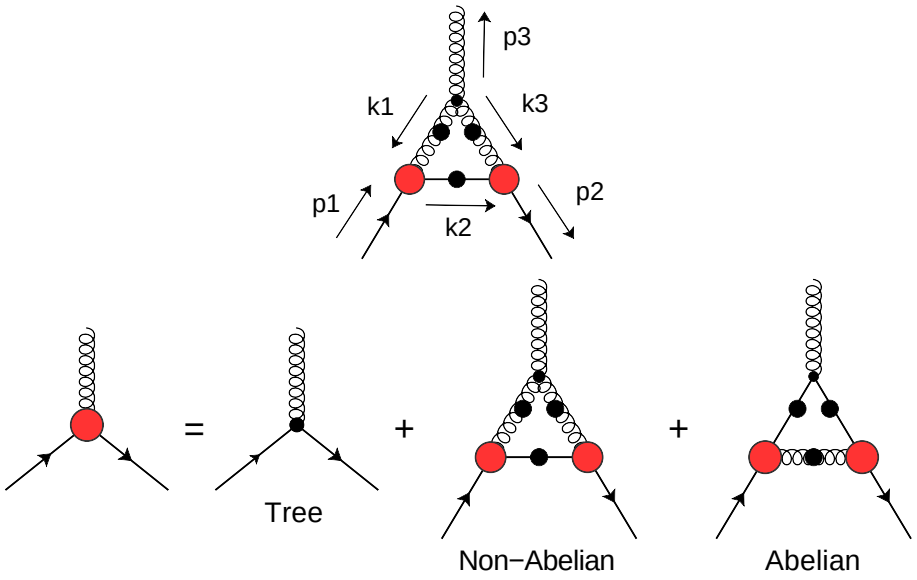

Figure 6.1: Truncated DSE for the quark-gluon interaction (*bottom*), with employed momentum conventions (*top*).

With momentum conventions as defined in the top panel of Figure 6.1, the self-energy diagrams take the form (see also the bottom panel of Fig. 6.1):

$$\Lambda_\mu^{NA}(p_1,p_2,p_3) = \frac{g^2 N_c}{2}\int_k \Gamma_\alpha(p_1,k_2,k_1)S(k_2)\Gamma_\beta(k_2,p_2,k_3)D_{\alpha\tau}(k_1)D_{\beta\sigma}(k_2)\Gamma^{(0)}_{\tau\sigma\mu}(k_1,k_3,p_3)\ ,$$
$$\Lambda_\mu^{AB}(p_1,p_2,p_3) = \frac{g^2}{2N_c}\int_k \Gamma_\alpha(k_1,-p_1,k_2)S(k_1)\Gamma^{(0)}_\mu(-k_1,k_3,p_3)S(k_3)\Gamma_\beta(-k_3,-p_2,-k_2)D_{\alpha\beta}(k_2)\ . \tag{6.2}$$

This particular approximation is usually employed since the non-Abelian and Abelian diagram are the only one-loop terms which do not contain non-primitively divergent vertex functions. One can partially account for the missing contributions by dressing all three vertices in loop diagrams, a truncation reminiscent of the 3PI formalism [70]. Keeping in mind the upcoming applications of the quark-gluon interaction in our study of bound states, we will make two additional simplifications.

The first simplification is that we neglect the Abelian diagram. From the standpoint of the quark-gluon DSE itself, this seems like a reasonable truncation since the Abelian loop is colour suppressed with respect to the non-Abelian one, and possibly kinematically suppressed as well, see [202] for the results on the scalar-gluon vertex. From the standpoint of the Bethe-Salpeter equation and its kernel, the inclusion of the Abelian loop would bring about the so-called crossed ladder exchange [181], a piece which significantly increases the technical difficulty (more on this in section 6.3) while apparently having no appreciable influence on meson masses [203]. This fact holds special weight in our calculation, since we will be judging the merits of our approach by comparing the results with those of lattice computations. As the said lattice results have uncertainites on the order of twenty percent, it seems unreasonable to invest a lot of effort in a diagram which, according to previous investigations, produces at most a few percent effect.

Before continuing, we wish like to point out that in this and the next section we will be working with arbitrary units, and any kind of unit denotation will be left out of the upcoming equations. The connection to physical scales will be established in section 6.4 by fixing f_π^{tc}. Our second simplification is considerably more severe than the first, and it amounts to a rainbow truncation inside the non-Abelian loop. The full quark-gluon vertices are replaced with their tree-level forms augmented by a model dressing which depends on gluon momentum alone:

$$\Gamma_\alpha(p_1, k_2, k_1) \to \lambda(k_1^2) \cdot \gamma_\alpha \ . \tag{6.3}$$

The connection to the fully self-consistent treatment is not completely lost, because the function $\lambda(k^2)$ is based on the tree-level projection of the calculated quark-gluon interaction. It is parametrised in the following way:

$$\lambda(k^2) = hZ_{1f} \left\{ \frac{L(M_0)}{1+y} + \frac{1}{1+z} \left[\frac{4\pi}{\beta_0 \alpha_\mu} \left(\frac{1}{\log(x)} + \frac{1}{1-x} \right) \right]^{18/44} \right\} \ . \tag{6.4}$$

The parameters are $h = 2.302,\ x = k^2/0.6,\ y = k^2/0.35,\ z = k^2/0.33,\ \beta_0 = 11N_c/3$, and $\alpha_\mu = 1.114$ at the renormalisation point $\mu^2 = 9$. The IR enhancement function $L(M_0)$ depends on the dynamical quark mass at zero momentum M_0. For fitting purposses we use the function

$$L(M_0) = \frac{a + bM_0 + cM_0^2}{M_0 + dM_0^2} \ . \tag{6.5}$$

The parameters of the fit are $a \approx 2.44,\ b \approx 1.79,\ c \approx -0.20$ and $d \approx 0.29$. Through $L(M_0)$, the model dressing $\lambda(k^2)$ is implicitly flavour-dependant, see [188]. In our calculation this does not have a great practical impact as we will only be working with chiral and very light quarks.

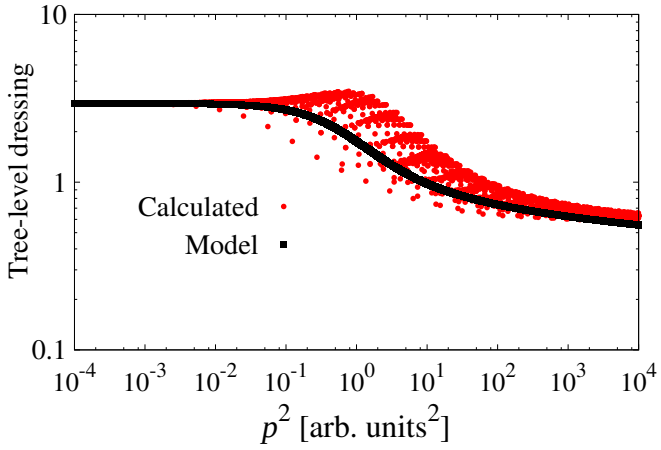

Figure 6.2: Comparison of the calculated quark-gluon vertex dressing and the model of Eq. (6.4), as functions of gluon momentum p^2. The angular spread in the calculated vertex comes from the fact that the object depends on additional momentum variables, see Eq. (6.2).

To demonstrate how (un)well the model function of equation (6.3) represents the actual tree-level dressing of the calculated vertex, we compare the two in Figure 6.2 (we will soon comment on how is the coupled system of quark and quark-gluon DSEs solved). As it depends on gluon momentum alone, the model λ cannot reproduce the angular dependence of the full vertex, but within these constraints it seems to do a decent job. In the context of bound state studies, the rainbow approximation of equation (6.3) is almost mandatory for several reasons. One is that, in Euclidean spacetime, the quark propagator and quark-gluon vertex have to be probed at complex momenta in order to be useful for investigations of hadronic observables. Solving the vertex DSE for real momenta alone is a formidable challenge already, whereas working on the timelike momentum axis raises the complexity to an even higher level. An additional detriment is that the fully self-consistent quark-gluon vertex implicitly depends on the quark propagator. Thus, when the cutting technique of equation (3.30) is employed, there will arise contributions in the BSE kernel which are much more difficult than anything we will consider here, see [90] for some examples of this in the 3PI approach. The truncated axWTI-preserving Bethe-Salpeter kernel in our simplified framework is given in Figure 6.3.

Now let us comment on the solution method for the coupled system of DSEs of the quark propagator and quark-gluon vertex. The quark DSE formally stays the same as in QCD, see equation (2.32). One practical difference is that the colour Casimir operator changes to 3/4 for an $SU(2)$ theory. As compared to simple rainbow-ladder treatments of sections 2.3 and 3.3, we now have to be more careful with the renormalisation procedure and our inputs for the quark-gluon vertex and other relevant Greens functions. We begin with the inverse quark propagator in Eq. (2.31), and project out the $A(p^2)$ and $B(p^2)$ components. In a symbolic notation, this gives us (cutoff dependence of renormalisation constants is left out):

$$A(p^2,\mu^2) = Z_2(\mu^2) + Z_{1f}(\mu^2)\Sigma_A(p^2,\mu^2)\ , \tag{6.6}$$

$$B(p^2,\mu^2) = Z_m(\mu^2)m + Z_{1f}(\mu^2)\Sigma_B(p^2,\mu^2). \tag{6.7}$$

Σ denotes the appropriate self-energies. With some help from the Slavnov-Taylor identitites of equation (2.29), we can express the quark-gluon renormalisation Z_{1f} in terms of the one for the quark field Z_2. In miniMOM scheme this relation takes a particularly simple form, with $Z_{1f} = Z_2/\tilde{Z}_3$. $\tilde{Z}_3$ is a part of our input for the gluon propagator, which is detailed in the next section. Here we only comment that we use a decoupling solution similar to the one of the previous Chapter, and that the renormalisation constant has the same value as already cited there, $\tilde{Z}_3 = 1.529$. The renormalisation for the three-gluon vertex is also unchanged compared

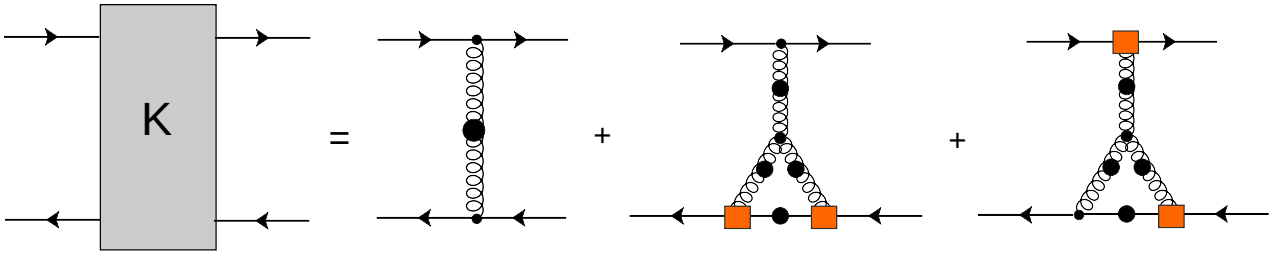

Figure 6.3: Approximated axWTI-preserving Bethe-Salpeter kernel. The 'full' quark-gluon vertices (orange squares) are modeled, see Eqs. (6.3) and (6.4).

to the QCD case, with $Z_1 = 2.213$. In the next section we comment on why we are allowed to simply transfer the Yang-Mills input from the QCD calculation to an $SU(2)$ one without any apparent changes. Since the gluon renormalisation remains a constant in the process of solving Eqs. (6.6) and (6.7), we absorb the factors of $1/\tilde{Z}_3$ into the self-energies. With a slight manipulation of equation (6.6), one then gets

$$\frac{1}{Z_2(\mu^2)} = \frac{1}{A(p^2,\mu^2)} + \frac{\Sigma_A(p^2,\mu^2)}{A(p^2,\mu^2)} \ . \tag{6.8}$$

By subtracting the above equation at $p^2 = \mu^2$ and using the renormalisation condition $A(\mu^2,\mu^2) = 1$, we arrive at

$$A(p^2,\mu^2) = \frac{1+\Sigma_A(p^2,\mu^2)}{1+\Sigma_A(\mu^2,\mu^2)} \ . \tag{6.9}$$

At each iteration step the $A(p^2)$ component is calculated from (6.9), and then used in the evaluation of quark field renormalisation in (6.8). With Z_2 specified, the $B(p^2)$ component follows as

$$\text{chiral limit :} \quad B(p^2,\mu^2) = Z_2(\mu^2)\cdot\Sigma_B(p^2,\mu^2) \ , \tag{6.10}$$

$$\text{non-chiral :} \quad B(p^2,\mu^2) = M(\mu^2) + Z_2(\mu^2)\left(\Sigma_B(p^2,\mu^2) - \Sigma_B(\mu^2,\mu^2)\right) . \tag{6.11}$$

In our approach we start with an initial guess for $A(p^2), B(p^2)$ and Z_2, and use these to evaluate the quark-gluon interaction Γ^μ first. The vertex is calculated at exactly those grid points for which it is used in the quark DSE, thus avoiding the need for interpolation. It takes 8 tensor structures to describe this three-point function in Landau gauge: we employ an orthonormal basis specified in Eq. (C.6). The coupled system of DSEs is iterated until mutual convergence. The ending result is shown in Figure 6.4.

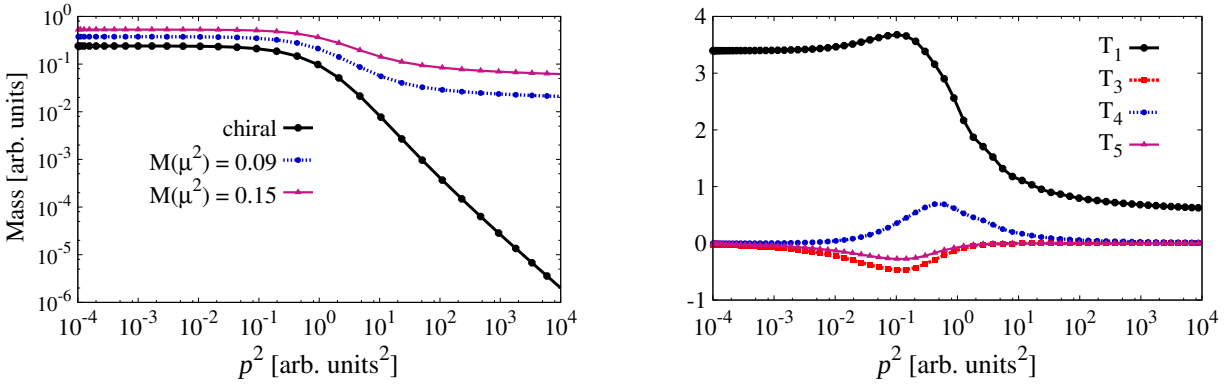

Figure 6.4: Quark propagators for several current quark masses (*left*) and the chiral quark-gluon vertex dressings $T_i(p^2, 2p^2, 3p^2)$ (*right*). The q-g basis is given in Eq. (C.6). T_2 and T_7 were left out as negligible, whereas T_6 and T_8 significantly overlap with T_1 and T_3 respectively.

To provide at least some sense of scale for the plots of Figure 6.4, we note that one arbitrary unit would roughly correspond to one GeV in QCD. All of the these calculations were also performed with the Abelian diagram included in the quark-gluon self-energy. We do not plot the results as they are virtually indistinguishable from the ones where the Abelian contribution is neglected. Finally, a remark is in place regarding the overall model dependence of our approach. Although it might not seem as such at a first glance, our calculation is highly constrained. Once the ghost/gluon input has been fixed and the truncation for the quark-gluon DSE chosen, all other parts of the computation are fixed by symmetry arguments. Admittedly, one still has some freedom in constructing the model dressing $\lambda(k^2)$ for the quark-gluon interaction, but this should be done so as to resemble the tree-level component of the full calculated vertex. Apart from the consideration of a fully self-consistent system, there are not many things which could be significantly altered or improved in our treatment. In order to at least partially assess the effect of missing contributions in the quark-gluon DSE, we will also employ a 3PI-inspired truncation where the three-gluon vertex will be dressed. Model for the three-gluon coupling will be based on the analysis done in the previous Chapter.

6.2 The Yang-Mills input

The decoupling ghost and gluon propagators used in our bound state calculations are shown in the left panel of Figure 6.5. In the right panel we plot the three-gluon interaction, evaluated for two different truncations of the corresponding DSE. In one model we keep only the ghost triangle diagram in the self-energy, while in the other we include all the one-loop terms with superficially divergent vertices. Only the tree-level tensor structure is employed. As already noted in section 5.3, with the former approximation one ends up with a vertex dressing which changes sign deep in the infrared region. Despite the simplicity of this truncation, we believe that it gives a function which is closer to the 'true' three-gluon vertex than the one resulting from a more elaborate treatment. This idea will be corroborated by some results which we will show here. However, before discussing the influence of different vertex models we would like to comment on the transition of the Yang-Mills input from a 'QCD' calculation of Chapter 5 to the $SU(2)$ case considered here.

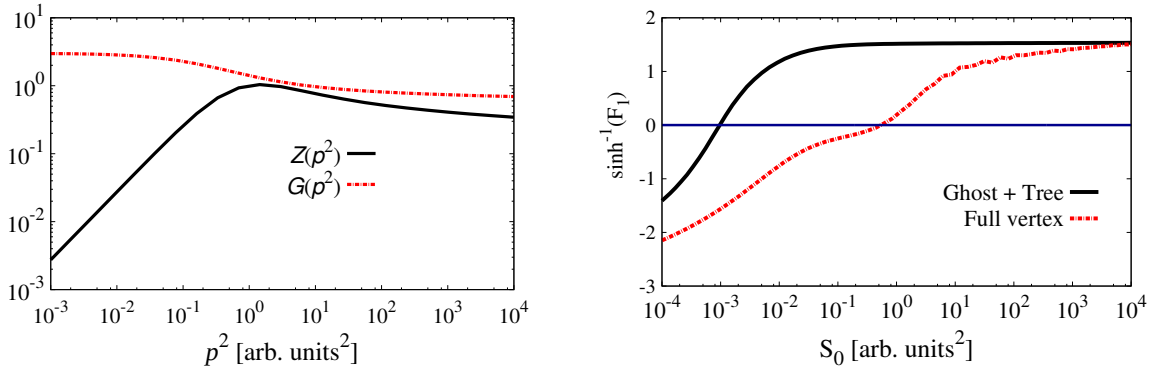

Figure 6.5: Yang-Mills propagators (*left*) and the models for the three-gluon vertex (*right*).

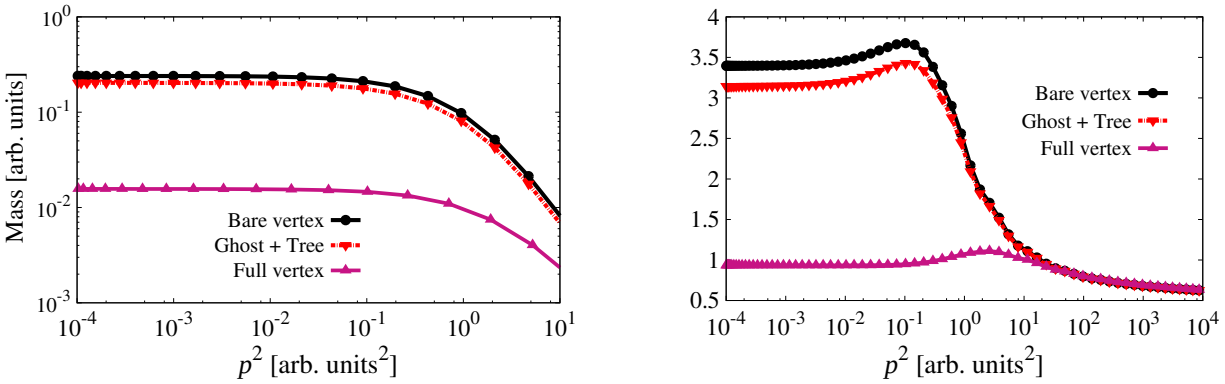

Figure 6.6: Influence of the three-gluon vertex model on the chiral limit quark propagator (*left*) and the leading component $T_1(p^2, 2p^2, 3p^2)$ for the quark-gluon interaction (*right*). The 'Full vertex' results are not converged: the quark mass would continue to collapse indefinitely, with little influence on vertex dressings.

In the ghost/gluon calculation of [22], only those diagrams were kept which are proportional to the product $g^2 N_c$. This practically means that the results are formally valid for any $SU(N_c)$ theory. Any changes in N_c can be compensated by a redefinition of the gauge coupling g^2 such that the above product stays the same. This is exactly the trick which we employ here. Accidentally, if the Abelian diagram is disregarded, the same argument holds for the truncated three-gluon and quark-gluon DSEs as well. As compared to a QCD calculation, the only thing which is different for an $SU(2)$ theory in our approach is the colour Casimir operator in the quark propagator DSE. It should thus not come as a surprise that many of our results for meson masses will resemble those of similar QCD evaluations, once the appropriate rescaling $f_\pi^{tc} \to f_\pi^{\rm qcd}$ is applied.

The influence of the three-gluon vertex models on the matter sector is shown in Figure 6.6. The model where only the ghost loop and tree-level terms are kept leads to moderate modifications of about 10 percent, which seems like a reasonable result. In stark contrast to this, the 'full' three-gluon vertex brings about drastic changes where there is virtually no chiral symmetry breaking in the quark DSE. This is yet another clue that the gluon three-point function is not well represented by our full solution of the previous Chapter. There is one interesting thing to note about this, however. By looking at these results one might start contemplating the idea that the 'strange' three-gluon coupling represents a possible way for the conformal phase to set in in a strongly interacting theory, as it leads to massless solutions for the quark in a rather non-trivial way. Any serious investigation along these lines would have to wait for unquenching effects to be included in the Yang-Mills sector in a reliable way.

As one of the final checks on the overall model dependence of our results, we wish to see how the three-gluon dressing affects the analytic properties of the quark propagator. We assess this by evaluating the Fourier transform of equation (2.34), both with a bare and a dressed three-gluon coupling. Understandably, we only consider the vertex model with a ghost loop included. The results are shown in Figure 6.7. One can see that the analytic structure looks almost the same in the two cases, and that the quarks are 'confined' within our model. The fact

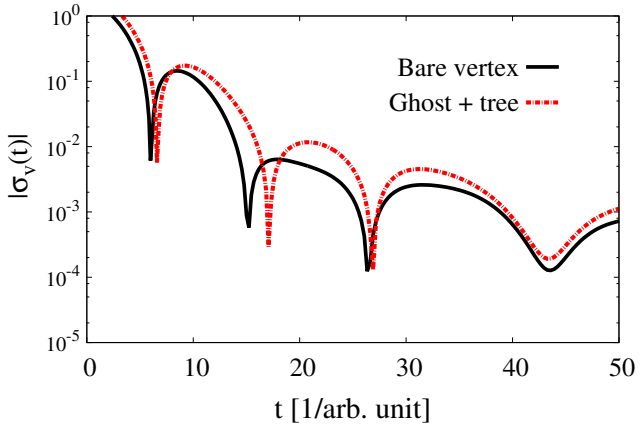

Figure 6.7: Influence of the three-gluon vertex dressing on the analytic structure of the quark propagator.

that the vertex dressing does not change the function $|\sigma_V(t)|$ appreciably is in accord with the main conclusions of [62], where it is suggested that it is only the differing tensor components in the quark-gluon interaction which can bring about significantly different results.

6.3 Numerical procedure

Although most of the technicalities related to this study are delegated to Appendix C, we will provide some basic details here. This is mostly to ease the interpretation of results to come. Firstly, we wish to comment on how we obtain the meson masses. We noted on several occasions that investigating bound states in Euclidean spacetime entails working with complex values for the total bound state momentum. This is not a big problem in principle owing to various well-established methods in the literature [192, 204–206]. One of these techniques, which is here applied for rainbow-ladder calculations, is also described in section C.1.

Apart from these, there are also approximate routines which allow one to gather limited information on the timelike P^2 axis by extrapolating from purely real P values [207, 208]. In our calculations we we will use one of these approximate approaches to alleviate the overall numerial effort. Either the homogeneous or vertex Bethe-Salpeter equations, given by (3.25) and (3.28), respectively, can be used for extrapolations. To test these methods, we compare them with the 'exact' computation in rainbow-ladder (RL) framework, where results in the complex plane can be obtained without too much trouble. Our RL setup in QCD is identical to the one in [61] for Maris-Tandy interaction. When using the homogeneous equation, instead of working directly with the eigenvalue λ, it is advantageous to introduce the function [79]:

$$g(\lambda) = 1 - \frac{1}{\lambda} \,. \tag{6.12}$$

The solution of the homogeneous BSE then corresponds to $g(\lambda) = 0$. We extrapolate from the spacelike P^2 axis by first transforming the data with $g(\lambda)$, and afterwards performing a

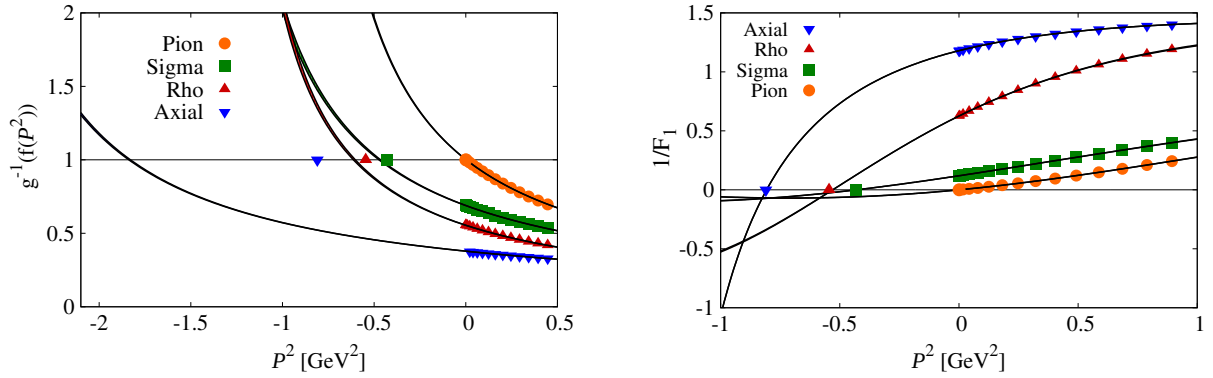

Figure 6.8: The eigenvalue (*left*) and inverse vertex (*right*) extrapolation for meson masses, compared to the 'exact' complex plane calculation in rainbow-ladder QCD.

linear fit $f(x) = a + b \cdot x$, with $x = P^2$. Finally, we go back to the original eigenvalue with the inverse function $\lambda_{\text{fit}} = g^{-1}\left(f(P^2)\right)$ and look where the resulting curves intersect the $\lambda = 1$ line. The results are shown in the left panel of Figure 6.8, where they are also compared to an exact (complex plane) calculation. It is quite evident that, except for the very lightest states, the method performs rather poorly. An alternative is to use the inhomogeneous BSE, and look for zero crossings in either of the inverse dressing functions $1/F_i(P^2)$ (relative momentum is set to zero for convenience). If the method is used for extrapolations, the following fit functions (sometimes wrongly referred to as 'Pade approximations') have proven to be useful::

$$R^{(n,m)}(x) = \frac{\sum_{i=0}^{n} a_i x^i}{1 + \sum_{i=1,m} b_i x^i} \,. \tag{6.13}$$

The results of this procedure with $R^{(2,2)}$ are shown in the right panel of Figure 6.8 and in Table 6.1. One can see that the technique gives surprisingly good results, even for the relatively heavy 1^{++} meson. The error bars cited in the Table come from the uncertainties for the fitting coefficients a_i, b_i in equation (6.13). These will also be included in our upcoming calculation of $SU(2)$ hadrons. One should keep in mind that there is an additional source of errors, which

J^{PC}	calc	$R^{(2,2)}$ $(L = 0.5)$	$R^{(2,2)}$ $(L = 1.0)$
0^{-+}	0	1	1
0^{++}	658	657(23)	656(23)
1^{--}	738	731(27)	728(27)
1^{++}	900	899(33)	899(33)

Table 6.1: Results of inverse vertex extrapolation for chiral-limit QCD in rainbow-ladder, compared with the results of direct analytic continuation. All units are in MeV. The points P^2 are taken from the region $(0, L)$; cited errors come from the fitting procedure.

is related to the reliability of the extrapolation method itself. One would expect that any extrapolation approach becomes less trustworthy as one probes deeper into the timelike P^2 region, and thus the results for heavy mesons are less reliable that for the light ones. This error is much harder to evaluate, and we will not even attempt to do so here. Based on our results for the inverse vertex procedure, it is probably safe to say that for the bound states which we consider these uncertainties are among the smaller effects, and for most practical purposes they can be neglected.

It is worth noting that hadron masses are the only quantities which can be obtained in this approximate way. All other observables (form factors, decay widths) require the explicit calculation of bound state amplitudes Γ_i. Fortunately for us, except masses we only need one additional observable for scale-setting purposes, and this is the pion decay constant. In the chiral limit f_π can be obtained exactly without leaving the spacelike P^2 axis, and thus it does not introduce any additional errors into the calculation. The decay constant is calculated according to equation (3.31).

We are however not yet done with simplifications. From the kernel diagrams of Figure 6.3 one can see that the full BSE evaluation is a two-loop endeavor, and therefore computationally quite demanding. We reduce this to a one-loop effort by employing interpolation, as shown schematically in Figure 6.9. A part of the diagram (which is anyway almost identical to the quark-gluon vertex) is calculated prior to any bound state computations, and it is then included in the BSE via interpolation. The details on the interpolation procedure are provided in section C.2. This is the main reason why we have refrained from including the Abelian diagram in the quark-gluon vertex DSE. Among other things, it would bring about the crossed-ladder exchange in the bound state equation, and the non-planar topology of that diagram makes the above trick inapplicable.

In order to test how this procedure affects our results, we have compared it with the exact (two-loop) calculation at a single point $P^2 = 0$. In this limit the kinematics greatly simplifies, and even the two-loop computation becomes numerically cheap. For all mesons except the pion, we found very small deviations between the two sets of results, on the order of a few permil. We will thus completely ignore the error coming from this approximation in the following discussions. The pion is the only state which is significantly influenced by the method. This is not a problem, since the masslessness of the pion in the chiral limit can be checked by other means. It is enough to perform a single two-loop calculation, in the homogeneous BSE approach, at the point $P^2 = 0$. One can then check if the returned eigenvalue is close to unity:

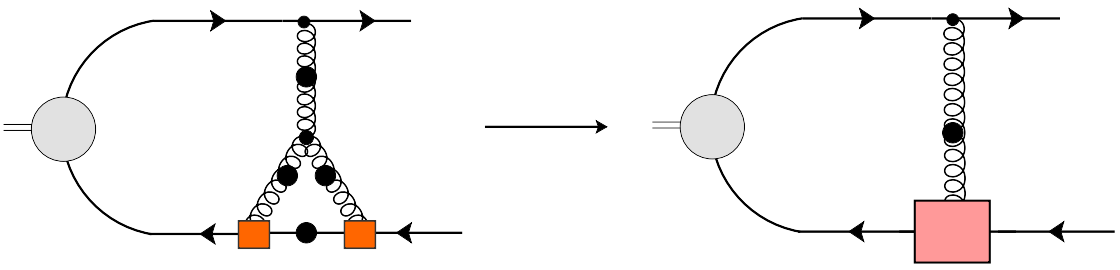

Figure 6.9: Sketch of an important approximation for the BSE. Part of the diagram is pre-calculated, stored and included in the bound-state equation via interpolation.

we have confirmed that it is, with $\lambda = 0.99998$. We are thus confident in citing the pion as 'exactly' massless in our approach.

One might have noticed that our truncations are slowly piling up. We have first neglected the Abelian contribution in the quark-gluon DSE, then abandoned the complex-plane evaluation of masses in favor of extrapolation from the spacelike P^2, and now we have additionaly introduced interpolation to render the computation easier. We believe that all these simplifications are justified if one keeps in mind our final aim. As stated before, we will judge the validity of our approach by comparing it with lattice calculations which have error bars on the order of twenty percent. We thus find our approximations reasonable, as the associated uncertainties are still well below the limit set by lattice results.

6.4 Ground state mesons

Our results for meson masses, in both rainbow-ladder and BRL settings, are shown and compared with lattice computations in Table 6.2. The scale is set by demanding $f_\pi = 246$ GeV. As there are yet no reliable lattice results for the σ meson, we will use an estimate based on group theory scaling arguments, with $m_\sigma \in [1, 1.5]$ TeV [108]. Unlike the situation in chromodynamics, it seems that RL performs rather well for the scalar particle, but considerably less so for the ρ meson. The axial-vector channel is equally badly described in both theories. Thus, despite the fact that the model in question is dynamically similar to QCD, the main conclusions on our results in the RL framework cannot be straightforwardly transfered between the two. This is a good example for our previous statements that rainbow-ladder approach itself cannot be simply applied to an arbitrary non-Abelian gauge theory and expected to perform as it would in QCD.

As for the BRL setting, it is hard to make definitive statements as there are considerable uncertainties present in both lattice and continuum studies, but it seems that the results are moving in the right direction. This is especially true if one employs the dressed three-gluon vertex (of course, we use a model with only the tree-level and ghost-triangle terms). What specifically captures the eye with regards to the influence of the three-gluon coupling is that using the non-perturbative version does not bring about a big difference in the results. This is perhaps unsurprising if one keeps in mind the relatively small changes introduced to the quark propagator and quark-gluon vertex in Fig. 6.6. This is quite encouraging as it points to a possibilty that more elaborate truncation schemes for the quark-gluon interaction (e. g.

J^{PC}	RL	BRL, bare 3g vertex	BRL, dressed 3g vertex	Lattice, from [29, 30]
0^{-+}	0	0	0	–
0^{++}	1.24	1.39(6)	1.33(6)	–
1^{--}	1.95	2.27(9)	2.36(8)	2.5 ± 0.5
1^{++}	2.36	2.87(10)	3.08(10)	3.3 ± 0.7

Table 6.2: Chiral limit results for meson masses in rainbow-ladder (RL) and beyond rainbow-ladder (BRL) frameworks, compared with lattice data for an $SU(2)$ gauge theory. All units are in TeV. Errors of the BRL results come from the extrapolation procedure.

the inclusion of the Abelian loop, or even a partial consideration of two-loop effects) might also not alter the results significantly. Thus even our approach, which is arguably the simplest improvement over the rainbow-ladder treatment one can make, might turn out to be sufficient for most practical purposes (see however [28] for the results on mesons and baryons in QCD in the same formalism, where the improvements over rainbow-ladder are not so clear-cut).

The σ meson (the Higgs boson of Technicolor) is an order of magnitude heavier than it should be based on experimental observations. This is a completely expected result for a QCD-like theory with $f_\pi^{tc} = v_{EW}$. As stated before, the large discrepancy might be partially remedied by explicitly considering the influence of the electroweak gauge sector [108], and/or adding fermionic matter to bring the theory closer to the conformal window. When citing conformal dynamics as a possible solution of these problems, one should not forget that both the hadronic masses and decay constants are supressed near the phase transition. Thus, if f_π^{tc} is always used to set the scale of the calculation, the walking behaviour might bring some improvement, as the results of [128, 130] suggest, but almost surely not enough to give a composite Higgs boson with a mass of just 126 GeV. It is probably a combination of multiple effects which will have to be included to arrive at phenomenologically truly acceptable Technicolor models.

In addition to chiral-limit results in the above Table, we also performed a few calculations with finite current quark masses. A particularly important check on our numerical procedure is to test if the Gell-Mann-Oakes-Renner (GMOR) relation [209] is satisifed. For two degenerate quarks with current mass m_q, the GMOR equality takes the form

$$m_\pi^2 = \frac{2m_q}{f_\pi^2}\langle\bar{q}q\rangle \ . \tag{6.14}$$

In this expression both the decay constant and the chiral condensate $\langle\bar{q}q\rangle$ ought to be evaluated in the chiral limit. For our checkup purposes the actual proportionality constant is irrelevant and we simply wish to demonstrate that $m_\pi^2 \sim m_q$ close to the chiral point. This is

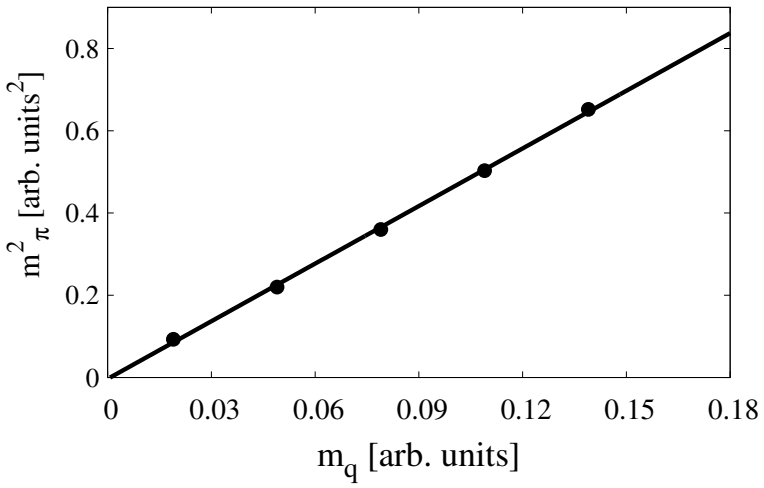

Figure 6.10: Numerical check of the GMOR relation in equation (6.14).

shown in Figure 6.10. The fact that the linear fit indeed describes the data points well tells us that our numerical method preserves the chiral dynamics to a high degree. Note that in our approach it is the dynamical quark mass $M(\mu)$, and not the current one m_q, which is used to specify the corresponding renormalisation condition, see equation (6.7). This is not an issue since m_q can always be extracted from the data, but if one forgets to make this adjustment the linear fit of Figure 6.10 would miss the origin by a considerable amount.

In Figure 6.11 we show how the masses of spin one mesons changes as the current quark mass is increased. With a vertical line we indicate a region where the decay mode $\rho \to \pi^+\pi^-$ becomes impossible as the pion is too heavy, with $2m_\pi \geq m_\rho$. This decay channel is of particular importance for Technicolor phenomenology as it is directly related to the process $\rho \to W^+W^-$: in unitarity gauge the technipions are nothing more than longitudinal polarisation states for the Ws. Unfortunately, reliable predicitions about these kinds of phenomena are hard to make for both functional and lattice methods. In continuum approaches the kinematics involved implies that even the relative momentum p^2 in the Bethe-Salpeter amplitude of Eq. (3.25) needs to be evaluated in the complex plane, which brings forth numerous complications, see [210] and references therein. In case of lattice studies, it is hard to perform simulations close to the chiral point, and as our estimate in Figure 6.11 shows, one needs to go to quite small current quark masses to be even able to see this specific decay channel. It thus appears that it will take quite some time for this highly coveted process to be investigated appropriately. As for the spin one meson mass dependencies themselves, our results are seemingly in good agreement with those of [30], but to make any certain statements about this we would have to make sure that our m_qs agree with those used on the lattice.

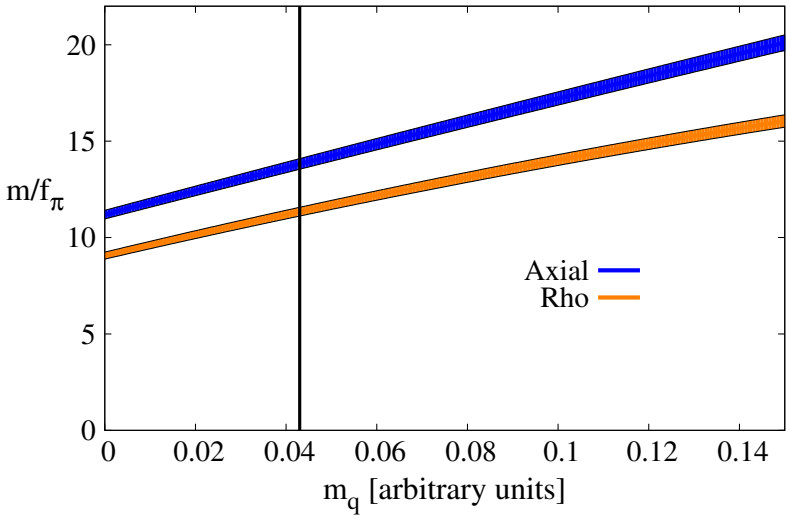

Figure 6.11: Spin one meson masses (in units of chiral f_π) as a function of current quark mass. Bands come from extrapolation uncertainties. To the right of the vertical line is a region where $2m_\pi \geq m_\rho$.

We finally wish to comment on the status of the enhanced flavour symmetry in our framework. The degeneracy of J^P mesons with J^{-P} diquarks has been checked in several lattice computations [29, 30, 135, 137, 138]. In the DSE/BSE formalism, working with diquarks entails the following change in the bound state equation:

$$\Gamma\left(P,p\right)_D = \int_k S\left(k_-\right)\Gamma\left(P,k\right)_D \left(S\left(-k_+\right)\right)^T K\left(P,p,k\right) \ . \tag{6.15}$$

In the above expression T denotes a matrix transpose. It would be perhaps unreasonable to expect that the above manipulation will bring about a scalar diquark equation which is consistent, in the axWTI-sense, with the truncated quark DSE. We have indeed explicitly checked, in the rainbow-ladder treatment, that there are no massless scalar diquarks present and thus the Pauli-Gürsey symmetry is explicitly broken. It would probably be quite hard, if not impossible, to come up with an approximation scheme in the continuum which would respect both the constraints of chiral dynamics and those of the enhanced flavour relations.

Chapter 7

Conclusions and outlook

The combined formalism of Dyson-Schwinger and Bethe-Salpeter equations (DSEs/BSEs) offers a powerful and versatile framework for the investigation of both the fundamental building blocks of strongly interacting theories, as well as their influence on hadronic bound state observables. In this thesis we have put the formalism to use by first exploring the three-gluon vertex as a simple Greens functions which describes the self-interaction of the gluon field. Our aim in this was to advance the general knowledge of QCD by studying one of its superficially divergent vertex functions, but also to obtain a possibly useful tool for probing bound states. We demonstrated that the tree-level term is the dominant one, with the sub-leading components contributing at most at a ten percent level: for modelling purposes it is thus probably safe to neglect them. For the uniform infrared limit we obtained the expected behaviour for both scaling and decoupling solutions, and have shown that the soft collinear divergences manifest themselves in the sub-dominant terms, while being mostly absent in the tree-level projection. This curious fact remains to be fully explained.

Despite our attempts to include as many pieces into this calculation as practicality would allow, there are clear signs that our treatment suffers from considerable deficiencies. These are most probably connected to our insufficient knowledge of the gluon four-point function, as well as the missing higher loop terms and diagrams with fermions. Some of these missing contributions (mostly related to the two-loop terms of the pure ghost-gluon sector) can be partially accounted for in a relatively simple way, and we are looking forward to including them in forthcoming studies. The ongoing functional investigations of the quark-gluon interaction will probably enable the inclusion of unquenching effects as well in a foreseeable future.

In our studies of hadrons we have mostly relied on chiral symmetry as a guideline when making truncations of relevant equations. Satisfaction of the corrresponding constraints gurantees the massless pions in the chiral limit, and in general greatly helps with the description of light meson spectrum. The simplest approximation consistent with the demands of chiral symmetry, the rainbow-ladder, has proven to be relatively successful in QCD phenomenology of mesons and baryons. We have, however, found it to be inadequate in an $SU(2)$ gauge theory, a strongly interacting template in which we are interested in as a possible unified description of dynamical electroweak symmetry breaking and Dark Matter. We believe that the biggest reason for the relatively poor performance of RL treatment has to do with its weak connection to the underlying gauge sector. To remedy some of these shortcomings we employed a more elaborate truncation scheme based on the diagrammatic expansion of the quark-gluon vertex DSE. Our results show a significant improvement over RL when compared to relevant lattice

computations.

Through the quark-gluon interaction, the three-gluon coupling also enters the bound state studies. We have found it to have an impact of about ten percent on meson masses, and in general it brings the results closer to lattice evaluations. These conclusions, however, heavily depend on the employed model for the three-gluon vertex: if the full solution of our DSE treatment is used, it brings about, in our approach, the 'trivial' quark propagator and quark-gluon vertex which have virtually none of the chirally-breaking components. This is another signal that there are important contributions missing in our approach to the gluon three-point function.

While we have here concentrated solely on masses and a pion decay constant for scale-setting purposes, there are many other interesting things left to study in these strongly-interacting templates, like the hadronic form factors and decay processes. In the context of Technicolor phenomenology, a particularly important decay channel is the $\rho \to \pi^+\pi^-$, which is directly related to the $\rho \to W^+W^-$ reaction. One should keep in mind that these are very demanding investigations, however, especially in the beyond rainbow-ladder setting, and that it will take some time to completely set up the formalism. In addition to this, in the future we would also like to eventually include the unquenching effects for both fundamental and phenomenological reasons. This would enable us to see how the conformal phase transition influences the Greens functions and hadronic observables of strongly interacting theories. While our bound state formalism would not change much in comparison to purely QCD-like models, the first and foremost challenge for these kind of investigations remains to reliably solve the coupled system of DSEs for the quark and Yang-Mills propagators and the quark-gluon vertex. We are looking forward to contributing to these endeavors.

Appendix A

Utilities

A.1 Euclidean conventions

Throughout we use the standard conventions for Euclidean spacetime, with a generic four-vector p in the form $p = (p_1, p_2, p_3, p_4)$, and the definitions

$$p \cdot q = \sum_{k=1}^{4} p_k q_k, \quad \not{p} = p \cdot \gamma, \quad \{\gamma^\mu, \gamma^\nu\} = 2\delta^{\mu\nu}, \quad (\gamma^\mu)^\dagger = \gamma^\mu. \tag{A.1}$$

A vector is said to be spacelike and timelike if $p^2 > 0$ and $p^2 < 0$ respectively. Additionally, we use

$$\sigma^{\mu\nu} = -\frac{i}{2}[\gamma^\mu, \gamma^\nu], \quad \gamma^5 = -\gamma^1\gamma^2\gamma^3\gamma^4 = -\frac{1}{24}\varepsilon^{\mu\nu\rho\tau}\gamma^\mu\gamma^\nu\gamma^\rho\gamma^\tau. \tag{A.2}$$

For the γ matrices we employ the Dirac basis, with

$$\gamma^k = \begin{pmatrix} 0 & -i\sigma^k \\ i\sigma^k & 0 \end{pmatrix}, \quad \gamma^4 = \begin{pmatrix} \mathbf{1} & 0 \\ 0 & -\mathbf{1} \end{pmatrix}, \quad \gamma^5 = \begin{pmatrix} \mathbf{1} & 0 \\ 0 & -\mathbf{1} \end{pmatrix}. \tag{A.3}$$

The charge conjugation operator is given by

$$C = \gamma^4\gamma^2, \quad C^\dagger = C^T = C^{-1} = -C. \tag{A.4}$$

The four-momenta are represented in terms of hyperspherical coordinates:

$$p = \sqrt{p^2}\begin{pmatrix} \sin\psi\sin\theta\sin\phi \\ \sin\psi\sin\theta\cos\phi \\ \sin\psi\cos\theta \\ \cos\psi \end{pmatrix} = \sqrt{p^2}\begin{pmatrix} z'y'w' \\ z'y'w \\ z'y \\ z \end{pmatrix}, \tag{A.5}$$

where we used the notation $z' = \sqrt{1-z^2}$, and similarly for y and w. In terms of these coordinates the four-dimensional momentum integration takes the form

$$\int_k = \int \frac{d^4k}{(2\pi)^4} = \frac{1}{(2\pi)^4}\frac{1}{2}\int_0^\infty dk^2 k^2 \int_{-1}^{+1} dz\sqrt{1-z^2}\int_{-1}^{+1} dy \int_{-1}^{+1} \frac{2dw}{\sqrt{1-w^2}}. \tag{A.6}$$

In this setup the w and z variables are ideally suited for the Chebyshev grids of the first and second kind respectively, see next section. In Euclidean spacetime, the generating functional of an arbitrary quantum field theory is expressed as

$$Z = \int \mathcal{D}\varphi e^{-\left(S[\varphi]+\int_x \varphi(x)J(x)\right)}, \tag{A.7}$$

while a generic n-point vertex function is derived as

$$G(x_1 \dots x_n) = \frac{(-1)^n \delta^n}{\delta J(x_1) \dots \delta J(x_n)} \frac{Z[J]}{Z[0]}\Big|_{J=0}. \tag{A.8}$$

A.2 Chebyshev expansion

In many of our calculations it is very convenient to take care of the angular dependence of vertex dressing functions by performing a Chebyshev expansion. If we concentrate only on the angular part, we can write

$$f(z) = \sum_{j=0}^{N_{ch}} a_j T_j(z), \tag{A.9}$$

where $z \in [-1, 1]$, $T_j(z)$ are Chebyshev polynomials of the first kind (we could have used the second kind just as well), and a_j are the appropriate expansion coefficients. In principle, one should take infinitely many terms into consideration, with $N_{ch} \to \infty$. In practice, it is enough to approximate the above expression with a finite and relatively small number of Chebyshev moments: in our computations we never needed terms higher than $N_{ch} = 7$ to adequately describe the angular variation. Note that the expansion of equation (A.9) starts with the zeroeth moment and thus $N_{ch} = 7$ actually corresponds to first 8 polynomials being present in the decomposition. The fact that it takes a relatively small number of Chebyshev basis functions to describe the function $f(z)$ sufficiently well is one of the main reasons why the above procedure is useful. It saves both the computational time and storage space when compared to calculations where one works directly with the angular grid z_k, where it usually takes at least 12 points to obtain good results. Another advantage of the Chebyshev expansion is that it replaces the dependence on discrete points z_k with the dependence on continuous functions $T_j(z)$. This is of importance if a relatively high precision is required, for instance if there should occur certain delicate cancellations in the angular integrals. As noted earlier, both the Chebyshev polynomials of the first and the second kind can be used for these manipulations. We shall now provide some basic formulas needed when working with these objects.

The Chebyshev polynomials of the **first kind** are given in the trigonometric form as

$$T_n(z) = \cos(n \arccos(x)). \tag{A.10}$$

They satisfy the orhtogonality relation

$$\int_z dz \frac{T_n(z) T_m(z)}{\sqrt{1-z^2}} = \begin{cases} 0 & : n \neq m \\ \pi & : n = m = 0 \\ \pi/2 & : n = m \neq 0 \end{cases}. \tag{A.11}$$

When working with these polynomials it is very useful to take the angular grid points z_k as roots of $T_n(z)$:

$$z_k = \cos\left(\frac{2k+1}{2n}\pi\right), \quad k = 0 \ldots n. \tag{A.12}$$

In the above expression n should be at least $N_{ch} + 1$ (e. g. if one is working with 8 polynomials in total, then there should be at least 9 angular points). The use of the grid defined by equation (A.12) is advantageous for any integrations with the measure $dx/\sqrt{1-x^2}$, for an example, the w integral in Eq. (A.6).

The trigonometric form for the Chebyshev polynomials of the **second kind** is

$$U_n(\cos(x)) = \frac{\sin((n+1)x)}{\sin x}. \tag{A.13}$$

The corresponding orthogonality relation is

$$\int_z dz\sqrt{1-z^2}U_n(z)U_m(z) = \begin{cases} 0 & : n = m = 0 \\ \pi/2 & : n = m \neq 0 \end{cases}. \tag{A.14}$$

For the evaluation of the above integral it is highly recommended to use grid points z_k which are zeroes of $U_n(z)$:

$$z_k = \cos\left(\frac{k+1}{n+1}\pi\right), \quad k = 0 \ldots n. \tag{A.15}$$

As in the case of the Chebies of the first kind, n should be at least $N_{ch}+1$. The grid points of Eq. (A.15) are well suited for all integrals with the measure $dx\sqrt{1-x^2}$, as is the z integral in equation (A.6). While in principle the $T_n(z)$ and $U_n(z)$ are equally useful for polynomial expansion of vertex dressing functions, in most cases we have found the Chebies of the second kind to be slightly superior in terms of grid sizes needed for a faithful representation of angular dependencies. And while the exact numbers varied from one investigation to the other, we have always found it to be sufficient to terminate the series expansion at most at $N_{ch} = 7$.

Appendix B

Basis construction and numerics for three-gluon vertex

B.1 Bose-symmetric basis

In this section we will describe a way to construct a tensor basis for the three-gluon vertex which makes its Bose symmetry manifest. We will rely heavily on the fact that the only colour factor which seems to be relevant for this vertex is the totally antisymmetric structure f^{abc}. The methods which will be shown here can easily be adapted to the symmetric combination d^{abc} as well. Due to the antisymmetry property of f^{abc}, the tensor part should also change sign when any two momenta and their corresponding indices swap places, i. e. we should have

$$\Gamma_{\mu\nu\rho}(p_1,p_2,p_3) = -\Gamma_{\nu\mu\rho}(p_2,p_1,p_3) = \Gamma_{\nu\rho\mu}(p_2,p_3,p_1), \quad \text{etc.} \tag{B.1}$$

A convenient way to construct a basis which satisfies the above criterion is to use permutation group analysis. In the following we briefly describe how to construct product representations of the permutation group S_3. Let us start with a generic function of three four-momenta $\psi(p_1,p_2,p_3)$: it can be a Lorentz scalar, a four-vector or a tensor basis element. We define the following combinations which are (anti)symmetric under the interchange of indices 1 and 2:

$$\begin{aligned}
\psi_1^{\pm} &= \psi(p_1,p_2,p_3) \pm \psi(p_2,p_1,p_3) \ , \\
\psi_2^{\pm} &= \psi(p_2,p_3,p_1) \pm \psi(p_1,p_3,p_2) \ , \\
\psi_3^{\pm} &= \psi(p_3,p_1,p_2) \pm \psi(p_3,p_2,p_1).
\end{aligned} \tag{B.2}$$

The above combinations are obtained from $\psi(p_1,p_2,p_3)$ by applying the permutation operators:

$$1 \pm P_{12}, \quad P_{31}P_{12} \pm P_{23}, \quad P_{32}P_{21} \pm P_{13} \ . \tag{B.3}$$

The operators P_{ik} act on momentum indices, for example $P_{31}P_{12}\psi(p_1,p_2,p_3) = \psi(p_2,p_3,p_1)$. The combinations of Eq. (B.2) can be arranged into the S_3 group multiplets:

$$
\begin{aligned}
S &= \psi_1^+ + \psi_2^+ + \psi_3^+ \ , \\
A &= \psi_1^- + \psi_2^- + \psi_3^- \ , \\
\mathcal{D}_1 &= \begin{bmatrix} \psi_2^- - \psi_3^- \\ -\frac{1}{\sqrt{3}}(\psi_2^+ + \psi_3^+ - 2\psi_1^+) \end{bmatrix} \ , \\
\mathcal{D}_2 &= \begin{bmatrix} \frac{1}{\sqrt{3}}(\psi_2^- + \psi_3^- - 2\psi_1^-) \\ \psi_2^+ - \psi_3^+) \end{bmatrix} .
\end{aligned} \tag{B.4}
$$

S and A are respectfully symmetric and antisymmetric under the interchange of momenta, while $\mathcal{D}_i$ transform as doublets. By using the properties of permutation operators $P_{ik} = P_{ki}, P_{ik}^2 = 1$ and $P_{ij}P_{jk} = P_{jk}P_{ki} = P_{ki}P_{ij}$ (no summation is implied), it is straightforward to show that $\mathcal{D}_i$ transform according to the following rules:

$$
\begin{aligned}
P_{12}\mathcal{D}_i &= \mathrm{M}\mathcal{D}_i, \quad & P_{13}P_{12}\mathcal{D}_i &= \mathrm{M}\mathrm{M}_+\mathcal{D}_i, \\
P_{13}\mathcal{D}_i &= \mathrm{M}_+\mathcal{D}_i, \quad & P_{23}P_{12}\mathcal{D}_i &= \mathrm{M}\mathrm{M}_-\mathcal{D}_i, \\
P_{23}\mathcal{D}_i &= \mathrm{M}_-\mathcal{D}_i. & &
\end{aligned} \tag{B.5}
$$

The orthogonal matrices M and $\mathrm{M}_\pm$ are given by

$$
\mathrm{M} = \begin{pmatrix} -1 & 0 \\ 0 & 1 \end{pmatrix}, \quad \mathrm{M}_\pm = \frac{1}{2}\begin{pmatrix} 1 & \pm\sqrt{3} \\ \pm\sqrt{3} & -1 \end{pmatrix}. \tag{B.6}
$$

The six operators of Eq. (B.3) exhaust all possibilities to permute any three elements. Note that the doublets $\mathcal{D}_1$ and $\mathcal{D}_2$ transform in the same way under all rotations. The next step is to form product representations. We denote a generic doublet by:

$$
\mathcal{D} = \begin{bmatrix} a \\ s \end{bmatrix}. \tag{B.7}
$$

A symmetric singlet in the product space can be formed in the following way:

$$
\mathcal{D} \cdot \mathcal{D}' = aa' + ss', \quad SS', \quad AA' \ . \tag{B.8}
$$

The fact that the inner product $\mathcal{D}\cdot\mathcal{D}'$ transforms as a symmetric singlet follows immediately from the orthogonality of matrices of Eq. (B.6). Antisymmetric singlets can be obtained in the product space as:

$$
\mathcal{D} \times \mathcal{D}' = as' - sa', \quad SA \ . \tag{B.9}
$$

The antisymmetry of $\mathcal{D} \times \mathcal{D}'$ can be easily shown as follows. Let $O = \left(\begin{smallmatrix} p & t \\ q & u \end{smallmatrix}\right)$ denote any orthogonal matrix of Eq (B.5) (it is either $\mathrm{M}, \mathrm{M}_\pm$ or their product). Then we have

$$
(O\mathcal{D}) \times (O\mathcal{D}') = (pu - tq)(as' - sa') = -(as' - sa') \ . \tag{B.10}
$$

The most general construction principle will also involve two-dimensional product representations: apart from the trivial combination $S\mathcal{D}$ one can also have

$$
\mathcal{D} * \mathcal{D}' = \begin{bmatrix} as' + sa' \\ aa' - ss' \end{bmatrix}, \quad \mathcal{D} * A = \begin{bmatrix} s \\ -a \end{bmatrix} \ . \tag{B.11}
$$

This exhausts all possibilities which we will need in the following. We begin the construction of Bose-symmetric basis by grouping the Lorentz invariants into the multiplet structure of Eq. (B.4). Taking into account the momentum conservation $p_1 + p_2 + p_3 = 0$, a total of three Lorentz invariants are needed to uniquely specify the four-vectors p_1, p_2 and p_3. We choose to work with invariants p_1^2, p_2^2 and p_3^2 and take $\psi(p_1, p_2, p_3) = p_3^2$ as the permutation group 'seed'. This results in:

$$\begin{aligned} S &= 2(p_1^2 + p_2^2 + p_3^2) \ , \\ \mathcal{D}_1 &= \begin{bmatrix} a \\ s \end{bmatrix} = -2 \begin{bmatrix} (p_2^2 - p_1^2) \\ \frac{1}{\sqrt{3}}(p_1^2 + p_2^2 - 2p_3^2) \end{bmatrix} . \end{aligned} \tag{B.12}$$

A and $\mathcal{D}_2$ are zero. We actually choose a sligthly different normalisation and work with the invariants (a and s were divided by S_0 to make them dimensionless):

$$\begin{aligned} S_0 &= \frac{1}{6}(p_1^2 + p_2^2 + p_3^2) \ , \\ a &= \sqrt{3}\frac{p_2^2 - p_1^2}{p_1^2 + p_2^2 + p_3^2}, \quad s = \frac{p_1^2 + p_2^2 - 2p_3^2}{p_1^2 + p_2^2 + p_3^2} \ . \end{aligned} \tag{B.13}$$

We now employ the same procedure for the tensor basis. A complete, linearly independent tensor basis (with 14 elements in total) can be generated by applying the permutation operators to the following six seed elements (permutations are understood to act both on the four-momentum $\{i, j, k\}$ and Lorentz indices $\{\mu, \nu, \rho\}$):

$$\begin{aligned} \psi_1^{\mu\nu\rho} &= \frac{1}{2}\delta^{\mu\nu} q_3^\rho \ , \quad & \psi_4^{\mu\nu\rho} &= \frac{1}{2} p_1^\mu p_2^\nu q_3^\rho \ , \\ \psi_2^{\mu\nu\rho} &= \frac{1}{6} q_1^\mu q_2^\nu q_3^\rho \ , \quad & \psi_5^{\mu\nu\rho} &= \frac{1}{6} p_1^\mu p_2^\nu p_3^\rho \ , \\ \psi_3^{\mu\nu\rho} &= \frac{1}{2} q_1^\mu q_2^\nu p_3^\rho \ , \quad & \psi_6^{\mu\nu\rho} &= \frac{1}{2}\delta^{\mu\nu} p_3^\rho \ . \end{aligned} \tag{B.14}$$

In the above expression we used the notation $q_i = p_j - p_k$, with $\{i, j, k\}$ an even permutation of $\{1, 2, 3\}$. Not all of the 14 elements are required to describe the three-gluon vertex in Landau gauge. Here we will only write down the multiplets which survive the transverse projection:

$$\begin{aligned} A'(\psi_1^{\mu\nu\rho}) &= \delta^{\rho\nu} q_1^\mu + \delta^{\rho\mu} q_2^\nu + \delta^{\mu\nu} q_3^\rho \ , \\ A'(\psi_2^{\mu\nu\rho}) &= q_1^\mu q_2^\nu q_3^\rho \ , \\ \mathcal{D}_2'(\psi_1^{\mu\nu\rho}) &= \begin{bmatrix} \frac{1}{\sqrt{3}}(\delta^{\rho\nu} q_1^\mu + \delta^{\rho\mu} q_2^\nu - 2\delta^{\mu\nu} q_3^\rho) \\ \delta^{\rho\nu} q_1^\mu - \delta^{\rho\mu} q_2^\nu \end{bmatrix} . \end{aligned} \tag{B.15}$$

We denoted the tensor basis multiplets with primes to distinguish them from momentum multiplets of equation (B.11). $A'(\psi_1^{\mu\nu\rho})$ and $A'(\psi_2^{\mu\nu\rho})$ are already antisymmetric: further anti-symmetric combinations can be obtained by using the doublets $\mathcal{D}_2'(\psi_1^{\mu\nu\rho})$ and $\mathcal{D}_1(p_3^2)$. Applying the rules of Eqs. (B.8), (B.9) and (B.11) we arrive at:

$$\mathcal{D}_1 \times \mathcal{D}_2', \quad (\mathcal{D}_1 * \mathcal{D}_1) \times \mathcal{D}_2' \ . \tag{B.16}$$

In practice we work with the linear combinations of these elements. In a standard notation our Bose-symmetric basis has the form:

$$\begin{aligned}
\tau_1^{\mu\nu\rho} &= q_1^\mu \delta^{\nu\rho} + q_2^\nu \delta^{\rho\mu} + q_3^\rho \delta^{\mu\nu} \ , \\
S_0\tau_2^{\mu\nu\rho} &= q_1^\mu q_2^\nu q_3^\rho \ , \\
S_0\tau_3^{\mu\nu\rho} &= p_1^2 q_1^\mu \delta^{\nu\rho} + p_2^2 q_2^\nu \delta^{\rho\mu} + p_3^2 q_3^\rho \delta^{\mu\nu} \ , \\
S_0\tau_4^{\mu\nu\rho} &= \omega_1 q_1^\mu \delta^{\nu\rho} + \omega_2 q_2^\nu \delta^{\rho\mu} + \omega_3 q_3^\rho \delta^{\mu\nu},
\end{aligned} \tag{B.17}$$

where $\omega_i = -p_j^2 + p_k^2$. $\tau_1^{\mu\nu\rho}$ is the tree-level term. Other $\tau_i^{\mu\nu\rho}$ were divided by S_0 so that all have the same mass dimension. We draw attention to the fact that the structure $\tau_4^{\mu\nu\rho}$ is actually symmetric with respect to the interchanges of equation (B.1), and thus the corresponding dressing function is antisymmetric. This choice was made for purposes of presentation: it leads to a dressing of $\tau_4^{\mu\nu\rho}$ which is sufficiently smooth and well-behaved. Finally, we note that the basis which appears in our calculations (both for external momentum variables and for internal loop calculations) is actually the transversely projected version of Eq. (B.17):

$$\tau_{i\perp}^{\mu\nu\rho}(p_1,p_2,p_3) = T_{\mu\alpha}(p_1)T_{\nu\beta}(p_2)T_{\rho\gamma}(p_3)\tau_i^{\alpha\beta\gamma}(p_1,p_2,p_3) \ . \tag{B.18}$$

Since the operator $T_{\mu\alpha}(p_1)T_{\nu\beta}(p_2)T_{\rho\gamma}(p_3)$ is Bose-symmetric, this projection does not affect the symmetry property of the basis.

B.2 Orthonormal basis

The Bose-symmetric basis is well suited for the presentation of results and for back-coupling of the three-gluon vertex (more on this later). However, certain steps in the numerical procedure are made considerably easier if one employs a basis which is not symmetric, but instead has a desirable property of orthonormality. Here we shall describe a construction principle of this orthonormal transverse basis and the role it plays in our calculations.

When discussing the orthonormal basis it is convenient to work with relative k and total momentum Q: their relation to standard external momenta p_1, p_2 and p_3 is (see also Figure B.1):

$$k = \frac{p_2 - p_1}{2}, \quad Q = -p_3 \ . \tag{B.19}$$

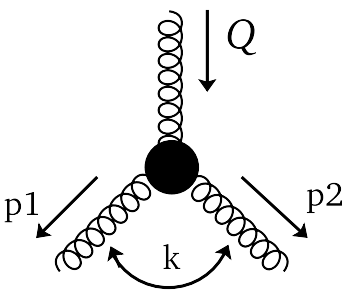

Figure B.1: Kinematics of the three-gluon vertex.

In the following we will also use the notation

$$k_- = -p_1, \quad k_+ = p_2 \ . \tag{B.20}$$

We start by defining the vectors s^μ and d^μ as

$$d^\mu = \hat{Q}^\mu, \quad s^\mu = \hat{k}_T^\mu, \tag{B.21}$$

where the hat denotes normalisation and $k_T^\mu = T^{\mu\nu}(Q)k^\nu$ is the projection of k transverse to Q. With the help of the definitions

$$\begin{aligned} \mathbf{T}_1^{\mu\nu} &= \delta^{\mu\nu}, \qquad \mathbf{T}_4^{\mu\nu} = s^\mu d^\nu + d^\mu s^\nu, \\ \mathbf{T}_2^{\mu\nu} &= s^\mu s^\nu, \quad \mathbf{T}_5^{\mu\nu} = s^\mu d^\nu - d^\mu s^\nu, \\ \mathbf{T}_3^{\mu\nu} &= d^\mu d^\nu, \end{aligned} \tag{B.22}$$

we can write down the complete basis for three-gluon vertex in the following way:

$$\begin{aligned} &\{s^\rho, d^\rho\} \times \{\mathbf{T}_1^{\mu\nu}, \mathbf{T}_2^{\mu\nu}, \mathbf{T}_3^{\mu\nu}, \mathbf{T}_4^{\mu\nu}, \mathbf{T}_5^{\mu\nu}\}, \\ &\{s^\mu, d^\mu\} \times \delta^{\rho\nu}, \quad \{s^\nu, d^\nu\} \times \delta^{\rho\mu}. \end{aligned} \tag{B.23}$$

Combinations in the above expression exhaust all possibilities to get a third rank tensor out of s, d and the Kronecker symbols. We now wish to make a basis which is transverse to all the four-vectors k_+, k_- and Q. We define the auxiliary variables

$$a = \sqrt{3\xi} z, \quad b = \sqrt{3\xi}\sqrt{1-z^2}, \tag{B.24}$$

where $\xi = 4k^2/3Q^2$ and $z = \hat{k} \cdot \hat{Q}$. Variable a is not to be confused with the doublet component of Eq. (B.7). Linear combinations of elements in equation (B.23) which have definitive transversality properties with respect to four-vectors k_-^μ and k_+^ν were found in [173]. In terms of the variables a, b these combinations read

$$\begin{aligned} \mathbf{Y}_1^{\mu\nu} &= \frac{1}{\sqrt{2}}(\mathbf{T}_1^{\mu\nu} - \mathbf{T}_2^{\mu\nu} - \mathbf{T}_3^{\mu\nu}) \ , \\ \mathbf{Y}_2^{\mu\nu} &= \frac{1}{\sqrt{n_1 n_2}}[(1-a^2)\mathbf{T}_2^{\mu\nu} - b^2\mathbf{T}_3^{\mu\nu} + ab\mathbf{T}_4^{\mu\nu} - b\mathbf{T}_5^{\mu\nu}] \ , \\ \mathbf{Y}_3^{\mu\nu} &= \frac{1}{\sqrt{n_1 n_2}}[(1-a^2)\mathbf{T}_3^{\mu\nu} - b^2\mathbf{T}_2^{\mu\nu} - ab\mathbf{T}_4^{\mu\nu} - b\mathbf{T}_5^{\mu\nu}] \ , \\ \mathbf{Y}_4^{\mu\nu} &= \frac{1}{2\sqrt{n_1 n_2}}[(1-a^2+b^2)\mathbf{T}_4^{\mu\nu} - 2ab(\mathbf{T}_2^{\mu\nu} - \mathbf{T}_3^{\mu\nu})] \ , \\ \mathbf{Y}_5^{\mu\nu} &= \frac{1}{2\sqrt{n_1 n_2}}[(1-a^2-b^2)\mathbf{T}_5^{\mu\nu} + 2b(\mathbf{T}_2^{\mu\nu} + \mathbf{T}_3^{\mu\nu})]. \end{aligned} \tag{B.25}$$

Here we used the abbreviations

$$n_1 = 1 + a^2 + b^2, \quad n_2 = n_1 - \frac{4a^2}{n_1} \ . \tag{B.26}$$

The tensors $\mathbf{Y}_1^{\mu\nu}$ and $\mathbf{Y}_2^{\mu\nu}$ are transverse in both indices μ and ν. From them we can thus get two basis elements which are fully transverse, the $s^\rho \mathbf{Y}_1^{\mu\nu}$ and $s^\rho \mathbf{Y}_2^{\mu\nu}$. Further elements can

be found by using the projection of four-vector s which is tranverse to $k_\pm$, i. e. $s^\mu_\pm = T^{\mu\nu}(k_\pm)s^\nu$. By normalising this projection we arrive at a vector

$$\hat{s}^\mu_\pm = \frac{1}{\sqrt{n_1 \pm 2a}}[(a \pm 1)s^\mu - bd^\mu]. \tag{B.27}$$

We now have all the ingredients ready to construct a fully transverse orthonormal basis. It takes the form

$$\begin{aligned} \rho_1^{\mu\nu\rho} &= \mathbf{Y}_1^{\mu\nu} s^\rho, \quad & \rho_2 &= \mathbf{Y}_2^{\mu\nu} s^\rho, \\ \rho_3^{\mu\nu\rho} &= \mathbf{Y}_1^{\rho\nu} \hat{s}^\mu_-, \quad & \rho_4 &= \mathbf{Y}_1^{\rho\mu} \hat{s}^\nu_+. \end{aligned} \tag{B.28}$$

This basis is very convenient when projecting out the components of the three-gluon vertex. One first contracts the right-hand side of the vertex DSE with $\rho_i^{\mu\nu\rho}$, which gives the dressing functions in transverse orthonormal basis. To get the dressings corresponding to the Bose-symmetric elements $\tau_{i\perp}^{\mu\nu\rho}$ one applies rotation. The matrix which rotates the coefficient functions of $\rho_i^{\mu\nu\rho}$ basis onto those of $\tau_{i\perp}^{\mu\nu\rho}$ is given by

$$R = \frac{1}{l\sqrt{2}b\sqrt{t}} \begin{bmatrix} \frac{c}{2} & 0 & \frac{b^2-a(m+a)-3}{2n_-} & \frac{-b^2-a(m-a)+3}{2n_+} \\ \frac{l(-m+4)}{32b^2t} & \frac{-l\sqrt{n_1 n_2}}{16\sqrt{2}b^2t} & \frac{-l(a+1)}{32b^2n_-t} & \frac{-l(a-1)}{32b^2n_+t} \\ \frac{m-6}{2t} & 0 & \frac{-m+6(a+1)}{8n_-t} & \frac{m+6(a-1)}{8n_+t} \\ -\frac{2}{t} & 0 & \frac{m-6+2a}{8n_-t} & \frac{m-6-2a}{8n_+t} \end{bmatrix}. \tag{B.29}$$

Here $t = Q^2/4$ and the other abbreviations were introduced as follows

$$\begin{aligned} l &= (a^2+b^2)^2 + 6(a^2-b^2) + 9, \\ c &= (a^2+b^2)^2 - 2(a^2-b^2) + 3, \\ m &= a^2 + b^2 + 3, \\ n_\pm &= (n_1 \pm 2a)^{-\frac{1}{2}}. \end{aligned} \tag{B.30}$$

B.3 Solution method

As mentioned in section 5.3, the use of Lorentz invariants (S_0, a, s) is of central importance for unveiling the properties of the vertex related to its Bose symmetry. Because of their significant role in this investigation, we choose to define our external grids directly in these variables. They can easily be connected to more common ones via transformation

$$t = \frac{1-s}{2} S_0, \quad \xi = \frac{1+s}{1-s}, \quad z = \frac{a}{\sqrt{1-s^2}}\ . \tag{B.31}$$

For convenience, here we repeat the definitions

$$t = \frac{Q^2}{4}, \quad \xi = \frac{4k^2}{3Q^2}, \quad z = \hat{k}\cdot\hat{Q}, \tag{B.32}$$

with k and Q relative and total momentum, respectively, see Figure B.1. Since variables a and s form the interior of a unit circle, it is convenient to express (a, s) in terms of cylindrical coordinates (r, ϕ) and perform a Chebyshev expansion in ϕ, see section A.2. Thus, if we expand the three-gluon vertex in transverse Bose-symmetric basis

$$\Gamma^{\mu\nu\rho}(S_0, r, \phi) = \sum_{i=1}^{4} F_i(S_0, r, \phi)\tau_{i\perp}^{\mu\nu\rho}(S_0, r, \phi), \tag{B.33}$$

the dressing functions F_i themselves are further expanded into Chebyshev polynomials of the second kind U^m:

$$\begin{aligned} F_i(S_0, r, \phi) &= \sum_{m=0}^{N_{ch}} f_i^m(S_0, r)U^{2m}(\phi), \quad i = 1, 2, 3 \quad , \\ F_4(S_0, r, \phi) &= \sum_{m=0}^{N_{ch}} f_4^m(S_0, r)U^{2m+1}(\phi). \end{aligned} \tag{B.34}$$

Note that for $F_{1,2,3}$ the even Chebies are used, whereas for F_4 the odd ones. This is due to symmetry properties of the dressing functions in (a, s) plane, see Figure 5.4. For our purposes a relatively small number of moments has proven sufficient to represent the dressing functions reasonably well, with $N_{ch} = 4$. Thus, in the interpolation procedure the Chebyshev expansion takes care of the ϕ dependence of the dressing functions. For the dependence on S_0 and r variables, we use the bilinear interpolation. It should be noted that this computationally cheap interpolation method has proven sufficient mostly owing to a relatively mild angular variation of the dressing functions, which is itself a consequence of the nice properties of Bose-symmetric basis. If one instead employs, for instance, the orthonormal basis for all steps of the calculation, one would have to resort to at least the bicubic method, or something even more demanding to get reasonable results.

The Chebyshev expansion and subsequent interpolations are performed with transformed dressings $\sinh^{-1}(F_i)$. The $\sinh^{-1}(x)$ function has a desirable property that for large arguments it behaves like a logarithm, while for small ones it is linear. And unlike the logarithm, the inverse hyperbolic sine is defined for both positive and negative arguments. The use of this transformation is especially convenient when working with scaling solutions. In the scaling scenario (but also for some 'extreme' decoupling solutions) the ghost triangle grows rapidly as the uniform limit $S_0 \to 0$ is approached. Thus interpolating directly in F_i would in general produce large errors in the IR, unless some sophisticated and expensive procedure is used. With the help of the above trick, a numerically cheap linear interpolation in S_0 variable proves to be adequate.

As was already mentioned in the main chapter on three-gluon vertex, the truncated Dyson-Schwinger equation for the vertex is not Bose-symmetric. Bose symmetry is restored for the approximated equation by including diagrams with cyclically permuted gluon legs. Explicit numerical calculations are done with only one set of diagrams, shown in Figure 5.1. This results in a Bose non-symmetric solution $\Gamma_{\mu\nu\rho}(p_1, p_2, p_3)$. The fully symmetric solution is then obtained as

$$\Gamma_{\mu\nu\rho}^{BOSE}(p_1, p_2, p_3) = \frac{1}{3}(\Gamma_{\mu\nu\rho}(p_1, p_2, p_3) + \Gamma_{\rho\mu\nu}(p_3, p_1, p_2) + \Gamma_{\nu\rho\mu}(p_2, p_3, p_1)) \tag{B.35}$$

It is important to note that the above step does not involve interpolation (interpolation is not required to get $\Gamma_{\rho\mu\nu}(p_3, p_1, p_2)$ and $\Gamma_{\nu\rho\mu}(p_2, p_3, p_1)$ from $\Gamma_{\mu\nu\rho}(p_1, p_2, p_3)$). This is enabled by a nice property of (S_0, r, ϕ) variables. From the relations of equation (B.5) and the definitions of cylindrical coordinates $r = \sqrt{a^2 + s^2}$, $\phi = \tan^{-1}(s/a)$ (say), it is easy to check how variables (S_0, r, ϕ) behave under permutations of (p_1, p_2, p_3):

$$\begin{aligned}
&(p_1, p_2, p_3) \to (S_0, r, \phi) \ , \\
&(p_3, p_1, p_2) \to (S_0, r, \phi + \frac{2\pi}{3}) \ , \\
&(p_2, p_3, p_1) \to (S_0, r, \phi + \frac{4\pi}{3}).
\end{aligned} \tag{B.36}$$

Owing to this property, once the non-symmetric quantity $\Gamma_{\mu\nu\rho}(p_1, p_2, p_3)$ has been calculated and stored on a (S_0, r, ϕ) grid, the permuted versions $\Gamma_{\rho\mu\nu}(p_3, p_1, p_2)$ and $\Gamma_{\nu\rho\mu}(p_2, p_3, p_1)$ are easily obtained by changing the ϕ variable. With an appropriately defined grid, these changes of ϕ can be done in an exact manner, therefore completely avoiding the need for interpolation. Obviously, this procedure also makes the symmetrisation process very fast.

Finally, since the three-gluon DSE is solved iteratively, we wish to comment on how the initial guess for the iteration process is formed. In the UV the vertex is dominated by the bare part, and in the IR by the ghost triangle. Both the bare vertex and the ghost loop represent inhomogeneous contributions to the vertex equation, and it is therefore convenient to take these two contributions together to form the first guess for the solution. Additionaly, to make the iteration procedure faster, we add another inhomogeneous term to this guess, the swordfish diagram with a dressed four-gluon vertex. As these contributions will not change during the iterations, they are calculated and stored on a special dense grid, in order to alleviate the interpolation procedure.

Appendix C

Technicalities of bound state studies

C.1 Quark DSE in the complex plane

For convenience we will write here again the quark propagator DSE and the meson BSE in momentum space:

$$\text{DSE}: \; S^{-1}(p) = Z_2 S_0^{-1}(p) + g^2 Z_{1f} C_F \int_k \gamma^\mu S(k) \Gamma^\nu(k,p) D_{\mu\nu}(p-k), \tag{C.1}$$

$$\text{BSE}: \; \Gamma(P,p) = \int_k S(k_-)\, \Gamma(P,k)\, S(k_+)\, K(P,p,k)\,. \tag{C.2}$$

Note the different momentum routing in quark DSE than in equation (2.32). As can be seen from the BSE, the bound state studies require the knowledge of the quark propagator at the points $k_\pm = k \pm P/2$ (we will employ equal momentum partitioning only). In the rest-frame of the bound state, the Euclidean 'on-shell' condition $P^2 = -M^2$ translates to $P = i(0,0,0,M)$, where M is the meson mass. Plugging this into the quark momenta $k_\pm^2$ in the BSE, and keeping in mind the angular integrals $k \cdot P$, gives rise to parabolic curves in the complex k^2 plane. The vertex of the outermost parabola is at $(M^2/4, 0)$ and its focus at $(0,0)$, see Figure C.1. The question now arises as how can the quark propagators along these parabolic lines be obtained.

Let us first tackle the simple case of the rainbow approximation in the quark DSE, with $\Gamma(k,p)^\nu \to \gamma^\nu$. Below we will address the more general truncation schemes. In the DSE the momentum routing is such that the loop propagator $S(k)$ is probed at real k values, and the complex piece flows through the quark-gluon vertex and gluon two-point function alone. In rainbow approximation gluon becomes the only part of the loop integral which is evaluated at complex momenta. Thus, once the quark propagator is calculated on the real axis, the above DSE can be straightforwardly solved for arbitrary momentum p with a single additional iteration. This procedure however assumes that the gluon is known and well-behaved in the complex plane, which does not hold for general rainbow-ladder models of effective running couplings. Also, the method cannot be simply generalised to the case where the momentum dependence in the full quark-gluon vertex is not neglected. These problems can be circumvented in the following way. The first step is to reroute the momenta in the quark DSE:

$$S^{-1}(p) = Z_2 S_0^{-1}(p) + g^2 Z_{1f} C_F \int_k \gamma^\mu S(p-k) \Gamma^\nu(p-k,p) D_{\mu\nu}(k). \tag{C.3}$$

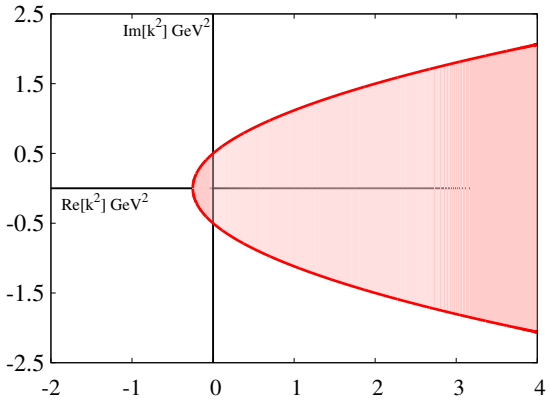

Figure C.1: The parabola along which the quark needs to be evaluated in the BSE, with $M = 1$. Due to angular integration, one needs in principle all the points in the shaded region. The parabola is symmetric with resp. to x axis owing to equal momentum partitioning in the BSE.

In the rainbow truncation the complex momentum now runs through the internal quark line only. The evaluation of the propagator along the lines $p^2 \in \mathbb{C}$ requires probing the points $(p-k)^2$: since the parabolic regions are nested, these all lie *inside* the desired line p^2. This suggests using the so-called shell method. With the propagator calculated for real momenta, one expands outwards from the real axis in the series of smaller steps (shells) until the parabola p^2 is reached: one does not move to the next shell until the results for the current one have converged. For interpolation purposes it is advantageous to define a rectangular grid which we label as (t^2, m^2), and then use a mapping onto the parabolic shells. The procedure is simple: t^2 and m^2 are stored as complex numbers $z = (\sqrt{t^2}, \sqrt{m^2})$, and the mapping is $f(z) = z^2$. This is shown schematically in Figure C.2. With this kind of setup we have found it sufficient to employ a spline interpolation in the t^2 direction and a linear one in the $\sqrt{m^2}$ direction.

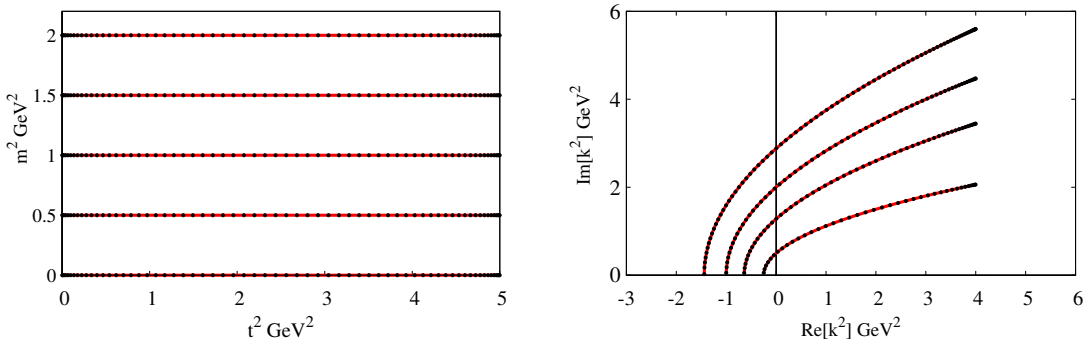

Figure C.2: For interpolation purposes we use a rectangular (t^2, m^2) grid (*left*) which is then mapped onto the parabolic shells in the complex k^2 plane (*right*).

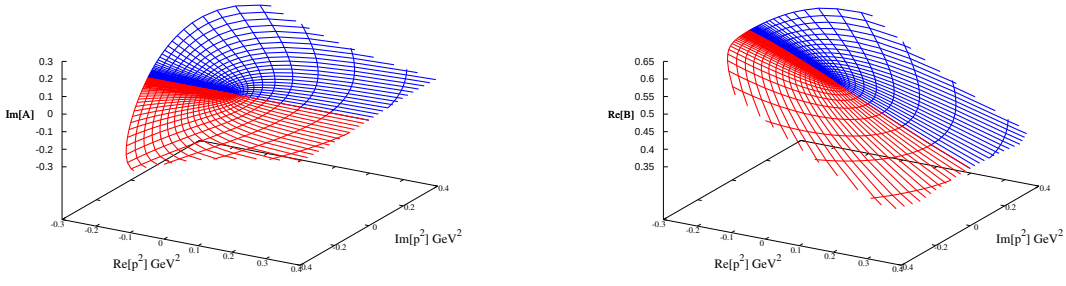

Figure C.3: The quark $A(p^2)$ and $B(p^2)$ functions in the complex plane, obtained with the shell integration method. The $A(p^2)$ function is in units 1/GeV.

Note that, while the BSE integrations will in general require information from both the lower and upper complex half-planes, see Figure C.1, it is actually enough to perform explicit calculations for only one of them: the corresponding data for the other plane can then be obtained by using the analyticity property of the quark propagator, e. g. $A(p_c^2) = A_c(p^2)$, with 'c' denoting complex conjugation. The results for the quark obtained with the shell method are shown in Figure C.3. The approach can be relatively straightforwardly generalised to the beyond rainbow ladder calculations which we performed (for real momenta only) in Chapter 6. The main difference as compared to a rainbow treatment is that the quark-gluon vertex needs to be evaluated in the complex plane as well. This is not a big problem in principle as the similar tricks can be used as in the quark DSE: with a careful choice of momentum routing all the complex-valued variables can be passed through internal quark lines, and the shell method can be applied for the quark-gluon interaction itself.

It should be pointed out that this technique has limited applicability. It will work good so long as the poles of the quark propagator are well outside the integration contour. However, if probing of the deep timelike P^2 region is required (i. e. one is investigating very heavy bound states), one will eventually run into these poles which will render the shell method useless. In that case alternative techniques need to be used, for instance deformations of the integration path and similar [211]. This can be easily illustrated by considering a chirally symmetric solution for the quark, with $B(p^2) = 0$. In that case the poles of $S(p)$ lie practically on the real axis and the shell method immediatelly fails. This is shown in Figure C.4, where it is compared to the calculation with the analytically continued gluon propagator: we consider the Maris-Tandy interaction which can be safely used in the complex plane. Model parameters are given in [61].

The fact that the shell approach cannot be directly applied to the case of (nearly)-conformal theories represents a big technical problem for the studies of bound states in those models. While there are alternative frameworks available for working with complex-valued momenta, most on them are still in development and cannot yet be generalised to beyond rainbow-ladder settings. For now, it might be more practical to resort to extrapolation methods when one is investigating walking theories. As we have shown in Chapter 6, extrapolation from the spacelike

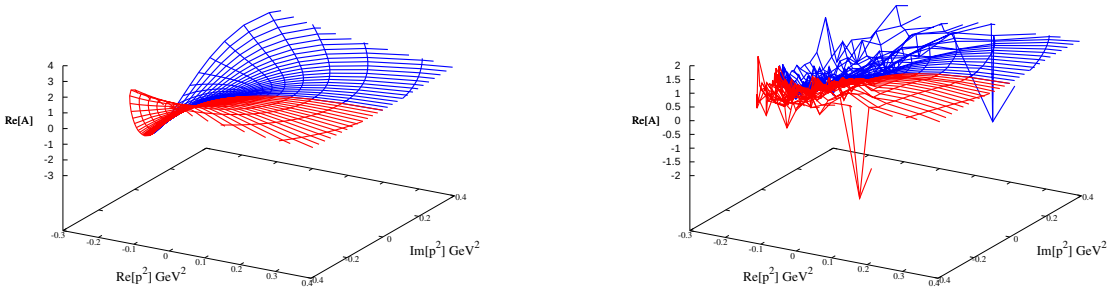

Figure C.4: The chirally symmetric solutions for the quark in the complex plane, obtained with analytic continuation of the gluon (*left*) and with the shell method (*right*). The effective interaction is Maris-Tandy, with the parameters given in [61].

P region works quite well even for relatively heavy mesons. Additionally, it is expected to be especially convenient for scenarios which feature hadronic mass suppression, as for the lighter states one does not have to extrapolate far along the negative P^2 axis.

C.2 The quark-gluon vertex: basis and interpolation

Let us first discuss the basis decomposition for the quark-gluon interaction. Taking into account its one Lorentz and two Dirac indices, and two independent momenta, the most naive basis one can write down for $\Gamma^\mu(p_1, p_2)$ would have the following form:

$$(\gamma^\mu, p_1^\mu, p_2^\mu) \times (\mathbf{1}, \not{p}_1, \not{p}_2, \not{p}_1\not{p}_2). \tag{C.4}$$

Here p_1 and p_2 denote the quark momenta. We now wish to combine the above elements into something which will be more convenient for our Landau gauge studies. More specifically, we want to exploit the transversality of Landau gauge gluon propagator, cf. equation (2.25), to eliminate some of the unneccessary components. With the routing conventions as depicted in Figure 6.1, we define the relative quark momentum $l = (p_2 + p_1)/2$ and gluon momentum $k = p_2 - p_1$ and construct the orthonormal combinations:

$$\begin{aligned} t^\mu &= \hat{k}^\mu, \\ s^\mu &= \hat{h}^\mu, \quad h^\mu = T^{(t)}_{\alpha\beta} l^\beta, \\ \gamma^\mu_{TT} &= T^{(t)}_{\mu\alpha} T^{(s)}_{\alpha\nu} \gamma^\nu = \gamma^\mu - \not{t} t^\mu - \not{s} s^\mu. \end{aligned} \tag{C.5}$$

In the above equations the hat denotes normalisation and $T^{(k)}_{\mu\nu} = \delta_{\mu\nu} - k^\mu k^\nu / k^2$ is the transverse projector. In Landau gauge any components proportional to t^μ will be projected out and so we need only the following 8 terms:

$$(\gamma^\mu_{TT}, s^\mu) \times (\mathbf{1}, \not{s}, \not{t}, \not{s}\not{t}). \tag{C.6}$$

This is our decomposition for the quark-gluon interaction. It is used when solving the coupled system of DSEs for the quark propagator and the vertex, as well as for interpolation purposes, see Figure 6.9 and the text above. In the right panel of Figure 6.4 we use the notation where $T_{1...4}$ correspond to the γ^μ_{TT} part and $T_{5...8}$ to an s^μ one. From the definition of γ^μ_{TT} one can see that the T_1 and T_6 reconstruct the tree-level term in Landau gauge.

While the transversality and orthonormality properties of the above basis are certainly useful, and the basis itself has proven adequate in most of our practical applications, it still leaves a few things to be desired. For instance, for the purposes of interpolation and displaying of results it would be highly convenient to have a decomposition akin to the Bose-symmetric one for the three-gluon vertex, where the symmetry principles are used to render the angular dependencies of dressing functions as weak as possible. One such was found in [212]: in terms of momenta l and k as defined above it takes the form (we leave out the explicit momentum dependence for the basis elements):

$$\begin{aligned}
\tau_1^\mu &= \gamma_T^\mu, & \tau_5^\mu &= (l\cdot k)\frac{i}{2}\left[\gamma_T^\mu, \not{l}\right], \\
\tau_2^\mu &= l_T^\mu \not{l}, & \tau_6^\mu &= \frac{1}{6}\left[\gamma^\mu, \not{l}, \not{k}\right], \\
\tau_3^\mu &= i l_T^\mu, & \tau_7^\mu &= t^{(kl)}_{\mu\nu}(l\cdot k)\gamma^\nu, \\
\tau_4^\mu &= \frac{i}{2}\left[\gamma^\mu, \not{k}\right], & \tau_8^\mu &= t^{(kl)}_{\mu\nu}\frac{i}{2}\left[\gamma^\nu, \not{l}\right].
\end{aligned} \tag{C.7}$$

Here T denotes the transverse projection with respect to momentum k, $[A,B,C] = [A,B]C + [B,C]A + [C,A]B$, and $t^{(kl)}_{\mu\nu} = (k\cdot l)\delta_{\mu\nu} - l^\mu k^\nu$ is the doubly-transverse projection operator. The above basis is charge-conjugation invariant. Among other things, this is expected to bring about the relatively mild angular dependence for the vertex dressing functions. Unfortunately, it is not easy to use the τ_i elements in conjunction with the transverse orthonormal (ON) ones of equation (C.6), as the corresponding rotation matrix seems to be full of kinematic singularities. To keep matters simple, and because the ON basis has proven to be 'good enough' in our tests of the interpolation for the quark-gluon vertex, we have chosen to refrain from using the quark/antiquark symmetric tensor elements. They should still be kept in mind for any future studies which might require better precision or performance. It is also worth noting that in our bound state studies we have managed to 'get away' with the simple decomposition of (C.6) mostly because we worked exclusively with real Euclidean momenta. If one probes the complex momentum values, it is highly advantageous to use basis constructions which isolate the complex piece at the price of introducing more elements, see [188] for details.

Now let us describe the interpolation procedure we used for the vertex dressing functions. These are calculated and stored on a three-dimensional grid of Lorentz invariants $(l^2, k^2, l\cdot k)$, where momenta l, k are as introduced above. For the angular dependence we used a polynomial interpolation (we found the four-point one to perform sufficiently good), the details of which can be easily found in many books with numerical recipes. Here we wish to elaborate in some detail on the two-dimensional part (l^2, k^2). Since the components corresponding to the orthonormal basis do not display any special symmetry properties, the cheapest option of bilinear interpolation has proven to be insufficient (contrast this to the situation with the three-gluon vertex). On the other hand, some other readily available algorithms, like the high-degree polynomial methods, are by far too much computationally demanding. For this reason

we chose the bicubic interpolator, which is not much slower than the bilinear one but provides considerably better results.

We shall start with the one-dimensional case. When interpolating for some function $f(x)$, the ordinary linear method uses only the values for f itself at certain grid points: the cubic spline approach improves this by employing the first derivative of the function as well. For simplicity, let us first look at the unit interval $x \in [0, 1]$. Given the values for the function and its first derivative at the end points, we can interpolate for $f(x)$ with a third-degree polynomial:

$$f(x) = ax^3 + bx^2 + cx + d, \tag{C.8}$$
$$f'(x) = 3ax^2 + 2bx + c. \tag{C.9}$$

Plugging in $f(0)$, $f'(0)$, $f(1)$ and $f'(1)$ into the above expressions easily gives

$$\begin{aligned} a &= 2f(0) - 2f(1) + f'(0) + f'(1), \\ b &= -3f(0) + 3f(1) - 2f'(0) - f'(1), \\ c &= f'(0), \\ d &= f(0). \end{aligned} \tag{C.10}$$

Using these coefficients in equation (C.8) and reshuffling terms finally yields

$$f(x) = h_{00}(x)f_0 + h_{10}(x)f'_0 + h_{01}(x)f_1 + h_{11}(x)f'_1 \ . \tag{C.11}$$

Here hs are the Hermite basis functions, given by

$$\begin{aligned} h_{00}(x) &= 2x^3 - 3x^2 + 1, \quad & h_{01}(x) &= -2x^3 + 3x^2, \\ h_{10}(x) &= x^3 - 2x^2 + x, \quad & h_{11}(x) &= x^3 - x^2. \end{aligned} \tag{C.12}$$

These are ploted in Figure C.5. Equation (C.11) is the basic formula for cubic Hermite spline interpolation on a unit interval.

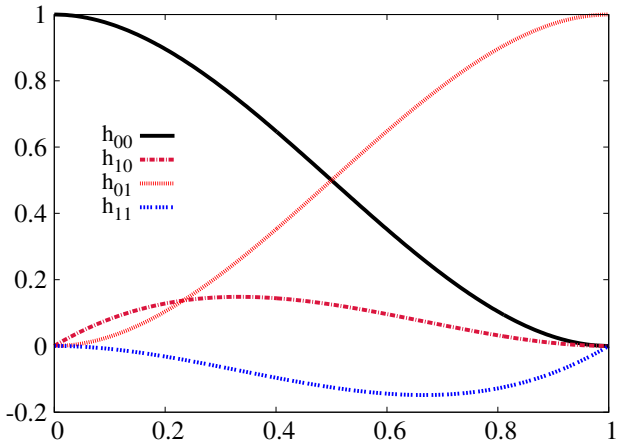

Figure C.5: The Hermite basis functions of equation (C.12).

Generalising the above method to an arbitrary interval $x \in [a, b]$ is straightforward through an affine transformation:

$$f(x) = h_{00}(t)f_a + h_{10}(t)(b-a)f'_a + h_{01}(t)f_b + h_{11}(t)(b-a)f'_b \,. \tag{C.13}$$

Here $t = (x-a)/(b-a)$. Since we usually work with data sets (as is the case here, for the quark-gluon vertex), we do not have explicit expressions for the derivatives f'. In that case one can employ numerical differentiation in any number of ways. We choose the following numerical evaluation for the derivative at the k-th grid point:

$$f'_k = \frac{f_{k+1} - f_{k-1}}{x_{k+1} - x_{k-1}}. \tag{C.14}$$

If the point lies at the beginning or the end of the data set, we use the ordinary forward and backward difference respectively. This framework is compared to linear interpolation in Figure C.6. It is perhaps not entirely fair to compare the two approaches (since cubic uses the function derivatives, it is obvious that it will much better represent the 'curvy' parts of the function), but the important point here is that the Hermite spline performs significantly better while still being relatively computationally cheap. When working with one-dimensional grids, the speed is usually not an issue and even higher-degree interpolations can be used without slowing things down too much. But when one starts considering two- or higher- dimensional problems, it really becomes important to find an interpolation procedure which will perform sufficiently good while not becoming the bottleneck of the calculation. For the three-gluon vertex, the bilinear method turned out to be good enough, but this was mostly due to the Bose-symmetry and the appropriatelly chosen representation for the momentum variables and basis elements. For the quark-gluon interaction this is not the case anymore, at least not with the 'naive' basis of equation (C.6) which we employ. Here, an almost perfect balance between speed and performance is offered by the 2d version of cubic Hermite spline.

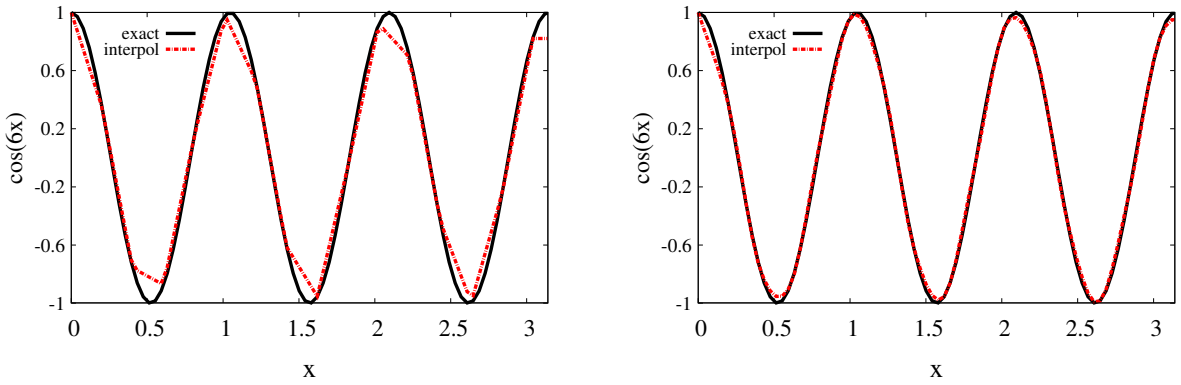

Figure C.6: Test of the linear (*left*) and cubic (*right*) interpolation. Function was stored on a coarse grid with 32 points, then interpolated for and compared with the exact values on a dense grid with 160 points.

The generalisation of the above described method to a two-dimensional computation is straightforward, but one has to keep in mind that it involves the evaluation of the second derivatives as well. While we did not test the bicubic interpolation for the quark-gluon vertex directly (as we did for the 1d case in Figure C.6), its performance was probed by using it in the bound-state equation. As stated in section 6.3, it brings about a difference in the homogeneous BSE eigenvalues on the order of a few permil when compared to an exact two-loop calculation at the point $P^2 = 0$.

C.3 Solving the BSE

Here we shall make some general short remarks on how the solutions of the (in)homogeneous BSEs can be obtained. Let us start with the homogeneous case, writing it in a shorthand notation as

$$\Gamma_i = \lambda M_{ij} \Gamma_j \tag{C.15}$$

M_{ij} is the 'BSE matrix' with superindices i, j which denote components and integration variables. For practical purposes it is very convenient to separate this into $M_{ij} = L_{ik} R_{kj}$, where R_{ij} is the matrix which 'attaches the quark legs', i. e.

$$\chi_i = R_{ij} \Gamma_j \tag{C.16}$$

$\chi(k, P)$ is the BSE wavefunction $\chi(k, P) = S(k_-)\Gamma(k, P)S(k_+)$. The matrix L_{ij} then surmises everything else, including the interaction kernel K. There are two reasons for this separation. One is that L_{ij} and R_{ij} are individually considerably simpler than the whole matrix M, which makes them easier for inspection in case of debugging. The other reason is that R_{ij} is independent of the BSE truncation. Thus, for instance, when going from beyond rainbow ladder to a RL framework it is enough to simply remove certain terms in L_{ij}: this would have been impossible if one was constructing only the whole M operator.

With this trick in store, let us look at how the equation (C.15) itself can be solved. If one is interested only in the properties of ground states (i. e. the states with the biggest eigenvalue λ), then it is enough to employ a simple power iteration method [213]. With an initial guess for the meson amplitude $|\Gamma^0\rangle$, one simply applies the BSE matrix to it repeatedly until some convergence criterion is met (i. e. until the difference between successive iterations has become small enough):

$$M^{N+1} \left|\Gamma^0\right\rangle \approx \lambda_0 M^N \left|\Gamma^0\right\rangle \tag{C.17}$$

λ_0 is the biggest eigenvalue, presumably corresponding to the ground state. Since we are dealing with a homogeneous equation, the amplitudes have to be normalised. As we are yet looking only at the mass spectra (and not at other hadronic observables), this normalisation condition can be almost completely arbitrary, for instance $\langle\Gamma|\Gamma\rangle = 1$. The method can be adjusted for studies of excited states as well, but this is computationally quite consuming, as each obtained bound state has to be projected out before looking for higher states. If the spectrum of excited mesons is desired, it is better to use other methods like e. g. the Arnoldi factorisation [214].

An alternative is to look at the inhomogeneous Bethe-Salpeter equation. Labeling the inhomogeneous term as Γ_i, is can be written in the form

$$\Gamma = (1 - M)^{-1} \Gamma_i \tag{C.18}$$

Here, M is the Bethe-Salpeter matrix. A very fast and convenient way to solve this expression is to use the bi-conjugate gradient method, or its stabilised version [215]. Note, however, that the results in this and similar approaches might heavily depend on the initial guess for the amplitude. This is usually not a problem if one merely wants to obtain bound state masses (the location of the poles is often stable in this regard), but it can become an issue if one wants to use the inhomogeneous BSE to describe 'virtual' meson propagators. In that case the results should at least once be cross-checked with a slower but more reliable method like e. g. the LU decomposition.

Finally, we wish to comment on the possibility of rendering the bound-state calculations simpler by employing the meson basis elements which have certain symmetry properties. We provide here an example of an orthogonal basis for the scalar meson which is even under the charge conjugation operation:

$$\begin{aligned} &\mathcal{T}_1(k,P) = \mathbf{1}, \quad \mathcal{T}_3(k,P) = \not{k} - \frac{\not{P}(k\cdot P)}{P^2}, \\ &\mathcal{T}_2(k,P) = \not{P}, \quad \mathcal{T}_4(k,P) = [\not{k},\not{P}]. \end{aligned} \tag{C.19}$$

In rainbow ladder framework, if one uses the basis for bound states which is either even or odd under C, one will end up with the matrices R and L which are, respectively, even or odd in the angle $k \cdot P$. This makes the corresponding Chebyshev expansion of meson amplitudes considerably simpler. Additionally, when working on the timelike P^2 axis, the angle $k \cdot P$ is the only piece which carries the imaginary unit i. Thus, by choosing the symmetry properties of the basis, one can get either purely real or purely imaginary (up to numerical artifacts, of course) meson dressing functions. Unfortunately, this argument does not extend to arbitrary beyond rainbow ladder treatments.

Appendix D

Constructing the Bethe-Salpeter kernel

D.1 Axial Ward-Takahashi identity

We wish to see how the theory behaves under infinitesimal local chiral rotations. Considering the flavour non-singlet case only, variations of the quark fields take the form

$$\begin{aligned} \psi &\longrightarrow \psi' = (1 + i\alpha\gamma_5)\psi, \\ \bar{\psi}' &\longrightarrow \bar{\psi}' = \bar{\psi}(1 + i\alpha\gamma_5). \end{aligned} \tag{D.1}$$

The transformation parameter α is explicitly given by $\alpha = \sum_f \alpha_f(x)\mathbf{t}_f$, with $\mathbf{t}_f$ the generators of $SU(N_f)$. We will keep the flavour structure implicit in what follows. The affected part of the Lagrangian and its change under these rotations are (we are assuming that the mass matrix commutes with α):

$$\mathcal{L} = \bar{\psi}\left(-\partial\!\!\!/ - igA\!\!\!/ + m\right)\psi \quad \longrightarrow \quad \delta\mathcal{L} = 2im\ \alpha P(x) - i\partial_\mu^x \alpha \mathcal{A}^\mu(x) \tag{D.2}$$

$\mathcal{A}^\mu(x)$ and $P(x)$ denote, respectively, the axial-vector and pseudoscalar currents

$$\begin{aligned} P(x) &= \bar{\psi}\gamma_5\psi, \\ \mathcal{A}^\mu(x) &= \bar{\psi}\gamma^\mu\gamma_5\psi. \end{aligned} \tag{D.3}$$

Now let us look at how the above transformation affects the quark propagator:

$$S(x_1, x_2) = \int \mathcal{D}_{[\psi,\bar{\psi}]} e^{iS[\psi,\bar{\psi}]} \psi(x_1)\bar{\psi}(x_2)\ . \tag{D.4}$$

Assuming that the integral measure does not change under chiral transformations (which is a valid assumption in the flavour non-singlet case), it is straightforward to arrive at the relation

$$\begin{aligned} 0 = \int \mathcal{D}_{[\psi,\bar{\psi}]} e^{iS[\psi,\bar{\psi}]} \{ i \int d^4x \left[\left(2m\alpha P(x) - \partial_\mu^x \alpha \mathcal{A}^\mu(x)\right) \psi(x_1)\bar{\psi}(x_2) \right] + \\ i\alpha(x_1)\gamma_5\psi(x_1)\bar{\psi}(x_2) + i\alpha(x_2)\psi(x_1)\bar{\psi}(x_2)\gamma_5 \} \end{aligned} \tag{D.5}$$

The final steps in this derivation are moving the derivative from α via partial integration, and introducing δ functions to get the quark propagators under the $\int_x$ integral. This finally yields the axial-vector Ward-Takahashi identity (axWTI) in coordinate space:

$$\partial_\mu^x G_5^\mu(x,x_1,x_2) = -2mG_5(x,x_1,x_2) - \delta(x-x_1)S(x_1,x_2)\gamma_5 - \delta(x-x_2)\gamma_5 S(x_1,x_2), \quad \text{(D.6)}$$

where $G_5^\mu(x,x_1,x_2)$ and $G_5(x,x_1,x_2)$ respectively stand for the non-amputated axial-vector and pseudoscalar vertex:

$$\begin{aligned} G_5^\mu(x,x_1,x_2) &= \int \mathcal{D}_{[\psi,\bar\psi]} \mathcal{A}^\mu(x)\psi(x_1)\bar\psi(x_2), \\ G_5(x,x_1,x_2) &= \int \mathcal{D}_{[\psi,\bar\psi]} P(x)\psi(x_1)\bar\psi(x_2). \end{aligned} \quad \text{(D.7)}$$

In what follows we only consider the chiral limit $m = 0$. It will prove convenient to Fourier-transform the axWTI to momentum space and recast it in terms of amputated vertices, leading to

$$iP_\mu \Gamma_5^\mu(P,p) = -S^{-1}(p_+)\gamma_5 - \gamma_5 S^{-1}(p_-). \quad \text{(D.8)}$$

Here $\Gamma_5^\mu(P,p) = S^{-1}(p_+)\; G_5^\mu(P,p)\; S^{-1}(p_-)$ is the amputated vertex with P and p its total and relative momentum respectively, and $p_\pm = p \pm P/2$. To connect the above equation to the bound state studies we use the fact that $\Gamma_5^\mu(P,p)$ is a solution of the Bethe-Salpeter equation (BSE):

$$[\Gamma_5^\mu(P,p)]^{ab} = \int_k [S(k_+)\gamma_5 + \gamma_5 S(k_-)]^{cd}\, K_{cd}^{ab}(P,p,k). \quad \text{(D.9)}$$

$K(P,p,k)$ is the Bethe-Salpeter 4-point interaction kernel. By combining Eqs. (D.8) and (D.9) and using the quark propagator DSE:

$$S^{-1}(p) = S_0^{-1}(p) + \Sigma(p), \quad \text{(D.10)}$$

it is straightforward to arrive at the form of the axWTI which is commonly encountered in calculations of hadronic observables:

$$\begin{aligned} &[\Sigma(p_+)\gamma_5 + \gamma_5\Sigma(p_-)]^{ab} = \\ &\qquad \int_k [\Sigma(k_+)\gamma_5 + \gamma_5\Sigma(k_-)]_{cd}\, K_{cd}^{ab}(P,p,k). \end{aligned} \quad \text{(D.11)}$$

D.2 DSE and BSE truncations from the effective action

In this section we will describe a general method of deriving 'consistent approximations' for propagator DSEs and bound state equations, based on the effective action formalism. By consistent truncations we mean those which do not break any global symmetries of the action. Our interest in this mostly comes from the considerations of chiral symmetry and the constraints it imposes for the combined treatment of quark DSEs and meson BSEs. The main ideas we present here can be straightforwardly applied to other systems as well, e. g. for the gluon propagator and the associated glueball BSE. Our discussion is mostly based on [90], but see also [216–218].

We introduce the formalism by first considering the case of local fields. For convenience we repeat the definition of the effective action and the associated derivatives, see also section 3.1:

$$\Gamma[\tilde{\varphi}] = W[J] + \int_x \tilde{\varphi}(x)J(x), \tag{D.12}$$

$$W'_x[J] = -\tilde{\varphi}(x), \quad \Gamma'_x[\tilde{\varphi}] = J(x). \tag{D.13}$$

$W[J] = -i \log Z[J]$ is the generating functional of connected Greens functions and $\tilde{\varphi}$ the quantum averaged field in the presence of sources. From the above expressions one can see that the 'classical' field φ in the absence of source terms is given by the stationarity condition

$$\frac{\delta\Gamma[\varphi]}{\delta\varphi} = 0. \tag{D.14}$$

A particular solution of this equation, which we label as $\varphi^{(0)}(x)$, is said to be stable if there exists an infinitesimal $\Delta\varphi(x)$ such that $\varphi^{(1)} = \varphi^{(0)}(x) + \Delta\varphi(x)$ is also a solution. By expanding around $\varphi^{(0)}(x)$ we get

$$\frac{\delta\Gamma[\varphi]}{\delta\varphi}\Big|_{\varphi(x)=\varphi^{(1)}(x)} = \frac{\delta\Gamma[\varphi]}{\delta\varphi}\Big|_{\varphi(x)=\varphi^{(0)}(x)} + \int_y \frac{\delta^2\Gamma[\varphi]}{\delta\varphi(x)\delta\varphi(y)}\Big|_{\varphi(x)=\varphi^{(0)}(x)} \Delta\varphi(y) + \ldots = 0. \tag{D.15}$$

Note that the above manipulation might involve an extra minus sign if $\varphi(x)$ is a fermionic field, but this fortunately has no bearing on the upcoming discussion. To a first order in $\Delta\varphi(x)$ the last equation implies

$$\int_y \frac{\delta^2\Gamma[\varphi]}{\delta\varphi(x)\delta\varphi(y)}\Big|_{\varphi(x)=\varphi^{(0)}(x)} \Delta\varphi(y) = 0. \tag{D.16}$$

In other words, $\varphi^{(0)}(x)$ is a stable solution if $\Delta\varphi(x)$ is an eigenvector of $\delta^2\Gamma[\varphi]/\delta\varphi\delta\varphi$ with eigenvalue zero. To see the significance of this, let us recall the following identity from section 3.1:

$$\int_y W''_{xy}[J]\Gamma''[\tilde{\varphi}]_{yz} = -\delta^4(x-z). \tag{D.17}$$

By considering an eigenvector $\xi(x)$ of $\delta^2 W[J]/\delta J\delta J$ with eigenvalue $1/\lambda$, i. e.

$$\int_y \frac{\delta^2 W[J]}{\delta J(x)\delta J(y)}\xi(y) = \frac{1}{\lambda}\xi(x), \tag{D.18}$$

and using the equation (D.17) it is straightforward to show

$$\int_y \frac{\delta^2\Gamma[\varphi]}{\delta\varphi(x)\delta\varphi(y)}\xi(y) = \lambda\xi(x). \tag{D.19}$$

This means that $\xi(x)$ is also an eigenvector of $\delta^2\Gamma[\varphi]/\delta\varphi\delta\varphi$ with an eigenvalue λ. As we have shown above the small quantity $\Delta\varphi(x)$ is an eigenvector with $\lambda = 0$, which entails a pole in the function $\delta^2 W[J]/\delta J\delta J$. Therefore, stable solutions $\varphi^{(0)}(x)$ are associated with poles

in the connected Greens functions $\delta^2 W[J]/\delta J \delta J$ (propagators if $\varphi(x)$ is a single field, e. g. $\varphi(x) = \psi(x)$ or similar).

Now let us generalise this discussion to the case of bilocal fields. To this end we add to the generating functional $Z[J]$ a bilocal source term $K(x,y)\mathcal{O}(x,y)$. To keep the argument as short as possible, we specialise immediately to the case of quark-antiquark bound states, so that $\mathcal{O}(x,y) = \psi(x)\bar{\psi}(y)$. The corresponding source term is Grassmann-valued, with $K(x,y) = -K(y,x)$. Apart from the field $\psi(x)$ there is now an additional solution, the two-point function

$$\frac{\delta W[J,K]}{\delta K(x,y)} = \frac{1}{2}\left(\psi(x)\bar{\psi}(y) + S(x,y)\right). \tag{D.20}$$

The two-particle irreducible (2PI) effective action is then defined as

$$\Gamma[\psi,S] = W[J,K] + \int_x J(x)\psi(x) + \frac{1}{2}\int_{xy} K(x,y)\psi(x)\bar{\psi}(y) + \frac{1}{2}\int_{xy} K(x,y)S(x,y). \tag{D.21}$$

In the above equation the symbolic notation $J(x)\psi(x)$ surmises both the $\psi(x)$ and $\bar{\psi}(x)$ source terms. In addition to the stationarity condition of equation (D.14) there is now also a solution corresponding to

$$\frac{\delta\Gamma[\psi,S]}{\delta S(x,y)} = 0. \tag{D.22}$$

We will shortly show that this is the equation of motion for the fermion (quark) propagator. In exactly the same manner as was done for the local case, it can be shown that the propagator $S^{(0)}(x,y)$ is a stable solution of Eq. (D.22) if $S^{(1)}(x,y) = S^{(0)}(x,y) + \Delta S(x,y)$ is also a solution and

$$\int_{zw} \frac{\delta^2\Gamma[\psi,S]}{\delta S(x,y)\delta S(z,w)}\Big|_{S=S^{(0)}} \Delta S(z,w) = 0. \tag{D.23}$$

In other words, a stable solution $S^{(0)}(x,y)$ is connected to the pole in the four-point function $\delta^2 W[J,K]/\delta K \delta K$. We now wish to demonstrate that this expression is nothing more than the usual meson Bethe-Salpeter equation. To do so we shall need the 'explicit' form of the 2PI effective action [219] ($S[A,\psi,\bar{\psi}]$ is the QCD action, not to be confused with the propagator S):

$$\Gamma[\psi,S] = S[A,\psi,\bar{\psi}] + i\mathrm{Tr}\log S - i\mathrm{Tr}S_0^{-1}S + \Gamma_2[\psi,S]. \tag{D.24}$$

$\Gamma_2[\psi,S]$ contains the two-particle irreducible diagrams only and S_0 is the tree-level fermion propagator. Exploiting the identity $\delta\mathrm{Tr}\log S = S^{-1}\delta S$ we can now write the equation (D.22) as

$$\frac{\delta\Gamma[\psi,S]}{\delta S(x,y)} = iS^{-1}(x,y) - iS_0^{-1}(x,y) + \frac{\delta\Gamma_2[\psi,S]}{\delta S(x,y)}. \tag{D.25}$$

Finally, by defining the quark self-energy as $\Sigma = -\delta\Gamma_2/\delta G$ we arrive at

$$S^{-1}(x,y) = S_0^{-1}(x,y) - \Sigma(x,y). \tag{D.26}$$

One can recognise this as the DSE for the fermion propagator. If a stable function $S^{(0)}$ solves the above gap equation, we can take one more functional derivative with respect to S and recast Eq. (D.23) as

$$0 = \int_{zw} \frac{\delta^2\Gamma[\psi,S]}{\delta S(x,y)\delta S(z,w)}\Big|_{S=S^{(0)}} \Delta S(z,w) = \int_{zw} \left(-S^{(0)}(x,z)S^{(0)}(y,w) + K(x,y;z,w)\Delta S(z,w)\right). \tag{D.27}$$

In the above derivation we used the identity $\delta M^{-1}_{ip} = -M^{-1}_{ij}\delta M_{jn}M^{-1}_{np}$. Equation (D.27) is precisely a meson BSE written in terms of the wavefunction $\Delta S = S\Gamma S$, with Γ the meson amplitude. The interaction kernel K is given by the functional derivative

$$K(x,y;z,w) = -\frac{\delta\Sigma(x,y)}{\delta S(z,w)}\Big|_{S=S^{(0)}}. \tag{D.28}$$

Note that the substitution $S = S^{(0)}$ in this expression is made only after the cutting technique has been performed. Finally, we wish to demonstrate that if the meson BSE is derived following the above procedure, the spontaneous breaking of chiral symmetry will give rise to massless pseudoscalar states, the pions. More details on this can be found in [180]. Let us consider a global chiral rotation, with the quark transforming as (like in the previous section, the flavour structure will be kept implicit in α):

$$S' = e^{i\gamma_5\alpha}Se^{i\gamma_5\alpha}. \tag{D.29}$$

Assuming that the effective action is invariant under these transformations, with $\delta\Gamma[S] = 0$, we get for the infinitesimal case

$$\frac{\varepsilon\ \delta\Gamma}{\delta S(x,y)}\left\{i\gamma_5, S(x,y)\right\} = 0. \tag{D.30}$$

Taking one more derivative $\delta/\delta S$ gives

$$\frac{\delta^2\Gamma[S]}{\delta S(x,y)\delta S(z,w)}\left\{i\gamma_5, S(z,w)\right\} + \frac{\delta\Gamma[S]}{\delta S(x,y)}\gamma_5 + \gamma_5\frac{\delta\Gamma[S]}{\delta S(x,y)} = 0. \tag{D.31}$$

By employing the stationarity condition the last two terms are eliminated, and one ends up with

$$\frac{\delta^2\Gamma[S]}{\delta S(x,y)\delta S(z,w)}\Big|_{S=S^{(0)}}\left\{i\gamma_5, S(z,w)\right\} = 0. \tag{D.32}$$

In the case of dynamical chiral symmetry breaking (i. e. the quark S has a chirally non-symmetric piece), the above equation can only be satisfied if $\delta^2\Gamma[S]/\delta S\delta S = 0$. This in turn implies that there is a bound state pole with pseudoscalar quantum numbers in the four-point function $\delta^2 W[K]/\delta K\delta K$. Additionally, the solution $S^{(0)}$ is translationally invariant, with $S^{(0)}(x,y) = S^{(0)}(x-y)$. This entails that, after Fourier-transforming to momentum space, the meson amplitude has a vanishing total momentum. The main point of this formalism is that

even after the effective action has been truncated/modeled, the above argument will hold so long as the approximated action still respects the relevant symmetry, and both the propagator DSE and the corresponding bound-state equation have been derived using the method outlined above. The derivation would follow along exactly the same lines for any symmetries left over in the simplified system.

Bibliography

[1] G. Gabrielse, D. Hanneke, T. Kinoshita, M. Nio and B. C. Odom, Phys. Rev. Lett. **97** (2006) 030802 [Phys. Rev. Lett. **99** (2007) 039902].

[2] P. Clade, E. de Mirandes, M. Cadoret, S. Guellati-Khelifa, C. Schwob, F. Nez, L. Julien and F. Biraben, Phys. Rev. Lett. **96** (2006) 033001.

[3] P. W. Higgs, Phys. Lett. **12** (1964) 132.

[4] P. W. Higgs, Phys. Rev. Lett. **13** (1964) 508.

[5] F. Englert and R. Brout, Phys. Rev. Lett. **13** (1964) 321.

[6] G. S. Guralnik, C. R. Hagen and T. W. B. Kibble, Phys. Rev. Lett. **13** (1964) 585.

[7] D. J. Gross and F. Wilczek, Phys. Rev. D **8** (1973) 3633.

[8] D. J. Gross and F. Wilczek, Phys. Rev. Lett. **30** (1973) 1343.

[9] H. D. Politzer, Phys. Rept. **14** (1974) 129.

[10] C. D. Roberts and A. G. Williams, Prog. Part. Nucl. Phys. **33** (1994) 477 [hep-ph/9403224].

[11] R. Alkofer and L. von Smekal, Phys. Rept. **353** (2001) 281 [hep-ph/0007355].

[12] C. S. Fischer, J. Phys. G **32** (2006) R253 [hep-ph/0605173].

[13] I. C. Cloet and C. D. Roberts, Prog. Part. Nucl. Phys. **77** (2014) 1 [arXiv:1310.2651 [nucl-th]].

[14] P. Maris, C. D. Roberts and P. C. Tandy, Phys. Lett. B **420** (1998) 267 [nucl-th/9707003].

[15] P. Maris and C. D. Roberts, Phys. Rev. C **56** (1997) 3369 [nucl-th/9708029].

[16] P. Maris and P. C. Tandy, Phys. Rev. C **60** (1999) 055214 [nucl-th/9905056].

[17] G. Eichmann, R. Alkofer, A. Krassnigg and D. Nicmorus, Phys. Rev. Lett. **104** (2010) 201601 [arXiv:0912.2246 [hep-ph]].

[18] D. Nicmorus, G. Eichmann and R. Alkofer, Phys. Rev. D **82** (2010) 114017 [arXiv:1008.3184 [hep-ph]].

[19] S. Weinberg, Phys. Rev. D **19** (1979) 1277.

[20] S. Dimopoulos and L. Susskind, Nucl. Phys. B **155**, 237 (1979).

[21] B. Holdom, Phys. Rev. D **24** (1981) 1441.

[22] C. S. Fischer and R. Alkofer, Phys. Lett. B **536** (2002) 177 [hep-ph/0202202].

[23] M. Q. Huber and L. von Smekal, JHEP **1304** (2013) 149 [arXiv:1211.6092 [hep-th]].

[24] A. Blum, M. Q. Huber, M. Mitter and L. von Smekal, Phys. Rev. D **89** (2014) 061703 [arXiv:1401.0713 [hep-ph]].

[25] M. Mitter, J. M. Pawlowski and N. Strodthoff, Phys. Rev. D **91** (2015) 054035 [arXiv:1411.7978 [hep-ph]].

[26] G. Eichmann, R. Williams, R. Alkofer and M. Vujinovic, Phys. Rev. D **89** (2014) 105014 [arXiv:1402.1365 [hep-ph]].

[27] M. Vujinovic and R. Williams, Eur. Phys. J. C **75** (2015) 3, 100 [arXiv:1411.7619 [hep-ph]].

[28] H. Sanchis-Alepuz and R. Williams, arXiv:1504.07776 [hep-ph].

[29] R. Lewis, C. Pica and F. Sannino, Phys. Rev. D **85** (2012) 014504 [arXiv:1109.3513 [hep-ph]].

[30] A. Hietanen, R. Lewis, C. Pica and F. Sannino, JHEP **1407** (2014) 116 [arXiv:1404.2794 [hep-lat]].

[31] A. Hietanen, R. Lewis, C. Pica and F. Sannino, arXiv:1308.4130 [hep-ph].

[32] G. Eichmann, arXiv:0909.0703 [hep-ph].

[33] M. E. Peskin and D. V. Schroeder, Reading, USA: Addison-Wesley (1995) 842 p

[34] S. F. Novaes, In *Sao Paulo 1999, Particles and fields* 5-102 [hep-ph/0001283].

[35] J. R. Andersen, O. Antipin, G. Azuelos, L. Del Debbio, E. Del Nobile, S. Di Chiara, T. Hapola and M. Jarvinen *et al.*, Eur. Phys. J. Plus **126** (2011) 81 [arXiv:1104.1255 [hep-ph]].

[36] J. Beringer *et al.* [Particle Data Group Collaboration], Phys. Rev. D **86** (2012) 010001.

[37] S. L. Adler, Phys. Rev. **177** (1969) 2426.

[38] J. S. Bell and R. Jackiw, Nuovo Cim. A **60** (1969) 47.

[39] L. D. Faddeev and V. N. Popov, Phys. Lett. B **25** (1967) 29.

[40] V. N. Gribov, Nucl. Phys. B **139** (1978) 1.

[41] C. Becchi, A. Rouet and R. Stora, Phys. Lett. B **52** (1974) 344.

[42] C. Becchi, A. Rouet and R. Stora, Commun. Math. Phys. **42** (1975) 127.

[43] J. C. Taylor, Nucl. Phys. B **33** (1971) 436.

[44] A. A. Slavnov, Theor. Math. Phys. **10** (1972) 99 [Teor. Mat. Fiz. **10** (1972) 153].

[45] P. Pascual and R. Tarrach, Lect. Notes Phys. **194** (1984) 1.

[46] S. Bethke, Eur. Phys. J. C **64** (2009) 689 [arXiv:0908.1135 [hep-ph]].

[47] D. Zwanziger, Nucl. Phys. B **518** (1998) 237.

[48] D. Zwanziger, Phys. Rev. Lett. **90** (2003) 102001 [hep-lat/0209105].

[49] J. Greensite and S. Olejnik, Phys. Rev. D **67** (2003) 094503 [hep-lat/0302018].

[50] C. Feuchter and H. Reinhardt, Phys. Rev. D **70** (2004) 105021 [hep-th/0408236].

[51] D. Zwanziger, Nucl. Phys. B **364** (1991) 127.

[52] C. Lerche and L. von Smekal, Phys. Rev. D **65** (2002) 125006 [hep-ph/0202194].

[53] R. Alkofer, C. S. Fischer, F. J. Llanes-Estrada and K. Schwenzer, Annals Phys. **324** (2009) 106 [arXiv:0804.3042 [hep-ph]].

[54] L. Fister and J. M. Pawlowski, Phys. Rev. D **88** (2013) 045010 [arXiv:1301.4163 [hep-ph]].

[55] T. Kugo and I. Ojima, Prog. Theor. Phys. Suppl. **66** (1979) 1.

[56] K. Osterwalder and R. Schrader, Commun. Math. Phys. **31** (1973) 83.

[57] K. Osterwalder and R. Schrader, Commun. Math. Phys. **42** (1975) 281.

[58] M. Stingl, Z. Phys. A **353** (1996) 423 [hep-th/9502157].

[59] J. Goldstone, Nuovo Cim. **19** (1961) 154.

[60] J. Goldstone, A. Salam and S. Weinberg, Phys. Rev. **127** (1962) 965.

[61] H. Sanchis-Alepuz, R. Alkofer, G. Eichmann and R. Williams, PoS QCD **-TNT-II** (2011) 041 [arXiv:1112.3214 [hep-ph]].

[62] R. Alkofer, W. Detmold, C. S. Fischer and P. Maris, Phys. Rev. D **70** (2004) 014014 [hep-ph/0309077].

[63] W. E. Caswell, Phys. Rev. Lett. **33** (1974) 244.

[64] T. W. Appelquist, D. Karabali and L. C. R. Wijewardhana, Phys. Rev. Lett. **57** (1986) 957.

[65] T. Appelquist and L. C. R. Wijewardhana, Phys. Rev. D **36** (1987) 568.

[66] T. Muta, World Sci. Lect. Notes Phys. **57** (1998) 1.

[67] M. Q. Huber and M. Mitter, Comput. Phys. Commun. **183** (2012) 2441 [arXiv:1112.5622 [hep-th]].

[68] M. Q. Huber and J. Braun, Comput. Phys. Commun. **183** (2012) 1290 [arXiv:1102.5307 [hep-th]].

[69] C. Wetterich, Phys. Lett. B **301** (1993) 90.

[70] J. Berges, Phys. Rev. D **70** (2004) 105010 [hep-ph/0401172].

[71] H. Gies and C. Wetterich, Phys. Rev. D **65** (2002) 065001 [hep-th/0107221].

[72] J. M. Pawlowski, Annals Phys. **322** (2007) 2831 [hep-th/0512261].

[73] J. Braun, L. Fister, J. M. Pawlowski and F. Rennecke, arXiv:1412.1045 [hep-ph].

[74] R. E. Cutkosky and M. Leon, Phys. Rev. **135** (1964) B1445.

[75] N. Nakanishi, Phys. Rev. **138** (1965) B1182.

[76] P. C. Tandy, Prog. Part. Nucl. Phys. **39** (1997) 117 [nucl-th/9705018].

[77] A. Krassnigg, Phys. Rev. D **80** (2009) 114010 [arXiv:0909.4016 [hep-ph]].

[78] M. Blank, A. Krassnigg and A. Maas, Phys. Rev. D **83** (2011) 034020 [arXiv:1007.3901 [hep-ph]].

[79] M. Blank and A. Krassnigg, Phys. Rev. D **84** (2011) 096014 [arXiv:1109.6509 [hep-ph]].

[80] H. L. L. Roberts, L. Chang, I. C. Cloet and C. D. Roberts, Few Body Syst. **51** (2011) 1 [arXiv:1101.4244 [nucl-th]].

[81] C. S. Fischer, S. Kubrak and R. Williams, Eur. Phys. J. A **50** (2014) 126 [arXiv:1406.4370 [hep-ph]].

[82] C. S. Fischer, S. Kubrak and R. Williams, arXiv:1409.5076 [hep-ph].

[83] G. Eichmann, Phys. Rev. D **84** (2011) 014014 [arXiv:1104.4505 [hep-ph]].

[84] H. Sanchis-Alepuz, R. Williams and R. Alkofer, Phys. Rev. D **87** (2013) 9, 096015 [arXiv:1302.6048 [hep-ph]].

[85] R. L. Jaffe, Phys. Rev. D **15** (1977) 281.

[86] N. Mathur, A. Alexandru, Y. Chen, S. J. Dong, T. Draper, I. Horvath, F. X. Lee and K. F. Liu *et al.*, Phys. Rev. D **76** (2007) 114505 [hep-ph/0607110].

[87] W. Heupel, G. Eichmann and C. S. Fischer, Phys. Lett. B **718** (2012) 545 [arXiv:1206.5129 [hep-ph]].

[88] A. Maas, JHEP **1105** (2011) 077 [arXiv:1102.5023 [hep-lat]].

[89] M. Hopfer, C. S. Fischer and R. Alkofer, JHEP **1411** (2014) 035 [arXiv:1405.7031 [hep-ph]].

[90] H. Sanchis-Alepuz and R. Williams, arXiv:1503.05896 [hep-ph].

[91] H. Sanchis-Alepuz, C. S. Fischer, C. Kellermann and L. von Smekal, arXiv:1503.06051 [hep-ph].

[92] S. L. Glashow, Nucl. Phys. **22** (1961) 579.

[93] J. S. Schwinger, Phys. Rev. **125** (1962) 397.

[94] J. S. Schwinger, Phys. Rev. **128** (1962) 2425.

[95] P. W. Anderson, Phys. Rev. **130** (1963) 439.

[96] S. Elitzur, Phys. Rev. D **12** (1975) 3978.

[97] N. Nakanishi and I. Ojima, World Sci. Lect. Notes Phys. **27** (1990) 1.

[98] G. 't Hooft, Nucl. Phys. B **35** (1971) 167.

[99] S. Chatrchyan *et al.* [CMS Collaboration], Phys. Lett. B **716** (2012) 30 [arXiv:1207.7235 [hep-ex]].

[100] G. Aad *et al.* [ATLAS Collaboration], Phys. Lett. B **716** (2012) 1 [arXiv:1207.7214 [hep-ex]].

[101] J. F. Gunion and H. E. Haber, Nucl. Phys. B **272** (1986) 1 [Erratum-ibid. B **402** (1993) 567].

[102] H. Georgi, Comptes Rendus Physique **8** (2007) 1029.

[103] E. Eichten and K. D. Lane, Phys. Lett. B **90** (1980) 125.

[104] D. F. Litim and F. Sannino, JHEP **1412** (2014) 178 [arXiv:1406.2337 [hep-th]].

[105] A. G. Cohen and H. Georgi, Nucl. Phys. B **314** (1989) 7.

[106] C. T. Hill, Phys. Lett. B **266** (1991) 419.

[107] D. D. Dietrich, F. Sannino and K. Tuominen, Phys. Rev. D **72** (2005) 055001 [hep-ph/0505059].

[108] R. Foadi, M. T. Frandsen and F. Sannino, Phys. Rev. D **87** (2013) 095001 [arXiv:1211.1083 [hep-ph]].

[109] A. Doff, A. A. Natale and P. S. Rodrigues da Silva, Phys. Rev. D **77** (2008) 075012 [arXiv:0802.1898 [hep-ph]].

[110] A. Doff, A. A. Natale and P. S. Rodrigues da Silva, Phys. Rev. D **80** (2009) 055005 [arXiv:0905.2981 [hep-ph]].

[111] T. Appelquist, J. Terning and L. C. R. Wijewardhana, Phys. Rev. Lett. **77** (1996) 1214 [hep-ph/9602385].

[112] T. Appelquist, G. T. Fleming and E. T. Neil, Phys. Rev. Lett. **100** (2008) 171607 [Erratum-ibid. **102** (2009) 149902] [arXiv:0712.0609 [hep-ph]].

[113] T. Appelquist, G. T. Fleming and E. T. Neil, Phys. Rev. D **79** (2009) 076010 [arXiv:0901.3766 [hep-ph]].

[114] T. Appelquist, G. T. Fleming, M. F. Lin, E. T. Neil and D. A. Schaich, Phys. Rev. D **84** (2011) 054501 [arXiv:1106.2148 [hep-lat]].

[115] A. Hasenfratz, Phys. Rev. Lett. **108** (2012) 061601 [arXiv:1106.5293 [hep-lat]].

[116] A. Cheng, A. Hasenfratz and D. Schaich, Phys. Rev. D **85** (2012) 094509 [arXiv:1111.2317 [hep-lat]].

[117] C. -J. D. Lin, K. Ogawa, H. Ohki and E. Shintani, JHEP **1208** (2012) 096 [arXiv:1205.6076 [hep-lat]].

[118] Y. Aoki *et al.* [LatKMI Collaboration], Phys. Rev. D **87** (2013) 9, 094511 [arXiv:1302.6859 [hep-lat]].

[119] T. Appelquist, R. C. Brower, M. I. Buchoff, M. Cheng, G. T. Fleming, J. Kiskis, M. F. Lin and E. T. Neil *et al.*, Phys. Rev. Lett. **112** (2014) 111601 [arXiv:1311.4889 [hep-ph]].

[120] M. E. Peskin and T. Takeuchi, Phys. Rev. Lett. **65** (1990) 964.

[121] M. E. Peskin and T. Takeuchi, Phys. Rev. D **46** (1992) 381.

[122] R. Barbieri, A. Pomarol, R. Rattazzi and A. Strumia, Nucl. Phys. B **703** (2004) 127 [hep-ph/0405040].

[123] K. Nakamura *et al.* [Particle Data Group Collaboration], J. Phys. G **37** (2010) 075021.

[124] E. Witten, Phys. Lett. B **117** (1982) 324.

[125] F. Sannino and K. Tuominen, Phys. Rev. D **71** (2005) 051901 [hep-ph/0405209].

[126] T. DeGrand, Y. Shamir and B. Svetitsky, Phys. Rev. D **82** (2010) 054503 [arXiv:1006.0707 [hep-lat]].

[127] T. DeGrand, Y. Shamir and B. Svetitsky, Phys. Rev. D **87** (2013) 074507 [arXiv:1201.0935 [hep-lat]].

[128] Z. Fodor, K. Holland, J. Kuti, D. Nogradi, C. Schroeder and C. H. Wong, Phys. Lett. B **718** (2012) 657 [arXiv:1209.0391 [hep-lat]].

[129] H. S. Fukano and F. Sannino, Phys. Rev. D **82** (2010) 035021 [arXiv:1005.3340 [hep-ph]].

[130] L. Del Debbio, B. Lucini, A. Patella, C. Pica and A. Rago. Phys. Rev. D **82** (2010) 014510 [arXiv:1004.3206 [hep-lat]].

[131] L. Del Debbio, B. Lucini, A. Patella, C. Pica and A. Rago, Phys. Rev. D **82** (2010) 014509 [arXiv:1004.3197 [hep-lat]].

[132] F. Bursa, L. Del Debbio, D. Henty, E. Kerrane, B. Lucini, A. Patella, C. Pica and T. Pickup *et al.*, Phys. Rev. D **84** (2011) 034506 [arXiv:1104.4301 [hep-lat]].

[133] D. August and A. Maas, JHEP **1307** (2013) 001 [arXiv:1304.4423 [hep-lat]].

[134] S. Hands, J. B. Kogut, M. P. Lombardo and S. E. Morrison, Nucl. Phys. B **558** (1999) 327 [hep-lat/9902034].

[135] R. Aloisio, V. Azcoiti, G. Di Carlo, A. Galante and A. F. Grillo, Nucl. Phys. B **606** (2001) 322 [hep-lat/0011079].

[136] R. Aloisio, V. Azcoiti, G. Di Carlo, A. Galante and A. F. Grillo, Phys. Lett. B **493** (2000) 189 [hep-lat/0009034].

[137] S. Hands, I. Montvay, S. Morrison, M. Oevers, L. Scorzato and J. Skullerud, Eur. Phys. J. C **17** (2000) 285 [hep-lat/0006018].

[138] J. B. Kogut, D. K. Sinclair, S. J. Hands and S. E. Morrison, Phys. Rev. D **64** (2001) 094505 [hep-lat/0105026].

[139] S. Hands, I. Montvay, L. Scorzato and J. Skullerud, Eur. Phys. J. C **22** (2001) 451 [hep-lat/0109029].

[140] J. B. Kogut, D. Toublan and D. K. Sinclair, Nucl. Phys. B **642** (2002) 181 [hep-lat/0205019].

[141] S. Muroya, A. Nakamura and C. Nonaka, Phys. Lett. B **551** (2003) 305 [hep-lat/0211010].

[142] B. Alles, M. D'Elia and M. P. Lombardo, Nucl. Phys. B **752** (2006) 124 [hep-lat/0602022].

[143] S. Hands, S. Kim and J. I. Skullerud, Eur. Phys. J. C **48** (2006) 193 [hep-lat/0604004].

[144] S. Cotter, P. Giudice, S. Hands and J. I. Skullerud, Phys. Rev. D **87** (2013) 3, 034507 [arXiv:1210.4496 [hep-lat]].

[145] T. Appelquist, P. S. Rodrigues da Silva and F. Sannino, Phys. Rev. D **60** (1999) 116007 [hep-ph/9906555].

[146] Z. -y. Duan, P. S. Rodrigues da Silva and F. Sannino, Nucl. Phys. B **592** (2001) 371 [hep-ph/0001303].

[147] Z. Ahmed *et al.* [CDMS-II Collaboration], Phys. Rev. Lett. **106** (2011) 131302 [arXiv:1011.2482 [astro-ph.CO]].

[148] E. Aprile *et al.* [XENON Collaboration], Astropart. Phys. **34** (2011) 679 [arXiv:1001.2834 [astro-ph.IM]].

[149] S. M. Barr, R. S. Chivukula and E. Farhi, Phys. Lett. B **241** (1990) 387.

[150] S. M. Barr, Phys. Rev. D **44** (1991) 3062.

[151] K. M. Zurek, Phys. Rept. **537** (2014) 91 [arXiv:1308.0338 [hep-ph]].

[152] T. Appelquist *et al.* [Lattice Strong Dynamics (LSD) Collaboration], Phys. Rev. D **89** (2014) 9, 094508 [arXiv:1402.6656 [hep-lat]].

[153] G. Cacciapaglia and F. Sannino, JHEP **1404** (2014) 111 [arXiv:1402.0233 [hep-ph]].

[154] J. S. Ball and T. -W. Chiu, Phys. Rev. D **22** (1980) 2550 [Erratum-ibid. D **23** (1981) 3085].

[155] W. Celmaster and R. J. Gonsalves, Phys. Rev. D **20** (1979) 1420.

[156] A. I. Davydychev, P. Osland and O. V. Tarasov, Nucl. Phys. Proc. Suppl. **51C** (1996) 289 [hep-ph/9605453].

[157] A. I. Davydychev, P. Osland and L. Saks, JHEP **0108** (2001) 050 [hep-ph/0105072].

[158] S. K. Kim and M. Baker, Nucl. Phys. B **164** (1980) 152.

[159] L. von Smekal, R. Alkofer and A. Hauck, Phys. Rev. Lett. **79** (1997) 3591 [hep-ph/9705242].

[160] C. S. Fischer, A. Maas and J. M. Pawlowski, Annals Phys. **324** (2009) 2408 [arXiv:0810.1987 [hep-ph]].

[161] R. Alkofer, C. S. Fischer and F. J. Llanes-Estrada, Phys. Lett. B **611** (2005) 279 [Erratum-ibid. **670** (2009) 460] [hep-th/0412330].

[162] A. Cucchieri, A. Maas and T. Mendes, Phys. Rev. D **74** (2006) 014503 [hep-lat/0605011].

[163] A. Maas, Phys. Rev. D **75** (2007) 116004 [arXiv:0704.0722 [hep-lat]].

[164] A. Cucchieri, A. Maas and T. Mendes, Phys. Rev. D **77** (2008) 094510 [arXiv:0803.1798 [hep-lat]].

[165] C. S. Fischer and R. Williams, Phys. Rev. Lett. **103** (2009) 122001 [arXiv:0905.2291 [hep-ph]].

[166] M. Q. Huber, A. Maas and L. von Smekal, JHEP **1211** (2012) 035 [arXiv:1207.0222 [hep-th]].

[167] L. von Smekal, K. Maltman and A. Sternbeck, Phys. Lett. B **681** (2009) 336 [arXiv:0903.1696 [hep-ph]].

[168] W. Schleifenbaum, A. Maas, J. Wambach and R. Alkofer, Phys. Rev. D **72** (2005) 014017 [hep-ph/0411052].

[169] P. Pascual and R. Tarrach, Nucl. Phys. B **174** (1980) 123 [Erratum-ibid. B **181** (1981) 546].

[170] C. Kellermann and C. S. Fischer, Phys. Rev. D **78** (2008) 025015 [arXiv:0801.2697 [hep-ph]].

[171] A. K. Cyrol, M. Q. Huber and L. von Smekal, Eur. Phys. J. C **75** (2015) 3, 102 [arXiv:1408.5409 [hep-ph]].

[172] A. C. Aguilar, D. Binosi, D. Ibaez and J. Papavassiliou, Phys. Rev. D **89** (2014) 085008 [arXiv:1312.1212 [hep-ph]].

[173] G. Eichmann and C. S. Fischer, PoS ConfinementX (2012) 090 [arXiv:1301.1194 [hep-ph]].

[174] R. Alkofer, M. Q. Huber and K. Schwenzer, Phys. Rev. D **81** (2010) 105010 [arXiv:0801.2762 [hep-th]].

[175] R. Alkofer, M. Q. Huber and K. Schwenzer, Eur. Phys. J. C **62** (2009) 761 [arXiv:0812.4045 [hep-ph]].

[176] M. Q. Huber, R. Alkofer, C. S. Fischer and K. Schwenzer, Phys. Lett. B **659** (2008) 434 [arXiv:0705.3809 [hep-ph]].

[177] M. Pelaez, M. Tissier and N. Wschebor, Phys. Rev. D **88** (2013) 125003 [arXiv:1310.2594 [hep-th]].

[178] R. Alkofer and C. S. Fischer, Fizika B **13** (2004) 65 [hep-ph/0309089].

[179] L. von Smekal, A. Hauck and R. Alkofer, Annals Phys. **267** (1998) 1 [Erratum-ibid. **269** (1998) 182] [hep-ph/9707327].

[180] H. J. Munczek, Phys. Rev. D **52** (1995) 4736 [hep-th/9411239].

[181] A. Bender, C. D. Roberts and L. Von Smekal, Phys. Lett. B **380** (1996) 7 [nucl-th/9602012].

[182] A. Bender, W. Detmold, C. D. Roberts and A. W. Thomas, Phys. Rev. C **65** (2002) 065203 [nucl-th/0202082].

[183] P. Watson, W. Cassing and P. C. Tandy, Few Body Syst. **35** (2004) 129 [hep-ph/0406340].

[184] P. Watson and W. Cassing, Few Body Syst. **35** (2004) 99 [hep-ph/0405287].

[185] M. S. Bhagwat, A. Holl, A. Krassnigg, C. D. Roberts and P. C. Tandy, Phys. Rev. C **70** (2004) 035205 [nucl-th/0403012].

[186] H. H. Matevosyan, A. W. Thomas and P. C. Tandy, Phys. Rev. C **75** (2007) 045201 [nucl-th/0605057].

[187] A. Windisch, M. Hopfer and R. Alkofer, Acta Phys. Polon. Supp. **6** (2013) 347 [arXiv:1210.8428 [hep-ph]].

[188] R. Williams, Eur. Phys. J. A **51** (2015) 5, 57 [arXiv:1404.2545 [hep-ph]].

[189] M. Gomez-Rocha, T. Hilger and A. Krassnigg, arXiv:1408.1077 [hep-ph].

[190] C. S. Fischer, P. Watson and W. Cassing, Phys. Rev. D **72** (2005) 094025 [hep-ph/0509213].

[191] C. S. Fischer, D. Nickel and J. Wambach, Phys. Rev. D **76** (2007) 094009 [arXiv:0705.4407 [hep-ph]].

[192] C. S. Fischer, D. Nickel and R. Williams, Eur. Phys. J. C **60** (2009) 47 [arXiv:0807.3486 [hep-ph]].

[193] C. S. Fischer and R. Williams, Phys. Rev. D **78** (2008) 074006 [arXiv:0808.3372 [hep-ph]].

[194] L. Chang and C. D. Roberts, Phys. Rev. Lett. **103** (2009) 081601 [arXiv:0903.5461 [nucl-th]].

[195] L. Chang and C. D. Roberts, Phys. Rev. C **85** (2012) 052201 [arXiv:1104.4821 [nucl-th]].

[196] W. Heupel, T. Goecke and C. S. Fischer, Eur. Phys. J. A **50** (2014) 85 [arXiv:1402.5042 [hep-ph]].

[197] J. Skullerud and A. Kizilersu, JHEP **0209** (2002) 013 [hep-ph/0205318].

[198] J. I. Skullerud, P. O. Bowman, A. Kizilersu, D. B. Leinweber and A. G. Williams, JHEP **0304** (2003) 047 [hep-ph/0303176].

[199] A. Kizilersu, D. B. Leinweber, J. I. Skullerud and A. G. Williams, Eur. Phys. J. C **50** (2007) 871 [hep-lat/0610078].

[200] E. Rojas, J. P. B. C. de Melo, B. El-Bennich, O. Oliveira and T. Frederico, JHEP **1310** (2013) 193 [arXiv:1306.3022 [hep-ph]].

[201] A. C. Aguilar, D. Binosi, D. Ibañez and J. Papavassiliou, Phys. Rev. D **90** (2014) 065027 [arXiv:1405.3506 [hep-ph]].

[202] M. Hopfer and R. Alkofer, Acta Phys. Polon. Supp. **6** (2013) 3, 929 [arXiv:1304.4360 [hep-ph]].

[203] R. Williams, EPJ Web Conf. **3** (2010) 03005 [arXiv:0912.3494 [hep-ph]].

[204] M. Gimeno-Segovia and F. J. Llanes-Estrada, Eur. Phys. J. C **56** (2008) 557 [arXiv:0805.4145 [hep-th]].

[205] S. Strauss, C. S. Fischer and C. Kellermann, Phys. Rev. Lett. **109** (2012) 252001 [arXiv:1208.6239 [hep-ph]].

[206] A. Windisch, M. Q. Huber and R. Alkofer, Acta Phys. Polon. Supp. **6** (2013) 3, 887 [arXiv:1304.3642 [hep-ph]].

[207] M. S. Bhagwat, A. Hoell, A. Krassnigg, C. D. Roberts and S. V. Wright, Few Body Syst. **40** (2007) 209 [nucl-th/0701009].

[208] S. M. Dorkin, L. P. Kaptari, T. Hilger and B. Kampfer, Phys. Rev. C **89** (2014) 034005 [arXiv:1312.2721 [hep-ph]].

[209] M. Gell-Mann, R. J. Oakes and B. Renner, Phys. Rev. **175** (1968) 2195.

[210] V. Mader, G. Eichmann, M. Blank and A. Krassnigg, Phys. Rev. D **84** (2011) 034012 [arXiv:1106.3159 [hep-ph]].

[211] A. Windisch, R. Alkofer, G. Haase and M. Liebmann, Comput. Phys. Commun. **184** (2013) 109 [arXiv:1205.0752 [hep-ph]].

[212] G. Eichmann and C. S. Fischer, Phys. Rev. D **87** (2013) 3, 036006 [arXiv:1212.1761 [hep-ph]].

[213] A. Krassnigg and C. D. Roberts, Fizika B **13** (2004) 143 [nucl-th/0308039].

[214] D. C. Sorensen, Tech. Rep. TR-96-40, Rice University, Houston, Texas (1996).

[215] H. A. van der Vorst, SIAM J. Sci. Stat. Comput. 13 (2) (1992) 631-644

[216] R. Fukuda, Prog. Theor. Phys. **78** (1987) 1487.

[217] M. Komachiya, M. Ukita and R. Fukuda, Phys. Rev. D **40** (1989) 2654.

[218] D. W. McKay and H. J. Munczek, Phys. Rev. D **40** (1989) 4151.

[219] J. M. Cornwall, R. Jackiw and E. Tomboulis, Phys. Rev. D **10** (1974) 2428.

Acknowledgements

First and foremost, I would like to thank my supervisor Reinhard Alkofer for his support, encouragement, guidance and (sometimes) great patience with me during my work on this doctoral thesis. I am also grateful for many discussions with him through which I learned a lot about quantum field theories and physics in general. I am greatly indebted to Richard Williams and Gernot Eichmann for teaching me the many useful 'tricks of the trade' and sharing their vast knowledge with me. I am additionally thankful to them and Christian Fischer for being excellent hosts during my stay at the University of Giessen. My thanks goes to Francesco Sannino, Claudio Pica and other ogranisers of interesting schools and conferences at CP3 Origins, where I learned a lot owing to the good atmosphere and excellent speakers.

I am very grateful for being allowed to enroll to the doctoral program 'Hadrons in vacuum, nuclei and stars' at the University of Graz. I wish to thank my fellow students, professors and staff members for making it such a pleasurable and stimulating experience.

To my friends and family, especially to my dear parents, Vesna and Marko, the words cannot express my gratitude. Thank you for always being there for me and supporting me in all the endeavors I have undertaken. I hope I have managed to return at least a small portion of this love and support to all of you.

Financial support. The work on this thesis was supported by the Austrian Science Fund (FWF), and from the Doktoratskolleg 'Hadrons in Vacuum, Nuclei and Stars' (FWF) DK W1203-N16.